Rebuttal

The authors like to thank the reviewers for their valuable comments leading to a great improvement of the present submission. We revised the manuscript with modifications marked in red color. We address the comments in detail as follows.

Referee #2

Reviewer:

In this study Herrmann et al. present a 1D modeling study investigating the potential for chemical oscillations (or more generally "recurrences") of ozone depletion episodes (ODEs) in the polar troposphere. Regular recurrences might be expected due to imbalances in the ozone-BrOx equilibrium that is central to the ozone depletion chemistry. For this study the authors used an advanced model involving gas and liquid phase chemistry, gas-aerosol interactions and vertical diffusion between the layers of their model. With initial conditions largely commensurate with observed data during polar ODEs their simulations predict recurrence of ODEs with periods from several days to a month, and ozone recovery from less than 1 to about 10 nmole/mole before depletion restarts. They follow this up with a parameter study to determine the impact of selected parameters in the model on the recurrence of ODEs. The paper is well written with a detailed description of their model, and every simulation result is extensively discussed in the context of the overall ODE mechanism. The main problem with this paper is that by ignoring large scale meteorological effects the model is too simplistic to be relevant.

Authors' Response: We disagree with the reviewer's statement about the relevance of our manuscript. Even though we do not model synoptic meteorological conditions, we are convinced that the results of the model are interesting and important. In the present study, we study whether recurrences are possible without considering large-scale meteorological effects. Therefore, we ignore them in our 1-D model. Also, we noticed that in some field studies, the occurrence of the ozone depletion is interpreted as being caused by the local chemistry (see Jacobi et al., 2006). While we agree that in reality, there will always be a combination of meteorological influences and chemical oscillations, this paper is meant as a contribution to fundamental research on the recurrences of ODEs and a proof of the concept. A perfect simulation including all known physics and chemistry might provide accurate results, but it would also make it very difficult to discern which physical and chemical mechanisms are actually responsible for the oscillations. In a simplified model, it can be tested whether a specific mechanism is responsible for the oscillations. While the results may likely be quantitatively incorrect (in the sense that reality may be different), they still allow to gain a deeper understanding of the specific mechanisms involved.

Reviewer:

There are many definitions on what constitutes a full ODE, but consensus exists that levels of ozone should be $<\sim 10$ nmole/mole, and that the end of an ODE features a return to levels of $>\sim 30$ nmole/mole. Measurements of the rate of ozone loss have been reported that implied total depletion in less than an hour. Satellite data have shown the occurrence of large systems containing enhanced levels of BrOx over the Arctic. All combined this suggests that ODEs as observed are driven by the change of air masses with high ozone/low BrOx and low ozone/high BrOx content, and that the ozone-BrOx chemistry that is responsible for the actual ozone depletion is not what is observed as ODE. Chemical oscillations may well occur during an ODE but are not what drives an ODE: recurrence of ODEs is driven by meteorological variability. Overall, I think the paper is publishable, although the scientific relevance is rather minor. The title should be modified so as not to suggest that the recurrence of ODEs is simulated (maybe into something along the lines of "simulation study of the oscillations in ozone levels during ODEs").

Authors' Response: We think that there is a misunderstanding. Up to now, the contribution of chemical oscillations to ODEs is not discussed in the literature. The reviewer's statement 'All combined this suggests that ODEs as observed are driven by the change of air masses with high ozone/low BrOx and low ozone/high BrOx content, and that the ozone-BrOx chemistry that is responsible for the actual ozone depletion is not what is observed as ODE.' is not supported by evidence, simply because models including chemical oscillations were not applied to date. While we agree with the reviewer that change of air masses (i.e. meteorology) certainly is important for recurring ODEs, the role of chemical oscillations is simply not known.
We agree, however, that the title should be modified to clarify what the study is about and propose the new title 'On the Contribution of Chemical Oscillations to Ozone Depletion Events in the Polar Spring'. In fact, we are presently extending our previous work (Cao and Gutheil, 2013) using 3D simulations so that the horizontal advection and the vertical convection can be explicitly considered. We have added this information into the last paragraph of the conclusions.

Reviewer:
And while at it I recommend rereading the text and see whether the model description and discussion of simulation results can be made more succinct; the paper is quite long for what it delivers.

Authors' Response: We believe we could save maybe about 1 to 1.5 pages by referring to Cao et al. (2016), however, we prefer to repeat the formulation for an easier understanding of the present model without having to consult other literature. Otherwise, we find it difficult to shorten the text without making the model description or discussion of the results much more difficult to understand.

Referee #3

Reviewer Summary:

Using a 1-D model of photochemistry and vertical diffusion in the lower troposphere, Herrmann et al. examine conditions leading to the self-oscillatory recurrences of ozone depletion events (ODEs) in the modelled polar boundary layer. This study finds that either the vertical diffusion of ozone from the free troposphere or the photochemical production of ozone via NOx chemistry can be a viable mechanism to recover the ozone mixing ratios after each episode of ODE in the boundary layer to drive a subsequent episode of bromine explosion and ozone depletion. Under some model conditions, the system can also approach the steady state after several recurrences of ODE. I have a mixed feeling about the present study. On one hand, the authors have done very thorough model experiments on the emergence and disappearance of the ODE recurrences, expanding a brief report on similar ODE recurrences simulated with a much simpler box model by Evans et al. (2003). On the other hand, the time scales of simulated ODE recurrences are in most cases longer than 10-20 days, whereas the shortest recurrence period simulated is about 5 days with invariant meteorology (turbulent diffusion). The constant meteorology ensures the delineation of the self-regulatory oscillation of the system without external excitation. In the real environment, however, meteorological conditions will certainly vary more or less at this time scale or shorter. Dry (and wet) deposition of aerosols seems to be ignored in the model runs so that particulate bromide accumulating in the model aerosols during the ODEs will stay intact over the recurrence time scales and available for the subsequent bromine explosion event, which I am not sure is realistic enough.

Authors' Response: We are aware of the fact that the aerosols may not stay intact for the entire simulation period. However, as outlined in our answer to major comment 3.) discussed below, the introduction of dry deposition of aerosols to the model does not significantly change the simulation results for the smaller dry deposition velocities. Furthermore, in polar regions aerosols can be also emitted from sources such as frost flowers or blowing snow, so that the loss of aerosols is compensated. The process how the aerosol is transported to the air is still unclear at present. Thus, we feel that it is realistic to consider the aerosols number concentration to be constant. This is made clear in the revised version of the paper, Section 2.1.2 Treatment of aerosols.

Reviewer:
Despite the novelty of this study, I rate its scientific significance somewhere between good and fair, because of the uncertain relevance of self-oscillatory ODE recurrences simulated here. I agree with Referee #2 in their opinion that the title of the paper is somewhat misleading and should be adapted to indicate that the authors have explored the likelihood of the chemically driven recurrence of ODEs in a more or less hypothetical fashion.

Authors' Response: As stated in the second response to Referee #2, we agree that the title should be modified to clarify what the study is about and thus, we propose the new title 'On the Contribution of Chemical Oscillations to Ozone Depletion Events in the Polar Spring'.

Reviewer:
However, who knows if someone will discover from the field data in the future the recurrent feature of ODEs similar to those simulated in this study? Yet it is fair to ask how the varying meteorological conditions can modify the self-oscillatory chemical behaviors. In my opinion, the paper is publishable with relatively minor revisions. It is an interesting paper.

Authors' Response: Thank you for the encouraging comment.

Major comments

Reviewer:
1.) P5, L30-, "To the authors' knowledge, recurrences of ODEs are hardly discussed in the literature": This sounds odd to me. Quite a few studies exist as the basis of our general understanding that variability in the meteorological conditions is the major source of the recurring nature of ODEs. To name a few, in addition to Bottenheim and Chan (2006), Oltmans et al. (2012) reported the role of synoptic air mass transport. Jacobi et al. (2010) pointed out the role of changing local and mesoscale weather conditions including the turbulent diffusion. One may regard model studies by Toyota et al. (2011) and Cao et al. (2016) as the demonstration of meteorological (external) drivers for the occurrence and termination of ODEs. Moore et al. (2014) pointed out the potential role of narrow openings in the sea ice in creating vastly different vertical mass exchange rates between the boundary layer and the free troposphere during the horizontal airmass transport. The authors should rephrase the statement by reflecting on some of such existing studies and should stress that the main value of the present study is in the exploration of other mechanisms potentially causing the ODE recurrences. I also wonder if there is a possibility for resonances with time-varying (periodic) vertical diffusivity profiles, but I guess it will be worth an entirely new study.

Authors' Response: We rephrased the statement to read: 'It is suggested (Hausmann and

Platt, 1994, Tuckermann et al., 1997, Bottenheim and Chan, 2006, Frieß et al., 2011, Oltmans et al., 2012, Helmig et al., 2012) that their cause is transport of air containing varying amounts of reactive Br and O_3 from different locations to the measurement site, leading to recurrence. Jacobi et al. (2010) discussed the role of changing local and mesoscale weather conditions as well as a possibility of a replenishment of ozone via vertical diffusion from aloft. Toyota et al. (2011) demonstrated the occurrence and termination of ODEs by meteorological drivers in a numerical modeling study. Moore et al. (2014) found that narrow openings in the sea ice create vastly different vertical mass exchange rates between the boundary layer and the free troposphere, allowing replenishment of ozone from aloft. Cao et al. (2016) demonstrated in a modeling study the recurrence of an ODE by an instantaneously changing boundary layer structure. Currently unknown is the contribution of chemical oscillations to ODEs, which is the focus of this study.'
We agree that finding resonances with time-varying vertical diffusivity profiles should be possible and interesting to look for, however, that would indeed have to be done in a new study.

Reviewer:
2.) P9, L17, "The pH value is fixed at 5": This assumption is probably good for the pH of moderately acidified sea-salt aerosols (Keene et al., 2002) and NH4-SO4-NO3 aerosols in the NH3-rich environment (Guo et al., 2017), but is perhaps too high for springtime haze aerosols (Li, 1994). Is there a rationale for your assumption and have you explored the role of aerosol acidity in your simulated results? You also mention, "HNO_3 tends to dissolve quickly in aerosols" (P9, L9). If you assumed lower pH values, the behavior of HNO_3 could be different.

Authors' Response: We conducted simulations testing different pH settings. Due to the fixed pH value, there is essentially an infinite amount of H^+ ions. Changing the pH value thus only changes the reaction rate for some of the liquid phase reactions and shifts acid-base equilibria. For a pH value smaller than 7, the recurrence periods do not change. The recycling of bromine for these settings is rate-limited by the aerosol-gas mass transfer, rather than by the aqueous phase reactions. The primary reason for why the bromine recycling is not working at pH values larger than 6, the limited amount of H^+ ions being used up quickly, is still circumvented by the fixed pH. For pH values larger than 7, the ODEs slow down or result in partial ODEs at a pH greater than 9. HNO_3 dissolves slower with decreasing pH, increasing in turn the NO_x mixing ratio for a fixed NO_y initial value. At a pH of approximately 1, HNO_3 mostly stays in the gas phase. It should be noted that the deposition of HNO_3 is overestimated due to the fixed pH, since for a variable pH, the deposition of HNO_3 reduces the pH of the aerosols and thus slows down. Also, HNO_3 is photolysed at the aerosol surface (Grannas et al. 2007), which is currently not implemented in the model. We added the following sentence to the manuscript: 'Simulations found little pH dependence of the oscillation periods for pH values below 7.'

Reviewer:
3.) It seems that the aerosol-phase species are not subject to dry deposition in the present model. Dry deposition velocities of fine aerosol particles are small but not necessarily negligible within the context of this study. If we take the dry deposition velocity of the order of 0.01-0.1 cm/s (e.g., Wu et al., 2018), the residence time of particle-bound species in the atmospheric boundary layer with the thickness of 200 mis estimated to be on the order of 2-20 days. This challenges the validity of neglecting the dry deposition of particle-bound species, in particular, bromide (Br-) (P17, L6-9;C3P19, L2-5). It is probably useful to perform additional model experiments for exploring the impact of dry deposition of aerosols and/or to discuss its implications.

Authors' Response: This is an interesting question. We conducted new simulations including dry deposition of the aerosol phase species Br^-, $HOBr_{aq}$, $Br_{2,aq}$, $BrCl_{aq}$ and HBr_{aq}, employing dry deposition velocities of $v_d = 0.01, 0.03$, and 0.1 cm s^{-1} for the base case settings and different initial values for $[NO_y]$ in steps of 25 pmol mol^{-1} from zero to 100 pmol mol^{-1} NO_y. For 100 pmol mol^{-1} NO_y, the recurrence period increases by approximately 10%, 20% and 40% for $v_d = 0.01, 0.03$ and 0.1 cm s^{-1}, respectively, see Fig. R1. The bromide concentration during the build-up phases decreases by approximately 10%, 20% and 30%, respectively. As a side effect, the ozone peak concentration increases by 3-8% for the smaller velocities and by approximately 20% for $v_d = 0.1$ cm s^{-1}. The NO_y mixing ratio for which the recurrences terminate does not seem to change (about 200 pmol mol^{-1} NO_y for all three cases), and the termination occurs after approximately the same amount of recurrences. However, if we introduce sinks for aerosol species, we should also include sources. New aerosols would likely not start with zero bromide molality. This, however, increases the parameter space further as well as the uncertainties in the implementation of aerosol emissions. These sources may introduce a new way to drive the recurrences. We added some discussion to the revised manuscript on P. 9, L 30-32: "Dry and wet depositions of aerosols as well as productions and emissions of aerosols are neglected. Exploratory simulations show that adding an aerosol deposition velocity in the range of 0.01-0.1 cm s^{-1} (Wu et al., 2018) increases the oscillation period by 10%-40% and decreases the bromide concentration during the build-up phases by approximately 10%-30%. However, if a sink for aerosol is introduced, sources for aerosols such as frost flowers or blowing snow should also be implemented. The produced/emitted aerosols are likely to have non-zero

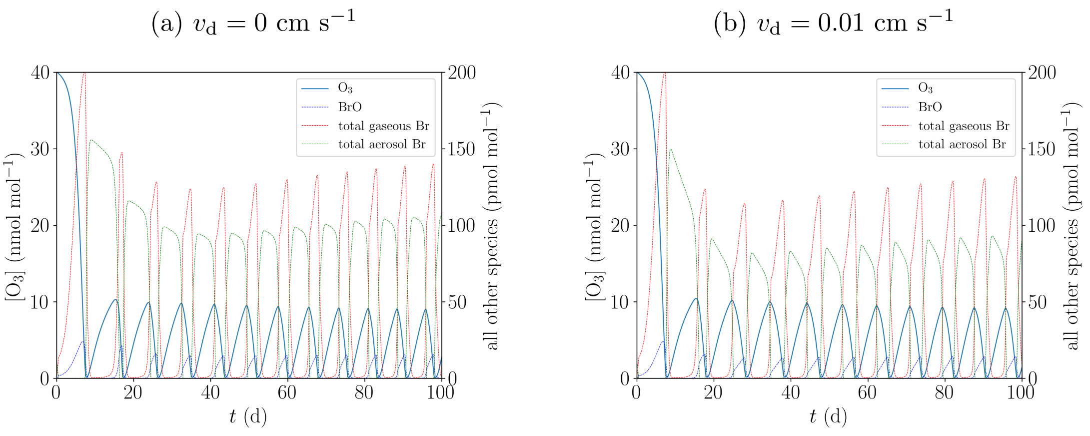
(a) $v_d = 0$ cm s^{-1}

(b) $v_d = 0.01$ cm s^{-1}

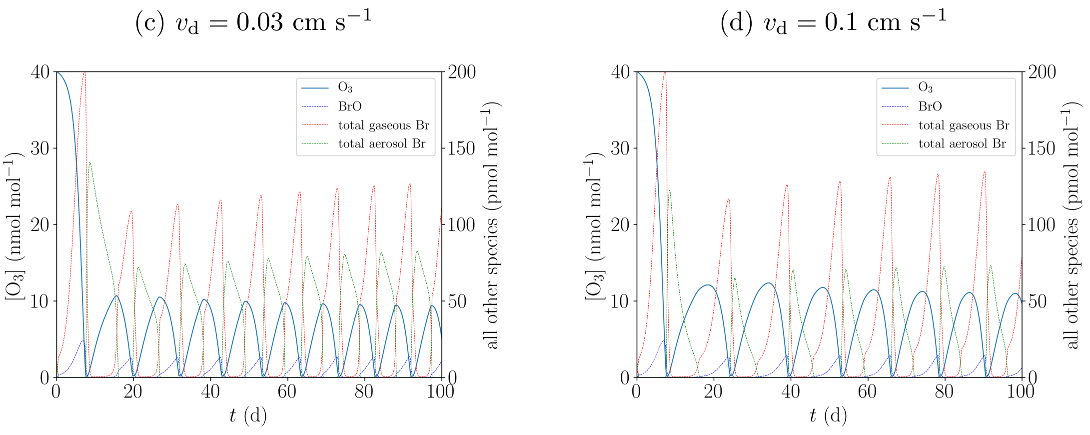
(c) $v_d = 0.03$ cm s^{-1}

(d) $v_d = 0.1$ cm s^{-1}

Figure R1: Simulations for base case settings with $NO_y = 100$ pmol mol^{-1} with different dry deposition velocities for aerosols.

bromide content, providing a source for bromine species and potentially countering the effects of the dry and wet depositions. Therefore, for simplicity and in order to avoid the uncertainties in the production and emission mechanisms of aerosols, both sources and sinks of aerosols are neglected."

Reviewer:
4.) Evans et al. (2003) seem to have assumed the mixing ratio of CH3CHO at 18 pmol/mol (see the end of their paragraph 15), whereas the default initial mixing ratio assumed in the present model is 150 pmol/mol (Table 2). It is not mentioned explicitly whether this value is adjusted for comparison with model results by Evans et al. (2003) in Section 3.3, even though the rate of bromine explosion can be highly sensitive to the CH3CHO mixing ratio. If the simulated mixing ratios of CH3CHO are still on the order of 100 pmol/mol in this case study, it is worthwhile conducting new model runs with CH3CHO = 18 pmol/mol.

Authors' Response: We conducted new simulations with fixed CH_3CHO mixing ratio: The recurrence period does not change at all, however, the first recurrence occurs approximately one day earlier, cf. Fig. R2. The ozone concentration drops only to approximately 2-3 nmol mol^{-1} instead of a mixing ratio smaller than 0.1 nmol mol^{-1}. The reason is probably the reaction of Br with CH_3CHO (R10 in Appendix A1), which produces HBr in the model. The fixed mixing ratio of CH_3CHO converts Br quickly to HBr, terminating the ODE earlier. For the variable case, the mixing ratio of CH_3CHO drops to zero during an ODE, which delays the termination of the ODE; after the ODE, the CH_3CHO concentration recovers to its background level. Evans et al. (2003) took the reaction

$$\mathrm{Br} + \mathrm{CH_3CHO} \longrightarrow \mathrm{HBr} + \mathrm{CH_3C(O)OO}$$

from Minkalowski et al. (2000) with approximately the same rate constant used in the present study. We are not sure why the model of Evans et al. (2003) does not also predict an ozone minimum of 2-3 nmol mol^{-1}. However, at this time, it cannot be determined which value is realistic because of the lack of measurements. Also, the motivation and justification for fixing the CH_3CHO concentration in the study of Evans et al. (2003) remains unclear. In Section 3.3 of the manuscript, it is now stated 'In contrast to the study of Evans et al. (2003), the mixing ratio of acetaldehyde CH_3CHO may evolve freely rather than being kept constant at 18 pmol mol^{-1}.'

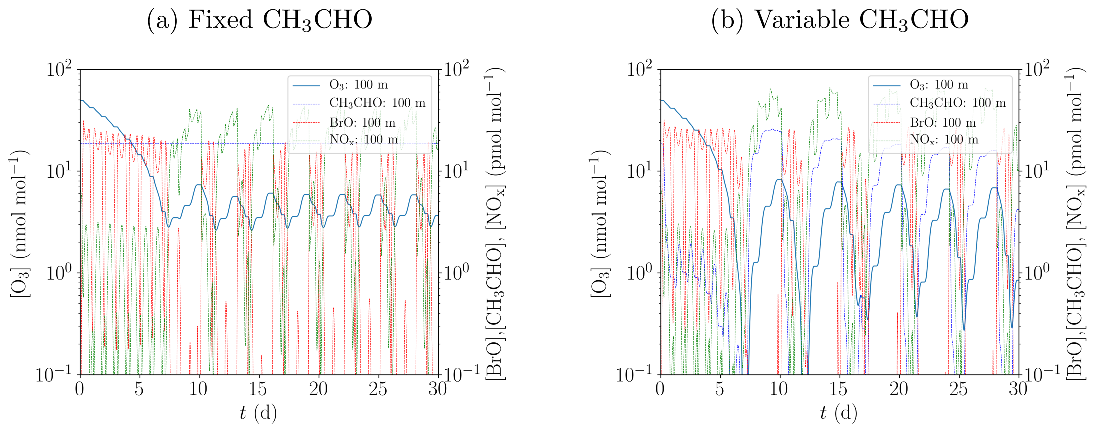
(a) Fixed CH_3CHO

(b) Variable CH_3CHO

Figure R2: Simulations of the recurrences of ODEs for the conditions of Evans et al. (2003) for the case with an initial bromide mixing ratio of 43 pmol mol^{-1}.

Reviewer:
5.) Processes that have been investigated in the past model studies but is missing in the present model study include in-snow multiphase photochemistry (e.g., Toyota et al., 2014) as a source of reactive bromine in the atmospheric boundary layer. They may accelerate the build-up of reactive bromine significantly and can thus modify the recurrent behavior of ODEs. This neglected aspect warrants some comments if not tested explicitly by extending the present model experiments.

Authors' Response: We agree that the snow pack may increase the recurrence behavior of ODEs. However, adding a snow pack model with additional physics for the snow pack and its exchange with the gas phase would require major changes to the code. Also, an additional (photo)chemistry mechanism in the snow pack would be necessary. In the conclusions section of the manuscript, P30, L26-29, adding a snow pack model is already suggested as an enhancement of the model in a future work.

Minor comments

Reviewer:
1.) The metric 'α' (defined in Eq. (1)) is referred to when discussing the simulated growth and decay of gaseous reactive bromine. It would be interesting if you can indeed manage to calculate the values of alpha from the model runs and to show their time series along with the mixing ratios of ozone and bromine species. Is it possible at all?

Authors' Response: In general, α is not a well-defined quantity. Considering the bromine explosion mechanism alone, after a time t_0 corresponding to one complete reaction cycle, the bromine mixing ratio has doubled resulting in $\alpha = 2$. The relation

$$[\mathrm{Br}_x](t) = [\mathrm{Br}_x](t=0)\,\alpha^{t/t_0} = [\mathrm{Br}_x](t=0)\,2^{t/t_0}$$

should hold in this simple case. However, if we add other reactions that may deplete or recycle bromine, it is not clear what the time t_0 is and since we can write

$$[\mathrm{Br}_x](t) = [\mathrm{Br}_x](t=0)\,\alpha^{t/t_0} = [\mathrm{Br}_x](t=0)\,e^{\ln(\alpha)t/t_0},$$

we must know t_0 in order to solve for alpha. $[\mathrm{Br}_x]$ is the total mixing ratio of gaseous bromine

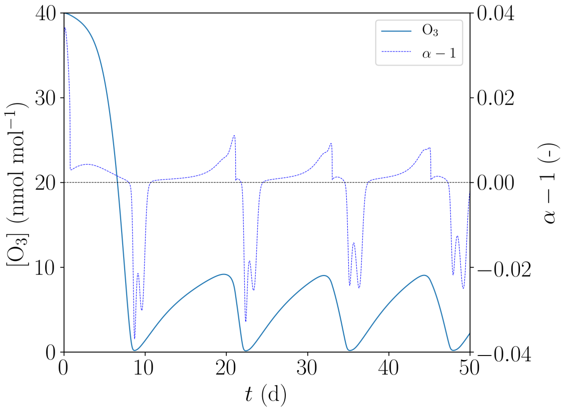

Figure R3: Mixing ratio of ozone and $\alpha - 1$ for base case settings. The dashed horizontal line indicates $\alpha - 1 = 0$

(with Br_2 counting twice). Solving for α and inserting the bromine mixing ratios of two successive time steps with time difference h, we find

$$\alpha = \left(\frac{[\mathrm{Br}_x(t_{n+1})]}{[\mathrm{Br}_x(t_n)]} \right)^{t_0/h} .$$

We estimated t_0 by adding the time scale of the dry deposition of HOBr to the time scales of the two reactions $\mathrm{Br} + \mathrm{O_3} \longrightarrow \mathrm{BrO} + \mathrm{O_2}$ and $\mathrm{BrO} + \mathrm{HO_2} \longrightarrow \mathrm{HOBr} + \mathrm{O_2}$. One might argue that only the slowest time scale should be used instead since the reactions occur simultaneously, however, t_0 is dominated by the slowest time scale in both cases anyway. t_0 is then in the range of 300..1600 seconds depending on the mixing ratio of O_3 and HO_2, with $t_0 \approx 400$ s during an ODE. As shown in Fig. R3, α varies only in the range of 0.96-1.04, where values above unity (i.e. values above the line $\alpha - 1 = 0$ in the figure) indicate bromine explosion and values of α below unity termination of the ODE. The results shown in Fig. R3 imply that already a quite small increase of α above unity is sufficient for the bromine explosion to occur. It should be noted that the value of α varies strongly with the definition of t_0. Also, even though α depends exponentially on t_0, the dependence should not deviate too far from the linear regime since the upper limit of α is 2.

Reviewer:
2.) P6, L17, "...Br instead reacts with HO2, aldehydes or alkenes to form HBr": Models (including the one used in this study) often assume that Br + alkenes produce HBr exclusively, but this is a surrogate approach to simplify complex reactions leading to the production of halogenated VOCs (e.g., Sander et al., 1997; Toyota et al., 2004; Keil and Shepson, 2006). Please consider rephrasing the statement.

Authors' Response: We rephrased the statement on P6, L17. It now reads: "...Br instead reacts with HO_2 or aldehydes to form HBr or with alkenes to form halogenated VOCs (e.g. Sander et al 1997, Toyota et al. 2004, Keil and Shepson, 2006). In many models, including the present formulation, the reactions forming halogenated VOCs are simplified in a surrogate approach to form HBr instead."

Reviewer:
3.) The model description in Section 2.1.1 appears to have significant overlaps with Cao et al. (2016). Please refer to (perhaps minor) changes from Cao et al. (2016) and consider shortening the description if possible.

Authors' Response: We may refer to the section describing the formulation of k_t to Cao et al. (2016) and simply say that we added an inversion layer. 2.1 Moreover, the description of the differential equations might be shortened somewhat. Sections 2.1.2, 2.1.3, 2.2.1, and the following are mostly describing differences to Cao et al. (2016), which cannot be removed. Section 2.4.2 might be shortened by stating that the heterogeneous reactions on snow/ice are described by Cao et al. (2016). Overall, the reference would save about 1 to 1.5 pages, however, we prefer to repeat the formulation for an easier understanding of the present model without having to consult the previous publication.

Reviewer:
4.) From Table A2, I do not see the photolysis of HNO_4 taken into account in this model. According to Stroud et al. (2003): "HNO_4 thermal decomposition and IR photolysis are the important loss mechanisms for HNO_4 in the arctic free troposphere. Our calculations result in

IR photodissociation contributing 20 % and 37 % to the total HNO_4 loss in February and May, respectively.” If you believe that this effect can notably change your model results in Section 3.4.2, please discuss.

Authors' Response: We ran new simulations using the HNO_4 photolysis rates of the CAABA/MECCA model. At an SZA of 80°, the photolysis rate of HNO_4 is 7.987×10^{-7} s^{-1} whereas the HNO_4 thermal decomposition at 238K is 7.97×10^{-6} s^{-1}. Thus, the HNO_4 decay is only approximately 10% higher with the added photolysis at that SZA. The results are barely changed by the addition of the photolysis: The NO_x mixing ratio increases by approximately 3% and the recurrence period decreases by approximately 3%.

Reviewer:
5. P26, L5-6: Define what BrNOx represents. BrNO2 + BrONO2?

Authors' Response: Yes, that is what we meant. It is now defined in the text.

Technical suggestions

Reviewer:
P1, L6: as low as → as short as
P1, L13: formulated by Lotka (1909), which are formulated in analogy to → formulated by Lotka (1909) in analogy to
P1, L16: in the order of → of the order of
P4, L25: iodine I (I^- and $IO_3{}^-$) → iodine (I^- and $IO_3{}^-$)
P4, L25: Specify the media (seawater, etc. ?) being referred to concerning the relative abundance of iodine against bromine.
P4, L27: due to the reduction of Cl → due to the reaction of Cl
P9, L14: ...heterogeneous reactions involving NOy ARE FORMULATED TO conserve gas-phase NOy.
P9, L19 and other places: Henry coefficients → Henry's law constants
P10, L4 and other places: uptake coefficient → mass accommodation coefficient
P17, L15: nitrogen oxygen → nitrogen oxides
P19, L2: starting at → restarting from
P19, L3-4: the aerosols are not diffusion limited → the multiphase reactions involving aerosols are not diffusion limited
P19, L4: All other EPISODES start FROM about 30 pmol mol^{-1} of BROMIDE...
P20, L1 and other places: aerosol transfer rates → gas-aerosol mass transfer rates
P23, L5: regenerated → replenished
P24, L13-15 (three times): upper troposphere → free troposphere
P24, L22: transported much MORE SLOWLY
P24, L23: decreasing with larger $k_{\mathrm{t,inv}}$
P24, L24-25: reducing the ozone RECOVERY RATE in the boundary layer and also limiting the maximum LEVELS TO WHICH OZONE CAN BE RECOVERED
P24, L27-: Also, the time between the two recurrences tends to increase PROGRESSIVELY AFTER EACH RECURRENCE since a larger turbulent diffusion coefficient in the inversion layer causes A GREATER loss of bromine to the free troposphere,...
P24, L31: If → In cases where
P26, L26: R59 → R57?
P26, L28: R67 → R65?

P26, L28: R86 → R84?

Authors' Response: We implemented all modifications as suggested by the reviewer.

Reviewer:
P9, L1: It is mentioned that $k_\mathrm{f} = 10\ \mathrm{m}^2\ \mathrm{s}^{-1}$ here, whereas Figure 1 indicates that $k_\mathrm{f} = 1\ \mathrm{m}^2\ \mathrm{s}^{-1}$. Please check the consistency between the two.

Authors' Response: We corrected the caption of Figure 1 of the original paper to clarify that $k_\mathrm{f} = 1\ \mathrm{m}^2\ \mathrm{s}^{-1}$ for this particular plot.

Reviewer:
P10, Eq. (12): Please double check if the factor "T/T0" is necessary.

Authors' Response: The factor is necessary for the dimensionless Henry coefficients H^cc. If the Henry coefficient H^cc in units [mol liter^{-1} Pa^{-1}] is used, the above factor is not necessary. In the present formulation, the factor T/T_0 arises due to the conversion factor $H^\mathrm{cc} = H^\mathrm{cp}RT$.

Reviewer:
P17, L2-5: You may want to rewrite these two sentences. I do not quite understand the message.

Authors' Response: We rewrote the sentence to read "Both a large ozone regeneration rate and a higher Br release efficiency reduce the drop in the total bromine mixing ratio in the gas as well as in the aerosol phase which occurs between successive oscillations. If the bromine release or the ozone regeneration rate are sufficiently large, the bromine mixing ratio may increase for successive oscillations, as shown in Fig. 7. The additional ozone production due to an increased initial NO_y mixing ratio shortens the oscillation period and therefore limits the bromine loss occurring between successive bromine explosions."

Reviewer:
P24, L23: I cannot see the connection between "drop to approximately 15 nmol mol^{-1}" and "converging to 12 nmol mol^{-1}". Can you rephrase to clarify?

Authors' Response: The '>' sign for 15 nmol mol^{-1} was wrong, it should have been an equal sign '=', thank you. We rewrote the sentence to read 'Ozone is also transported much more slowly to the lower layers of the free troposphere, causing the ozone levels to drop to approximately 15 nmol mol^{-1} at 500 m for $k_\mathrm{t,inv} = 25\ \mathrm{cm}^2\ \mathrm{s}^{-1}$; ozone levels decrease further with increased values of $k_\mathrm{t,inv}$, converging to 12 nmol mol^{-1} for $k_\mathrm{t,inv}$ exceeding a value of 50 $\mathrm{cm}^2\ \mathrm{s}^{-1}$.

Reviewer:
P26, L29-30: I do not quite understand the message here. Do you mean: "The shift from PAN to HNO_4 as the most abundant NO_y species at the lower temperature decreases the net ozone destruction rate during an ODE, resulting in earlier terminations of the ODEs?

Authors' Response: We rephrased the sentence to read "The shift from PAN as the most stable species towards HNO_4 for the lower temperature increases the ozone recovery during an ODE. Since a larger ozone recovery during an ODE facilitates chemical equilibrium with the reactive bromine, this results in earlier terminations of the oscillations of ODEs.'

Reviewer:
P28, L6, "photolyzrefered": Is this a word in German?

Authors' Response: This is a typo, it should read "photolyzed".

References

Cao, L. and Gutheil, E.: Numerical simulation of tropospheric ozone depletion in the polar spring, Air Quality, Atmosphere & Health, 6, 673–686, 2013.

Cao, L., Platt, U., Gutheil, E., Role of the boundary layer in the occurrence and termination of the tropospheric ozone depletion events in polar spring, Atmospheric Environment, Volume 132, 2016, Pages 98-110, https://doi.org/10.1016/j.atmosenv.2016.02.034.

Frieß, U., Sihler, H., Sander, R., Pöhler, D., Yilmaz, S., and Platt, U.: The vertical distribution of BrO and aerosols in the Arctic: measurements by active and passive differential opti- cal absorption sprectroscopy, J. Geophys. Res., 116, D00R04, doi:10.1029/2011JD015938, 2011.

Grannas, A. M., Jones, A. E., Dibb, J., Ammann, M., Anastasio, C., Beine, H. J., Bergin, M., Bottenheim, J., Boxe, C. S., Carver, G., Chen, G., Crawford, J. H., Dominé, F., Frey, M. M., Guzmán, M. I., Heard, D. E., Helmig, D., Hoffmann, M. R., Honrath, R. E., Huey, L. G., Hutterli, M., Jacobi, H. W., Klán, P., Lefer, B., McConnell, J., Plane, J., Sander, R., Savarino, J., Shepson, P. B., Simpson, W. R., Sodeau, J. R., von Glasow, R., Weller, R., Wolff, E. W., and Zhu, T.: An overview of snow photochemistry: evidence, mechanisms and impacts, Atmos. Chem. Phys., 7, 4329-4373, https://doi.org/10.5194/acp-7-4329-2007, 2007.

Guo, H., Weber, R. J., and Nenes, A. (2017), High levels of ammonia do not raise fine particle pH sufficiently to yield nitrogen oxide-dominated sulfate production, Scientific Reports, 7, 12109, doi:10.1038/s41598-017-11704-0.

Hausmann M. and Platt U. (1994), Spectroscopic measurement of bromine oxide and ozone in the high Arctic during Polar Sunrise Experiment 1992, J. Geophys. Res., 99, 25399-25413.

Helmig, D., Boylan, P., Johnson, B., Oltmans, S., Fairall, C., Staebler, R., Weinheimer, A., Orlando, J., Knapp, D. J., Montzka, D. D., Flocke, F., Frieß, U., Sihler, H., and Shepson, P. B.: Ozone dynamics and snow-atmosphere exchanges during ozone depletion events at Barrow, AK, J. Geophys. Res., 117, D20303, doi:10.1029/2012JD017531, 2012.

Jacobi, H.-W., S. Morin, and J. W. Bottenheim (2010), Observation of widespread depletion of ozone in the springtime boundary layer of the central Arctic linked to mesoscale synoptic conditions, J. Geophys. Res., 115, D17302, doi:10.1029/2010JD013940.

Jacobi, H. W. , Kaleschke, L. , Richter, A. , et al. Observation of a fast ozone loss in the marginal ice zone of the Arctic Ocean[J]. Journal of Geophysical Research, 2006, 111(D15):D15309.

Keene, W. C., Pszenny, A. A. P., Maben, J. R., and Sander, R., Variation of marine aerosol acidity with particle size, Geophys. Res. Lett., 29(7), doi:10.1029/2001GL013881, 2002.

Keil, A. D., and Shepson, P. B. (2006), Chlorine and bromine atom ratios in the spring- time Arctic troposphere as determined from measurements of halogenated volatile organic compounds, J. Geophys. Res., 111, D17303, doi:10.1029/2006JD007119.

Li, S.-M. (1994), Equilibrium of particle nitrite with gas-phase HONO: tropospheric measurements in the high arctic during polar sunrise, J. Geophys. Res., 99, 25469- 25478. Christopher W. Moore, Daniel Obrist, Alexandra Steffen, Ralf M. Staebler, Thomas A. Douglas, Andreas Richter, and Son V. Nghiem (2014), Convective forcing of mercury and ozone in the Arctic boundary layer induced by leads in sea ice, Nature, volume 506, pages 81-84.

Oltmans, S. J., B. J. Johnson, and J. M. Harris (2012), Springtime boundary layer ozone depletion at Barrow, Alaska: Meteorological influence, year-to-year variation, and long- term change, J. Geophys. Res., 117, D00R18, doi:10.1029/2011JD016889.

Sander, R., Vogt, R., Harris, G. W. and Crutzen, P. J. (1997), Modelling the chemistry of ozone, halogen compounds, and hydrocarbons in the arctic troposphere during spring. Tellus B, 49: 522-532. doi:10.1034/j.1600-0889.49.issue5.8.x

Stroud, C., Madronich, S., Atlas, E., Ridley, B., Flocke, F., Weinheimer, A., Talbot, B., Fried, A., Wert, B., Shetter, R., Lefer, B., Coffey, M., Heikes, B., and Blake, D. (2003), Photochemistry in the arctic free troposphere: NOx budget and the role of odd nitrogen reservoir recycling, Atmospheric Environment, 37, 3351-3364,
https://doi.org/10.1016/S1352-2310(03)00353-4.

Toyota, K., Kanaya, Y., Takahashi, M., and Akimoto, H.: A box model study on photochemical interactions between VOCs and reactive halogen species in the marine boundary layer, Atmos. Chem. Phys., 4, 1961-1987, https://doi.org/10.5194/acp-4- 1961-2004, 2004.

Toyota, K., McConnell, J. C., Lupu, A., Neary, L., McLinden, C. A., Richter, A., Kwok, R., Semeniuk, K., Kaminski, J. W., Gong, S.-L., Jarosz, J., Chipperfield, M. P., and Sioris, C. E.: Analysis of reactive bromine production and ozone depletion in the Arctic boundary layer using 3-D simulations with GEM-AQ: inference from synoptic-scale patterns, Atmos. Chem. Phys., 11, 3949-3979, https://doi.org/10.5194/acp-11-3949-2011, 2011.

Toyota, K., McConnell, J. C., Staebler, R. M., and Dastoor, A. P.: Air–snowpack exchange of bromine, ozone and mercury in the springtime Arctic simulated by the 1-D model PHANTAS – Part 1: In-snow bromine activation and its impact on ozone, Atmos. Chem. Phys., 14, 4101-4133, https://doi.org/10.5194/acp-14-4101-2014, 2014.

Tuckermann, M., Ackermann, R., Golz, C., Lorenzen-Schmidt, H., Senne, T., Stutz, J., Trost, B., Unold, W., and Platt, U.: DOAS- observation of halogen radical-catalysed arctic boundary layer ozone destruction during the ARCTOC-campaigns 1995 and 1996 in Ny-Alesund, Spitsbergen, Tellus B, 49, 533–555, 1997.

Wu, M., Liu, X., Zhang, L., Wu, C., Lu, Z., Ma, P.-L., et al. (2018). Impacts of aerosol dry deposition on black carbon spatial distributions and radiative effects in the Community Atmosphere Model CAM5. Journal of Advances in Modeling Earth Systems, 10, 1150-1171. https://doi.org/10.1029/2017MS00121

On the Contribution of Chemical Oscillations to Ozone Depletion Events in the Polar Spring

Maximilian Herrmann [1], Le Cao [2], Holger Sihler [3], Ulrich Platt [4,5], and Eva Gutheil [1,5]

[1]Interdisciplinary Center for Scientific Computing, Heidelberg University, Heidelberg, Germany
[2]Key Laboratory for Aerosol-Cloud-Precipitation of China Meteorological Administration, Nanjing University of Information Science and Technology, Nanjing, China
[3]Max-Planck Institute for Chemistry, Mainz, Germany
[4]Institute of Environmental Physics, Heidelberg University, Heidelberg, Germany
[5]Heidelberg Center for the Environment, Heidelberg University, Heidelberg, Germany

Correspondence: M. Herrmann (maximilian.herrmann@iwr.uni-heidelberg.de)

Abstract. This paper presents a numerical study of the ~~recurrences (or oscillations)~~ oscillations (or recurrences) of tropospheric ozone depletion events, ODEs, using the further developed one-dimensional chemistry transport model KINAL-T. Reactive bromine is the major contributor to the occurrence of ODEs. After the termination of an ODE, the reactive bromine in the air is deposited onto aerosols or on the snow surface, and the ozone may regenerate via $\mathrm{NO_x}$-catalyzed photochemistry or by turbulent transport from the free troposphere into the boundary layer. The replenished ozone then is available for the next cycle of autocatalytic bromine release (bromine explosion) leading to another ODE. The ~~recurrence~~ oscillation periods are found to be as ~~low~~ short as five days for the purely chemically $\mathrm{NO_x}$-driven oscillation and 30 days for a diffusion-driven ~~recurrence~~ oscillation. An important requirement for ~~recurrence~~ oscillation of ODEs to occur is found to be a sufficiently strong inversion layer. In a parameter study, the dependence of the ~~recurrence~~ oscillation period on the nitrogen oxides concentration, the inversion layer strength, the ambient temperature, the aerosol density, and the solar radiation is investigated. Parameters controlling the ~~recurrence~~ oscillation of ODEs are discussed.

1 Introduction

Oscillating chemical systems have been of scientific interest for well over a hundred years. One of the most simple, theoretical chemical oscillation was formulated by Lotka (1909) ~~which are formulated~~ in analogy to the predator–prey equations. Briggs and Rauscher (1973) found "an oscillating iodine clock", an oscillating reaction mechanism involving iodate, which could readily be reproduced in the laboratory.

Oscillations in tropospheric chemistry, involving the species $\mathrm{NO_x}, \mathrm{HO_x}, \mathrm{CO}$, and $\mathrm{O_3}$ with oscillation periods ~~in~~ of the order of several weeks to centuries were found by several researchers (e.g. White and Dietz, 1984; Poppe and Lustfeld, 1996; Hess and Madronich, 1997; Tinsley and Field, 2001). Kalachev and Field (2001) investigated a system involving the species $\mathrm{CO}, \mathrm{O_3}, \mathrm{NO}, \mathrm{NO_2}, \mathrm{HO}$, and $\mathrm{HO_2}$ with a total of seven reactions and three emissions. They found an oscillation period of one month and managed to reduce the chemical system to four species. Moreover, low $\mathrm{NO_x}$, high $\mathrm{HO_x}$, high $\mathrm{NO_x}$, and low $\mathrm{HO_x}$

regimes were identified.

Hess and Madronich (1997) investigated a similar but more complex chemical system which they were able to reduce to a two-variable system in which O_3 and CO oscillate on time scales of years to centuries. Tinsley and Field (2001) developed a two-variable model with a similar mechanism and used it to investigate the excitability behaviour of the phase space. It should be noted that these tropospheric chemical systems involve not only gas-phase chemistry, but are driven externally by the emission and the deposition of various species.

Fox et al. (1982) describe stratospheric instabilities involving three steady-state solutions for the partitioning of chlorine. Their chemical, purely gas-phase mechanism consists of chlorine compounds as well as the NO_y and HO_x families. Two of the steady-state solutions were found to be stable, which releases the potential of the system to oscillate which, however, was not investigated.

An oscillating chemical system can only occur, if the system comprises both non-linearities and feedback cycles. The chemistry of ozone depletion events (ODEs) consists of non-linearities and an auto-catalytic reaction cycle, suggesting the potential for an oscillating system.

Tang and McConnell (1996) studied the ozone depletion events using a box model where ~~the recurrence of an ODEs were found~~ an oscillation of an ODE was found after about five days. Evans et al. (2003) found indications for chemical oscillations involving ODEs, where only photochemical recovery of O_3 was considered, and ~~a recurrence~~ an oscillation period of approximately three days was found. This oscillation time scale is among the fastest found in a model of tropospheric chemistry. The chemical reaction mechanism consists of both gas-phase and aerosol-phase reactions. In addition, the oscillations are driven externally by emissions and depositions. In the present work, an extensive investigation of the oscillation potential of ODEs is conducted, and simulations with conditions similar to those described by Evans et al. (2003) are preformed in order to evaluate the present simulations, which, however, are preformed in a one-dimensional configuration considering a more advanced chemical reaction mechanism and a more sophisticated aerosol treatment. An overview of ODEs is given in the following paragraphs.

ODEs typically occur in the boundary layer in both, the Arctic and Antarctic during spring and sometimes also in fall. During a full ODE, ozone concentrations drop below 1 $\mathrm{nmol\,mol^{-1}}$ and for partial ODEs to levels of less than 10 $\mathrm{nmol\,mol^{-1}}$ (e.g. Oltmans, 1981; Bottenheim et al., 1986; Hausmann and Platt, 1994; Frieß et al., 2004; Wagner et al., 2007; Halfacre et al., 2014). Barrie et al. (1988) were the first to find an anti-correlation of the ozone and bromine concentrations during an ODE. Hausmann and Platt (1994) then found experimental evidence for the chemical reaction mechanism that is most likely responsible for the destruction of the ozone by Br atoms, which was suggested by Barrie et al. (1988):

$$2(\mathrm{Br} + \mathrm{O_3} \rightarrow \mathrm{BrO} + \mathrm{O_2}) \tag{R1}$$

$$\mathrm{BrO} + \mathrm{BrO} \rightarrow \begin{cases} 2\,\mathrm{Br} + \mathrm{O_2} \\ \mathrm{Br_2} + \mathrm{O_2} \end{cases} \tag{R2}$$

$$\mathrm{Br_2} + h\nu \rightarrow 2\mathrm{Br}, \tag{R3}$$

resulting in the following net reaction

$$2\mathrm{O_3} \rightarrow 3\mathrm{O_2}. \tag{R4}$$

In this mechanism, the destruction rate of $\mathrm{O_3}$ is limited by the BrO self-reaction (R2) and thus, a function of the square of the BrO concentration. The two different reactions paths in the self-reaction (R2) of BrO occur in a ratio of 78:22 at 258 K and 73:27 at 238 K, which are the two temperatures at which the present study is performed. The recycling of two Br atoms through reaction cycle (R1) through (R3) may occur 50-100 times before reacting to HBr via reactions of the type (R12), see below.

The primary source of the bromine in the polar boundary layer is still under discussion (e.g. Simpson et al., 2015). However, the snow-covered sea ice and the sea salt aerosols contain a significant amount of bromide $\mathrm{Br^-}$. Bromide can be released from both solid and liquid phases via the heterogenous reaction cycle (Fan and Jacob, 1992; McConnell et al., 1992; Platt and Janssen, 1995)

$$\mathrm{Br} + \mathrm{O_3} \rightarrow \mathrm{BrO} + \mathrm{O_2} \tag{R5}$$

$$\mathrm{BrO} + \mathrm{HO_2} \rightarrow \mathrm{HOBr} + \mathrm{O_2} \tag{R6}$$

$$\mathrm{HOBr} + \mathrm{H^+} + \mathrm{Br^-} \rightarrow \mathrm{Br_2} + \mathrm{H_2O} \tag{R7}$$

$$\mathrm{Br_2} + h\nu \rightarrow 2\mathrm{Br}, \tag{R8}$$

resulting in the net reaction

$$\mathrm{Br} + \mathrm{Br^-} + \mathrm{H^+} + \mathrm{O_3} + \mathrm{HO_2} \rightarrow 2\mathrm{Br} + 2\mathrm{O_2} + \mathrm{H_2O}. \tag{R9}$$

Thus, in each cycle, the number of gas-phase bromine atoms can grow by a factor $\alpha \leq 2$:

$$[\mathrm{Br}] \rightarrow \alpha\,[\mathrm{Br}]. \tag{1}$$

This process is termed the "bromine explosion" (Platt and Janssen, 1995; Platt and Lehrer, 1997; Wennberg, 1999) due to its auto-catalytic nature.

The bromine explosion requires acidity as can be seen from the net reaction (R 9). In fact, both laboratory and field measurements found that lower pH values as well as a higher bromide-to-chloride ratio in the snow speed up the evolution of the $\mathrm{Br_2}$ formation, whereas a pH value larger than six hinders the occurrence of a bromine explosion (Huff and Abbatt, 2002; Adams et al., 2002; Abbatt et al., 2012; Wren et al., 2013; Pratt et al., 2013). In particular, Pratt et al. (2013) reported that in the presence of snow with pH values in the range of 4.6 to 6.3 and $\mathrm{Br^-}$/$\mathrm{Cl^-}$ ratios between 1/38 and 1/148, a considerable amount of $\mathrm{Br_2}$ is produced, whereas for 7.3 $<$ pH $<$ 9.5 and 1/526 $<$ $\mathrm{Br^-}$/$\mathrm{Cl^-}$ $<$ 1/230, no BrO is obtained. In the presence of snow with pH = 5.3 and a $\mathrm{Br^-}$/$\mathrm{Cl^-}$ ratio of 1/468, $\mathrm{Br_2}$ is only produced if $[\mathrm{O_3}] > 100\ \mathrm{nmol\,mol^{-1}}$. Wren et al. (2013) found that in the case of pre-freezing and pH $>$ 6.2, no $\mathrm{Br_2}$ was released.

Bromide can also be activated by the species $\mathrm{BrONO_2}$, involving $\mathrm{NO_2}$, via the reactions

$$\mathrm{BrO + NO_2 + M \rightarrow BrONO_2 + M} \qquad \text{(R10)}$$

and

$$\mathrm{BrONO_2 + Br^- \rightarrow Br_2 + NO_3^-}\,. \qquad \text{(R11)}$$

In the snow, the produced nitrate is photolyzed to $\mathrm{NO_x}$ (Honrath et al., 2000; Dubowski et al., 2001; Cotter et al., 2003; Chu and Anastasio, 2003), so that this process is catalyzed by $\mathrm{NO_2}$, and it is auto-catalytic with respect to $\mathrm{Br_x}$. A major source of polar NOx, i.e. NO and $\mathrm{NO_2}$, might be a snow pack as discussed, for instance, by Jones et al. (2000, 2001). The release mechanism of NOx probably is that the UV absorption spectrum of $\mathrm{HNO_3}$ on ice is somewhat shifted towards longer wavelengths so that ice-adsorbed $\mathrm{HNO_3}$ can photolyze considerably faster than gas-phase $\mathrm{HNO_3}$, and thereby, it is reconverted into $\mathrm{NO_x}$ (Dubowski et al., 2001; Beine et al., 2003; Grannas et al., 2007).

Br atoms can also react with several organic species to form HBr and thus $\mathrm{Br^-}$, for instance with aldehydes

$$\mathrm{Br + CH_2O + O_2 \rightarrow HBr + CO + HO_2} \qquad \text{(R12)}$$

$$\mathrm{HBr \rightleftharpoons HBr_{aq}} \qquad \text{(R13)}$$

$$\mathrm{HBr_{aq} \rightleftharpoons H^+ + Br^-}, \qquad \text{(R14)}$$

effectively reducing α, cf. Eq. (1). During an ODE, once the ozone concentration has dropped sufficiently low, α drops to values of less than unity, causing the bromine explosion to retard and eventually to terminate.

Other halogen species such as iodine and chlorine radicals play a smaller role than bromine for the occurrence of ODEs. Detectable amounts of iodine were never found in the Arctic and rarely in the Antarctic (Saiz-Lopez et al., 2007), probably since the amount of iodine ($\mathrm{I^-}$ and $\mathrm{IO_3^-}$) is only 0.05% of that of $\mathrm{Br^-}$ in sea water (Luther et al., 1988; Grebel et al., 2010). $\mathrm{Cl^-}$ is more than 600 times more abundant than bromide in sea water and in frost flowers (Simpson et al., 2005; Millero et al., 2008). However, chlorine cannot undergo a "chlorine explosion" in the same way as bromine due to the ~~reduction~~ reaction of Cl with the very abundant methane to HCl, thus always reducing α in an hypothetical Cl-explosion to values below unity. HCl quickly deposits to aerosols or to the snow surface. However, the presence of even a few $\mathrm{pmol\,mol^{-1}}$ of chlorine or iodine could speed up the ODEs through a recycling of BrO since the reaction of ClO or IO with BrO is approximately one order of magnitude faster than the BrO self-reaction (R2), i.e. (Atkinson et al., 2007)

$$\mathrm{BrO} + \mathrm{XO} \rightarrow \mathrm{BrX} + \mathrm{O_2} \tag{R15}$$

and

$$\mathrm{BrX} + h\nu \rightarrow \mathrm{Br} + \mathrm{X} \tag{R16}$$

with X = Cl or I compared to X = Br. The presence of chloride may also increase the speed of the bromine explosion: In the liquid phase, the reaction of deposited HOBr with chloride (Simpson et al., 2007)

$$\mathrm{HOBr_{aq}} + \mathrm{H^+} + \mathrm{Cl^-} \overset{\mathrm{aq}}{\rightarrow} \mathrm{BrCl} + \mathrm{H_2O} \tag{R17}$$

occurs at a much faster rate than the reaction with bromide due to the larger concentration of chloride and the higher reaction constant of (R17) compared to (R7). A large fraction of the BrCl can then react with bromide to ultimately produce $\mathrm{Br_2}$, which is then released into the gas phase. However, some of the deposited HOBr instead releases BrCl, effectively reducing the α described above. Whether the presence of chloride speeds up or slows down the bromine explosion depends on the reduction of α and the quicker release of $\mathrm{Br_2}$ due to reaction (R17). A similar reaction involving HOCl also occurs

$$\mathrm{HOCl_{aq}} + \mathrm{H^+} + \mathrm{Br^-} \overset{\mathrm{aq}}{\rightarrow} \mathrm{BrCl} + \mathrm{H_2O}, \tag{R18}$$

although at a much smaller reaction rate.

As an alternative to the bromine explosion mechanisms, bromine may be released directly via a net heterogenous reaction involving ozone (e.g. Oum et al., 1998; Artiglia et al., 2017)

$$\mathrm{O_3} + 2\mathrm{Br^-} + 2\mathrm{H^+} \rightarrow \mathrm{Br_2} + \mathrm{H_2O} + \mathrm{O_2}. \tag{R19}$$

The underlying reaction mechanism may be an initial source for bromine, initiating the bromine explosion. The complete set of reactions can be found in Tables A3 and A4 in Appendix A. The release may need sunlight to occur efficiently (Pratt et al., 2013).

The meteorological conditions under which ODEs occur are also still under discussion. Often proposed are shallow, stable boundary layers (Wagner et al., 2001; Frieß et al., 2004; Lehrer et al., 2004; Koo et al., 2012). The inversion layer limits the loss of BrO from the boundary layer and also the replenishing of ozone from aloft.

ODEs occur predominantly at temperatures below $-20°$ C (Tarasick and Bottenheim, 2002), but could also be observed at temperatures of up to $-6°$ C (Bottenheim et al., 2009). Pöhler et al. (2010) found a nearly linear decrease of BrO concentrations with increasing temperature in the temperature range from$-24°$ C to $-15°$ C. Causes for the temperature dependence probably are a stronger surface-to-air flux of bromine, resulting from a stronger temperature gradient between the warm ice surface and cold air as well as the temperature-dependent reaction constants that may favor an ODE.

Frequently, successions of ODEs are measured at the same location over the year (e.g. Halfacre et al., 2014). ~~To the authors knowledge, recurrences of ODES are hardly discussed in the literature. It is suggested (Bottenheim and Chan, 2006) that their cause is that air containing varying amounts of reactive Br and $\mathrm{O_3}$ may be transported from different locations to the measurement site, leading to recurrence.~~

~~Alternatively, ozone in the polar boundary layer may also be replenished in-situ via two mechanisms:~~ It is suggested (Hausmann and Platt, 1994; Tuckermann et al., 1997; Bottenheim and Chan, 2006; Frieß et al., 2011; Oltmans et al., 2012; Helmig et al., 2012) that their cause is transport of air containing varying amounts of reactive Br and $\mathrm{O_3}$ from different locations to the measurement site, leading to recurrence. Jacobi et al. (2010) discussed the role of changing local and mesoscale weather conditions as well as a possibility of a replenishment of ozone via vertical diffusion from aloft. Toyota et al. (2011) demonstrated the occurence and termination of ODEs by meteorological drivers in a numerical modeling study. Moore et al. (2014) found that narrow openings in the sea ice create vastly different vertical mass exchange rates between the boundary layer and the free troposphere, allowing replenishment of ozone from aloft. Cao et al. (2016) demonstrated in a modeling study the recurrence of an ODE by an instantaneously changing boundary layer structure. Currently unknown is the contribution of chemical oscillations to ODEs, which is the focus of the present study. Ozone rich air is transported to the polar boundary layer from aloft by turbulent diffusion from the free troposphere. An inversion layer limits the rate of this replenishment. Ozone is also photochemically produced in-situ by the well-known $\mathrm{NO_x}$ catalyzed $\mathrm{O_3}$-formation mechanism:

$$\mathrm{NO_2} + h\nu \rightarrow \mathrm{NO} + \mathrm{O(^3P)}, \tag{R20}$$

$$\mathrm{O_2} + \mathrm{O(^3P)} + \mathrm{M} \rightarrow \mathrm{O_3} + \mathrm{M}. \tag{R21}$$

$\mathrm{NO_2}$ in turn is produced primarily by the reaction of NO and $\mathrm{HO_2}$

$$\mathrm{NO} + \mathrm{HO_2} \rightarrow \mathrm{NO_2} + \mathrm{OH}, \tag{R22}$$

where most of the $\mathrm{HO_2}$ is produced by

$$\mathrm{CO} + \mathrm{OH} + \mathrm{O_2} \rightarrow \mathrm{CO_2} + \mathrm{HO_2}. \tag{R23}$$

In the present study it is shown that the chemical system coupled with vertical turbulent diffusion shows periodicity even without horizontal transport. After a bromine explosion, the ozone concentration drops to a negligible level. As a consequence, the formation of BrO via (R5) drops to nearly zero, so that Br instead reacts with $\mathrm{HO_2}$ or aldehydes to form HBr or with alkenes to form halogenated VOCs (e.g. Sander et al., 1997; Toyota et al., 2004; Keil and Shepson, 2006). In many models, including the present formulation, the reactions forming halogenated VOCs are simplified in a surrogate approach to form HBr instead. HBr then dissolves in the aerosols. Both gas-phase and dissolved HBr are chemically inert. Now that there is no more active bromine to destroy the ozone, the ozone concentration can regenerate by either downward mixing into the boundary layer from the free troposphere or via $\mathrm{NO_x}$-catalyzed photochemical $\mathrm{O_3}$ formation. Together with the ozone, the active bromine species can also regenerate. However, due to the nonlinear nature of the bromine explosion, the reactivation speed of the inactive bromine in the aerosols scales with the amount of already active bromine. The reactivation of the inactive bromine thus starts out much slower than the ozone regeneration, allowing ozone to replenish before a new ODE occurs.

~~In the literature (e.g. Lotka, 1909; Tinsley and Field, 2001; Evans et al., 2003), reactions with periodic variations of some concentrations, such as the recurrences of ODEs, are called chemical oscillations. Since the term oscillation may suggest a constant recurrence period, the more general expression of recurrences is used in the remainder of this paper.~~

In the present study, the 1D Model KINAL-T (KInetic aNALysis of reaction mechanics with Transport) based on the work of Cao et al. (2016) is employed to calculate the ~~recurrence~~ oscillation of ODEs, where oscillation does not necessarily imply perfect periodic behavior. Finding experimental evidence for ~~recurrence~~ chemical oscillations is expected to be very difficult, since meteorological effects such as wind transport conceal the ~~recurrent~~ oscillating properties. It may be nearly impossible to disentangle the ozone regeneration via wind transport from the vertical diffusion or from the $\mathrm{NO_2}$ photolysis. Nevertheless, the present model provides important insight into the ~~recurrence~~ oscillations of ODEs.

2 Model and numerical solver

In the present study, the former model of Cao et al. (2016) is extended and optimized in order to account for the ~~recurrence~~ oscillations of ODEs. For simplicity, constant temperature, zero vertical velocity and prescribed turbulent diffusion coefficients (cf. section 2.1.1) are assumed.

2.1 The differential equations

The chemical reaction system is described by the temporal and spatial variations of the species concentrations $c_{i,j}$, where $i = 1,\ldots,N$ is the species number and $j = 1,\ldots,M$ denotes the discretized grid number. Since the gas temperature is assumed to be constant, density changes of the gas phase are neglected. Using central differences for the discretization of the physical space, the governing equations for the species concentrations yield (Cao et al., 2016)

$$\frac{\mathrm{d}c_{i,j}}{\mathrm{d}t} = \underbrace{P_{i,j} - D_{i,j}}_{\substack{\text{chemical production}\\ \text{and consumption}}} + \underbrace{\frac{F_{i,j+1/2} - F_{i,j-1/2}}{h_j}}_{\text{diffusion}} + \underbrace{F_{\mathrm{d},i,j}}_{\text{dry deposition}} + \underbrace{k_\mathrm{a}(c_{i,j} - c_{\mathrm{a,eq}})}_{\text{aerosol mass transfer}}. \tag{2}$$

The dry deposition term is assumed to be non-zero only in the lowest grid cell, $j = 1$. The diffusion flux is given by

$$F_{i,j+1/2} = \left(k_{j+1/2} + D\right) \frac{c_{i,j+1} - c_{i,j}}{z_{j+1} - z_j}, \tag{3}$$

where the molecular diffusion coefficient $D = 0.2\ \mathrm{cm^2\,s^{-1}}$ and $F_{i,1/2} = 0$. In the one-dimensional grid under consideration, z_j denotes the position of the center of grid cell j, and h_j is the size of the grid cell j, $h_j = (z_{j+1} - z_{j-1})/2$. The turbulent diffusion coefficient at the interface of the grid cell $j + 1/2$ is denoted by $k_{j+1/2}$, cf. Eq. (3).

The evaluation of the turbulent diffusion coefficient needs special attention since its parameterization depends on the meteorological conditions, which will be given in the next subsection. Moreover, the gas-phase reactions and the aerosol treatment will be provided.

2.1.1 Turbulent diffusion coefficient

The height-dependent turbulent diffusion coefficient $k(z)$ is chosen similar as by Cao et al. (2016), using the first-order parameterization of Pielke and Mahrer (1975) for neutrally stratified boundary layers using the following empirical polynomial equation:

$$k(z) = \begin{cases} \dfrac{z}{L_0} k_0 & \text{if } z < L_0 \\ k_\mathrm{f} + \left(\dfrac{L-z}{L-L_0}\right)^2 \left[k_0 - k_\mathrm{f} + (z - L_0)\left(\dfrac{k_0}{L_0} + 2\dfrac{k_0 - k_\mathrm{f}}{L - L_0}\right)\right] & \text{if } L_0 \leq z < L \\ k_{\mathrm{t,inv}} & \text{if } L \leq z \leq L + L_{\mathrm{inv}} \\ k_\mathrm{f} & \text{if } L + L_{\mathrm{inv}} < z \end{cases} \tag{4}$$

The discretized turbulent diffusion coefficients are determined by $k_{j+1/2} = k\left(z_j + h_j/2\right)$. In equation (4), L is the boundary layer height up to the inversion layer. L_0 is the height of the surface layer which is assumed to be 10% of the boundary layer height (Stull, 1988). $k_0 = \kappa u_* L_0$ is the turbulent diffusion coefficient at the top of the surface layer. $\kappa = 0.41$ is the von Karman constant and $u_* = \kappa v / \ln(L_0/z_0)$ the friction velocity, where v is the reference wind speed at the top of the surface layer, which is assumed to be $v = 5\,\mathrm{m\,s^{-1}}$. The surface roughness length for snow/ice, z_0, is taken as $z_0 = 10^{-5}$ m (Huff and Abbatt, 2000, 2002).

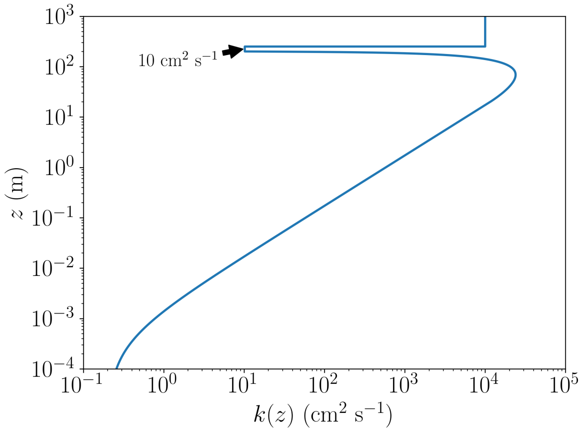

Figure 1. The turbulent diffusion coefficient $k(z)$ as a function of altitude z for a boundary layer height of 200 m, a wind speed of $5\,\mathrm{m\,s^{-1}}$, $k_\mathrm{f} = 1\ \mathrm{m^2\,s^{-1}}$ and the inversion layer thickness of 50 m

A relation of L and the vertical potential temperature gradient is described by Neff et al. (2008) as:

$$L = (1.2u_*)\,(fN_{\mathrm{B}})^{-0.5}, \tag{5}$$

with the Brunt-Vaisala frequency

$$N_{\mathrm{B}} = \sqrt{\frac{g}{T}\frac{\mathrm{d}\Theta}{\mathrm{d}z}}. \tag{6}$$

The Coriolis parameter $f = 1.458 \times 10^{-4}\ \mathrm{s}^{-1}$ is calculated at the north pole. $g = 9.81\ \mathrm{m\,s}^{-2}$ is the gravitational acceleration. For the two different temperatures of $T = 258$ K and 238 K under consideration, a vertical potential temperature gradient of $\mathrm{d}\Theta/\mathrm{d}z = 6.4 \times 10^{-4}\ \mathrm{K\,m}^{-1}$ and $5.9 \times 10^{-4}\ \mathrm{K\,m}^{-1}$, respectively, is considered both of which correspond to the boundary layer height of $L = 200$ m employed in this work. An inversion layer of thickness L_{inv} is inserted at the top of the boundary layer, where the turbulent diffusion coefficient $k_{\mathrm{t,inv}}$ is assumed to be constant and treated as a free parameter.

The turbulent diffusion coefficient k_{f} in the free troposphere is assumed to be constant throughout the free troposphere. The reported values for turbulence in the free troposphere vary strongly between 0.01 and 100 $\mathrm{m}^2\,\mathrm{s}^{-1}$ (Wilson, 2004; Ueda et al., 2012).

An example of the resulting profile of the turbulent diffusion coefficient as defined through Eq. (4) is displayed in Fig. 1 where the boundary layer height is 200 m, the wind speed is $5\ \mathrm{m\,s}^{-1}$ and inversion layer thickness is 50 m. The values of $k_{\mathrm{t,inv}}$ and k_{f} are 10 $\mathrm{cm}^2\,\mathrm{s}^{-1}$ and 10 $\mathrm{m}^2\,\mathrm{s}^{-1}$, respectively; these values refer to the base case discussed further below. The vertical diffusion between the boundary layer and the free troposphere is limited by a significantly reduced value of $k(z)$.

2.1.2 Chemical reaction mechanism

The chemical reaction mechanism is based on the bromine/nitrogen/chlorine mechanism of Cao et al. (2014) with a few modifications to the gas phase mechanism and more complex aerosol modeling. Both modifications are described below. The resulting mechanism encompasses 50 gas-phase species with 175 gas-phase reactions and 20 aerosol-phase species with 50 aerosol-phase reactions. The full reaction mechanism is described in Tables A1-A5 of Appendix A.

For simplicity, the gas-phase concentration of $\mathrm{NO_y}$ is assumed to be a conserved quantity in the model. In reality, this is only partly true, since $\mathrm{HNO_3}$ tends to dissolve quickly in aerosols and can become inert, acting as a strong sink. This sink may be compensated by the emissions of $\mathrm{NO_x}$ from the snow, which was discussed in the introduction. The modeling of these processes would add more uncertainties since the emissions and depositions of the various reactive nitrogen species need to be parameterized. Also, in order to correctly model the deposition of $\mathrm{HNO_3}$, detailed aerosol chemistry is needed, which would increase the simulation time. Therefore, gas-phase $\mathrm{NO_y}$ is assumed to be conserved in the present model, i.e. no emission and deposition of $\mathrm{NO_y}$ and heterogenous reactions involving $\mathrm{NO_y}$ are formulated to conserve gas-phase $\mathrm{NO_y}$.

2.1.3 Treatment of the aerosols

The aerosols are modeled as described by Sander (1999) and they are assumed to be liquid. A mono-disperse aerosol with a radius $r = 1$ µm is assumed. The pH value is fixed to 5. Simulations found little pH dependence of the oscillation periods for pH values below 7. The aerosols are assumed not to undergo any dynamics except for turbulent diffusion, and the aerosol volume fraction in air is fixed at a value of $\phi = 10^{-11}\ \mathrm{m}^3_{\mathrm{aq}}\mathrm{m}^{-3}_{\mathrm{air}}$. Dry and wet depositions of aerosols as well as productions and emissions of aerosols are neglected. Exploratory simulations show that adding an aerosol deposition velocity in the range of 0.01-0.1 $\mathrm{cm\,s^{-1}}$ (Wu et al., 2018) increases the oscillation period by 10%-40% and decreases the bromide concentration during the build-up phases by approximately 10%-30%. However, if a sink for aerosol is introduced, sources for aerosols such as frost flowers or blowing snow should also be implemented. The produced/emitted aerosols are likely to have non-zero bromide content, providing a source for bromine species and potentially countering the effects of the dry and wet depositions. Therefore, for simplicity and in order to avoid the uncertainties in the production and emission mechanisms of aerosols, both sources and sinks of aerosols are neglected. The aqueous reaction constants, acid/base equilibria, ~~uptake~~ mass accommodation coefficients, and ~~Henry coefficients~~ Henry's law constants are taken from the box model CAABA/MECCA, version 3.8l (Sander et al., 2011), and they are summarized as follows.

The transfer rate for a gas species is given by

$$\left(\frac{\mathrm{d}c_{i,j,\mathrm{g}}}{\mathrm{d}t}\right)_{\mathrm{transfer}} = k_{\mathrm{t}}\left(\phi c_{i,j,\mathrm{g}} - \frac{c_{i,j,\mathrm{a}}}{H_i(T)}\right) \tag{7}$$

with the species- and temperature-dependent non-dimensional Henry's law constants $H_i(T)$, cf. Eq. (12). The gas and the aerosol concentrations $c_{i,j,\mathrm{g}}$ and $c_{i,j,\mathrm{a}}$, respectively, are in $\mathrm{molec\,cm^{-3}}$. The transfer coefficient k_{t} is calculated as

$$k_{\mathrm{t}} = \frac{k_{\mathrm{in}}}{\phi} = \frac{1}{\phi}\left(k_{\mathrm{diff}}^{-1} + k_{\mathrm{coll}}^{-1}\right)^{-1}. \tag{8}$$

The diffusion limit for gas-aerosol mass transfer k_{diff} is

$$k_{\mathrm{diff}} = \frac{v_{\mathrm{th}}\lambda\phi}{r^2} = \frac{v_{\mathrm{th}}\lambda A}{3r}, \tag{9}$$

where $\lambda = 2.28 \cdot 10^{-5}\ \frac{T}{p}\ \mathrm{Pa\,m\,K^{-1}}$ (Pruppacher et al., 1998) is the mean free path with pressure p. In Eq. (9), use of

$$r = \frac{3\phi}{A} \tag{10}$$

has been made, including the assumption of a mono-disperse aerosol with radius r, the aerosol volume fraction ϕ, and aerosol surface area concentration A. The collision term k_{coll}, cf. Eq. (8), for the gas-aerosol mass transfer is

$$k_{\mathrm{coll}} = \frac{3v_{\mathrm{th}}\alpha_i\phi}{4r} = \frac{\alpha_i v_{\mathrm{th}} A}{4}. \tag{11}$$

Here, α_i is the species-dependent mass accommodation coefficient.

The temperature dependence of the Henry's law constants of species i is calculated by

$$H_i(T) = H_i(T_0)\frac{T}{T_0}\exp\left[T_{H_i}\left(\frac{1}{T} - \frac{1}{T_0}\right)\right], \tag{12}$$

where $T_{H_i} = -\Delta_{\mathrm{sol}}H/\mathrm{R}$ is the enthalpy of dissolution divided by the universal gas constant R, and the mass accommodation coefficients are obtained from

$$\alpha_i(T) = \left\{1 + (1/\alpha(T_0) - 1)\exp\left[-T_{\alpha_{\mathrm{i}}}\left(\frac{1}{T} - \frac{1}{T_0}\right)\right]\right\}^{-1}, \tag{13}$$

where $T_0 = 298.15$ K. The values for the Henry's law constants and the mass accommodation coefficients are given in Table A3. The transfer rate for the corresponding aerosol species from the aerosol phase to the gas phase has the opposite sign.

2.2 Numerical aspects of the model

2.2.1 The numerical grid

A sketch of the numerical grid is displayed in Fig. 2. The computational domain extends 1,000 m in vertical direction and the number of exemplary grid cells is $M = 32$. Different numerical grid resolutions were used to assure grid independence of the numerical solution of the equations, see discussion in the results' section. The lowest grid cell at the surface is $z_1 = 10^{-4}$ m. The lowest $M/2+1$ grid cells are distributed logarithmically up to 100 m of the computational domain, cf. Fig. 3. In an intermediate regime, it is assured that at least one grid cell resides inside the inversion layer and that there are grid cells on the borders of the inversion layer to ensure a proper resolution the inversion layer. The remaining grid cells are distributed linearly up to the upper boundary at $1,000$ m. The numerical grid is displayed in Fig. 3 where the first 17 grid cells are logarithmically distributed, followed by five grid cells to resolve the inversion layer. The remaining ten grid cells are distributed linearly. A black vertical line marks transition from the logarithmic to the linear regime, and the grey area marks the inversion layer.
The choice of switching from the logarithmic to the linear grid at 100 m and at 200 m was tested, and the numerical results were not affected. The boundary layer height L is 200 m in the present simulations, cf. Tab. 1, so that the choice of 100 m for the switch of the numerical grid is chosen in order not to interfere with the height of the boundary layer.
Most simulations were conducted with 16 grid cells, simulations with 32, 48, and 64 grid cells were also performed to assure

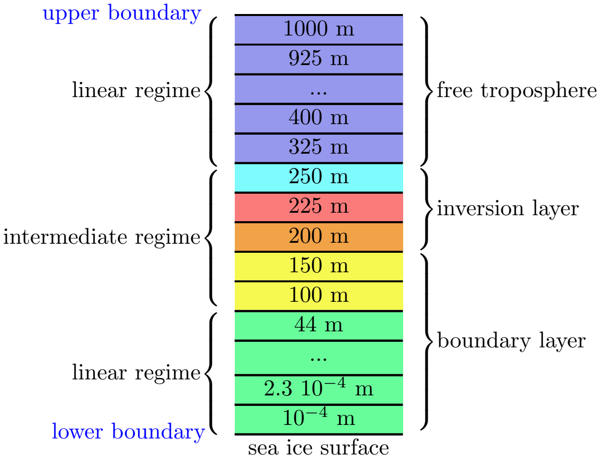

Figure 2. One-dimensional grid. Numbers are at the center of every numerical grid cell. Red grid cell resides inside the inversion layer. The grid cells at 200 m and 250 m are centered at the interface of the inversion layer

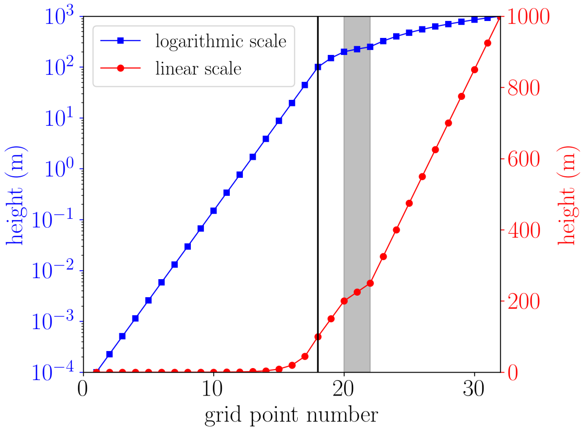

Figure 3. Numerical grid with M = 32 grid cells (cf. Fig. 2) plotted on a logarithmic scale (squares) and a linear scale (filled circles). The grey area shows the inversion layer

grid independence of the results. In subsection 3.1.1 it is shown that 16 grid cells are sufficient to calculate the ~~recurrence~~ oscillation periods with errors smaller than one percent. In total, several hundred simulations for 200 real-time days were conducted in order to study the model parameters (see Tab. 1), so that the small grid size is convenient to minimize the total runtime of the simulations.

2.2.2 The numerical solver

In order to study the ~~recurrence~~ oscillation of ODEs for different parameter settings, the typical realtime of about 20 days that was used by Cao et al. (2016) is extended to 200 days in the present study. Scanning the parameter space shown in Tab. 1 requires hundreds of simulations, so that at first, an optimization of the KINAL-T code (Cao et al., 2016) was conducted.

Cao et al. (2016) decoupled the diffusion terms, the chemical reactions were solved in an implicit way using the Rosenbrock 4 solver (Gottwald and Wanner, 1981), and diffusion was treated in an explicit way. The heterogenous reactions were solved as part of the chemistry equations.

This procedure has some disadvantages. Since the grid is logarithmic for $z < 100\ \mathrm{m}$, the cell size h_j is $h_j \propto z$ in that regime. The diffusion time scale $t_\mathrm{d} = h_j^2/k(z) \propto z$ becomes very small for small z, which limits the time steps to the order of milliseconds if an explicit solver is chosen. Also, the heterogenous reactions on the ice surface destroy all HOBr in the lowest cell in some tens to hundreds of microseconds, depending on the size of the grid cells, so that the heterogenous reactions have to be solved as part of the diffusion equations in order to allow mixing of upper layers into the lowest cell during a single time step. Even then, however, time steps smaller than seconds are needed due to the strong coupling of the diffusion and the chemical reactions caused by the heterogenous reactions, if the equations are solved completely decoupled. Thus, in the present code, the diffusion equations and the chemical reactions are solved fully coupled with the implicit, A-stable Rosenbrock 4 solver, resulting in a quite large Jacobian matrix of dimension $n = N \times M$, i.e. the product of the number of species, N, and grid cells, M. The time steps are chosen adaptively, where most time steps are of the order of minutes.

The base parameter settings as well as the range in which they are varied are shown in Tab. 1. The values for the temperature T, pressure p, boundary layer height L, aerosol volume fraction ϕ, and solar zenith angle are chosen following Cao et al. (2016).

2.3 Base parameters

An inversion layer thickness of $L_{\mathrm{inv}} = 50\ \mathrm{m}$ is chosen. Palo et al. (2017) found values ranging from $20\ \mathrm{m}$ to $1000\ \mathrm{m}$, with a mean of $337\ \mathrm{m}$. In the study of Neff et al. (2008), a shallow boundary layer with $L \approx 165\ \mathrm{m}$ and an inversion layer thickness of $L_{\mathrm{inv}} \approx 70\ \mathrm{m}$ were found. In the present study it was found that a larger inversion layer thickness $\mathrm{L_{inv}}$ can be compensated (i.e. leads to asimilar behaviour in the boundary layer) by choosing a correspondingly larger turbulent diffusion coefficient $k_{\mathrm{t,inv}}$, with a nearly linear relationship $k_{\mathrm{t,inv}} \sim L_{\mathrm{inv}}^{1.2}$. The base parameter settings for the diffusion coefficient in the inversion layer has been determined by searching for the oscillating solutions of the numerical simulations.

Table 1. Parameter definition for the base case settings and variations used in the parameter study

Parameter	Symbol	Unit	Base Case	Values
Boundary layer height	L	m	200	
Inversion layer thickness	L_{inv}	m	50	
Temperature	T	K	258	238, 258
Pressure	p	Pa	101,325	
Turbulent diffusion coefficient in the inversion layer	$k_{\mathrm{t,inv}}$	$\mathrm{cm^2\,s^{-1}}$	10	$0 \dots 60$
Turbulent diffusion coefficient in the free troposphere	k_{f}	$\mathrm{m^2\,s^{-1}}$	10	$0.1,\ 1,\ 10$
Aerosol volume fraction	ϕ	$\mathrm{m^3_{aq} m^{-3}_{air}}$	10^{-11}	$10^{-12} \dots 3 \cdot 10^{-10}$
Total concentration of all nitrogen oxides	$[\mathrm{NO_y}]$	$\mathrm{pmol\,mol^{-1}}$	50	$0 \dots 300$
Solar zenith angle	SZA	°	80	$70 \dots 90$
Chlorine chemistry			active	active, deactivated

The dependence of the ~~recurrence~~ oscillation period on $[\mathrm{NO_y}]$ was investigated for two different temperatures of 258 K and 238 K and with the chlorine mechanism turned on and off. The diffusion coefficients in the free troposphere k_{f} were varied along with $k_{\mathrm{t,inv}}$. For sake of simplicity, the SZA was assumed to be constant during a simulation. The base setting of a constant 80° corresponds to the conditions on the north pole in mid-April.

2.4 Initial and boundary conditions

2.4.1 Initial conditions

The initial species concentrations are shown in Tab. 2. Initial concentrations of organic species are chosen to be consistent with the study of Hov et al. (1989). Nitrogen-contraining species concentrations are varied as shown in Tab. 2. Emissions of nitrogen from the snow are not considered, instead $\mathrm{NO_y}$ is a conserved quantity in the model. Initial concentrations of bromine are zero in both the free troposphere and in the inversion layer. Starting with non-zero gas-phase bromine concentrations means that the initialization of the bromine explosion is not simulated, the simulation starts during the build-up stage of the bromine explosion.

Table 2. Initial trace-gas concentrations

Species	Concentration
O_3	40 $\mathrm{nmol\,mol^{-1}}$
Br_2	0.3 $\mathrm{pmol\,mol^{-1}}$
HBr	0.01 $\mathrm{pmol\,mol^{-1}}$
CO	160 $\mathrm{nmol\,mol^{-1}}$
CH_4	2 $\mathrm{\mu mol\,mol^{-1}}$
C_2H_6	3.5 $\mathrm{nmol\,mol^{-1}}$
C_2H_4	400 $\mathrm{pmol\,mol^{-1}}$
C_2H_2	1 $\mathrm{nmol\,mol^{-1}}$
C_3H_8	2.35 $\mathrm{nmol\,mol^{-1}}$
CH_3CHO	150 $\mathrm{pmol\,mol^{-1}}$
HCHO	0.5 $\mathrm{pmol\,mol^{-1}}$
NO	$0.05\ [\mathrm{NO_y}]$
NO_2	$0.02\ [\mathrm{NO_y}]$
HNO_3	$0.01\ [\mathrm{NO_y}]$
PAN	$0.92\ [\mathrm{NO_y}]$
Br^-	0.05 $\mathrm{mol\,l^{-1}}$
Cl^-	30 $\mathrm{mol\,l^{-1}}$

2.4.2 Boundary conditions and heterogenous reactions at the ice surface

The upper boundary of the calculation domain at 1,000 m is a Dirichlet boundary where all species concentrations are set to the initial concentrations given in Tab. 2. The presumed large diffusion coefficient of $10\ \mathrm{m^2\,s^{-1}}$ ensures that the free troposphere is nudged to the initial concentrations on a time scale of hours.

For the boundary at the ice surface, zero flux is assumed. The exchange with the snow/ice surface is modeled via the heterogenous reactions listed in Appendix A in Tab. A5. An example of the general treatment of a representative heterogenous reaction is

$$\mathrm{HOBr} + \mathrm{H}^+ + \mathrm{Br}^- \overset{\mathrm{aq}}{\rightarrow} \mathrm{Br}_2 + \mathrm{H}_2\mathrm{O}, \tag{R24}$$

which is represented as dry deposition reaction that occurs only in the lowest computational cell. The ice/snowpack itself is not modeled, instead, it is assumed that the salt content is infinite so that heterogenous reactions on the ice surface are effectively treated as

$$\mathrm{HOBr} \rightarrow \mathrm{Br}_2. \tag{R25}$$

The first-order reaction constants are parameterized by

$$k = \frac{v_\mathrm{d}}{h_1}, \tag{14}$$

where the thickness of the lowest layer is h_1, cf. Eq. (3), and the dry deposition velocity is v_d. The dry deposition velocity is modeled following the work of Seinfeld and Pandis (2006) as the inverse of the sum of three resistances R_a, R_b, and R_c

$$v_\mathrm{d} = \frac{1}{R_a + R_b + R_c} \tag{15}$$

described as follows. First, the gas is transported from the center of the lowest grid cell z_1 to the top of the interfacial layer at the surface roughness length z_0 by turbulent diffusion, which leads to the aero-dynamic resistance

$$R_a = \int\limits_{z_0}^{z_1} (K(z) + D)^{-1}\, dz = \int\limits_{z_0}^{L_1} (\kappa u_* z + D)^{-1}\, dz = \ln\left(\frac{\kappa u_* z_1 + D}{\kappa u_* z_0 + D}\right) / (\kappa u_*). \tag{16}$$

Then, the gas must be transported through the interfacial layer via molecular diffusion resulting in the quasi-laminar resistance

$$R_b = z_0 / D. \tag{17}$$

Finally, the surface resistance is estimated by

$$R_c = 4 / (v_\mathrm{th} \gamma) \tag{18}$$

with the thermal velocity $v_\mathrm{th} = \sqrt{8\mathrm{R}T/(\pi M_i)}$. M_i is the molar mass of the gas species undergoing the heterogenous reaction and R is the universal gas constant. For the range of γ in the present study (see Tab. A5), the aero-dynamic resistance is the largest out of the three resistances. Due to the small size of the lowest grid cell, the heterogenous reactions are very fast and their speed is actually limited by the turbulent diffusion of the depositing species from the upper grid cells to the lowest grid cell. The dry depositions of HCl and HBr provide sinks that prevent halogen concentrations to increase infinitely.

3 Results and discussion

In this section, the mechanism of ~~recurrences~~ oscillations of ozone depletion events as well as their possible termination are investigated. First, the reasons for ~~recurrence~~ oscillation to occur is discussed and the ~~recurrence~~ oscillation period is defined. Second, a closed system with aerosols as the only surface for the recycling of bromine is investigated. Moreover, a comparison to an earlier study (Evans et al., 2003) is presented. Finally, parameter studies are performed on the base parameters presented in Tab. 1 in order to investigate the variation of the ~~recurrence~~ oscillation period.

3.1 ~~Recurrence~~ Oscillation and termination of ODEs

This section concerns the study of ~~recurrence~~ oscillation and termination of ODEs.

3.1.1 ~~Recurrence~~ Oscillation of ODEs

The ~~recurrence~~ oscillation period of an ODE is defined as the average time difference of two consecutive ozone maxima. An ozone maximum is only accepted, if the difference in mixing ratio to the preceding ozone minimum is at least 2 $\mathrm{nmol\,mol^{-1}}$, which is used as a threshold value to distinguish between oscillations and noise.

Figure 4 shows the ~~recurrence~~ oscillation of ODEs for the base setting of the present model, cf. Tab. 1, for 16, 32, 48, and 64 grid cells. The differences between the different grid sizes are small, the average ~~recurrence~~ oscillation period varies by less than 1%, and thus, 16 grid cells are sufficient to properly represent the major features of the ODEs and their ~~recurrence~~ oscillation.

~~Recurrence~~ Oscillation of ODEs may be explained as follows: After the occurrence of an ODE, there is not enough ozone left

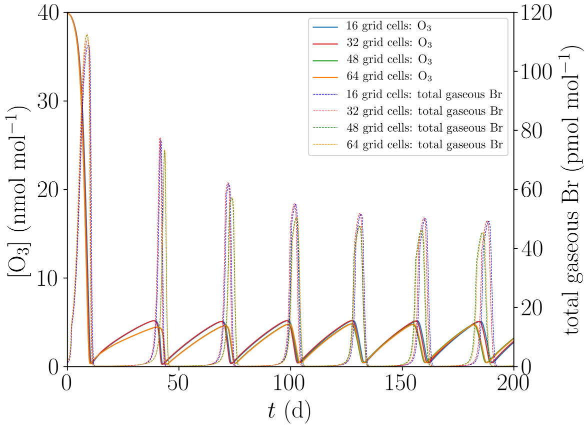

Figure 4. Evolution of O_3 and total gaseous bromine mixing ratios for four different numbers of grid cells of M = 16, 32, 48, and 64

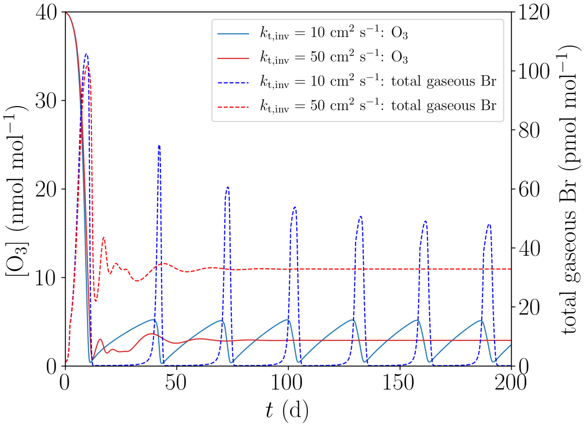

Figure 5. Evolution of O_3 and total gaseous bromine mixing ratios for $k_{\mathrm{t,inv}} = 10$ and 50 $\mathrm{cm^2\,s^{-1}}$

to sustain the BrO concentration through reaction (R1), causing bromine to be converted into HBr, which deposits onto the ice/snow surface or onto aerosols and then turns into bromide, cf. reaction (R12). The now inactive bromide needs to undergo another bromine explosion, see reaction (R9), in order to become reactive again, which does not occur in the absence of ozone. This allows the ozone in the boundary layer to replenish via the photolysis of $\mathrm{NO_2}$ or by diffusion from the free troposphere through the inversion layer. Once the ozone mixing ratio is large enough, α, defined in equation (1), becomes larger than unity, allowing for another bromine explosion. Ozone and reactive bromine now replenish simultaneously where the formation of reactive bromine is becoming faster, increasing the ozone mixing ratio. Once the BrO mixing ratio has reached approximately $10\ \mathrm{pmol\,mol^{-1}}$, the ozone destruction by bromine becomes larger than the ozone regeneration. Then, another ODE occurs and the cycle repeats. Another sink of bromine in the model is the diffusion of part of the bromine species through the inversion layer, since bromine may leave the computational domain through the upper boundary, where the Dirichlet boundary conditions enforce the bromine concentrations to zero.

However, ~~recurrences~~ oscillations do not occur for all parameter settings as can be seen in Fig. 5 where $k_{\mathrm{t,inv}}$ is increased from 10 to 50 $\mathrm{cm^2\ s^{-1}}$. For $k_{\mathrm{t,inv}} = 50\ \mathrm{cm^2\,s^{-1}}$, after the initial ODE and ~~a recurrence~~ an oscillation with a reduced value of $[\mathrm{O_3}]$, no further ~~recurrence~~ oscillation occurs. Instead, the reactive bromine and ozone establish a chemical equilibrium, and no further ~~recurrence~~ oscillation is observed, i.e. it terminates. The termination of ~~a recurrence~~ an oscillation will be further discussed next.

3.1.2 Termination of ODE ~~recurrences~~ oscillations

In order to study the termination of ODE ~~recurrence~~ oscillations, the initial concentration of $[\mathrm{NOy}]$ is reduced to zero compared to the base case, cf. Tab. 1. Moreover, the turbulent diffusion coefficient in the inversion layer is increased from the base parameter of $10\ \mathrm{cm^2\,s^{-1}}$ displayed in Fig. 6a to $20\ \mathrm{cm^2\,s^{-1}}$ shown in Fig. 6b.

If the ozone recovery rate during an ODE is too large compared to the amount of reactive bromine left for $\alpha < 1$ in Eq. (1), the remaining bromine is not sufficient to fully destroy the ozone, leading to shorter ~~recurrence~~ oscillation periods and lower levels of ozone peak concentrations as seen in Fig. 6b: Bromine levels drop until ozone can regenerate, the regeneration of ozone reactivates a part of the inactive bromine, which in turn depletes ozone until the ozone and the bromine concentrations achieve an equilibrium, and thus, only two ~~recurrences~~ oscillations occur.

The termination may occur directly after the initial ODE as shown in Fig. 5 or after a few ~~recurrences~~ oscillations as a dampened oscillation, see Fig. 6b. The initial ODE typically releases the largest amount of bromine because the initial ozone mixing ratio of $40\ \mathrm{nmol\,mol^{-1}}$ is much larger than the $10\ \mathrm{nmol\,mol^{-1}}$ mixing ratio of the ~~recurrences~~ oscillations. The total amount of bromine in boundary layer tends to drop after the initial ODE, mostly due to the dry deposition of HBr and to a lesser extent due to diffusion of bromine into the free troposphere.

This reduction in the bromine is the main dampening process. The smaller bromine mixing ratio may not be sufficient to destroy the remaining ozone once $\alpha < 1$ and can thus result in a termination at a later ~~recurrence~~ oscillation instead of the termination after the first ODE.

Both a large ozone regeneration rate and a higher Br release ~~for each $\mathrm{nmol\,mol^{-1}}$ of ozone reduce the drop in bromine for the~~

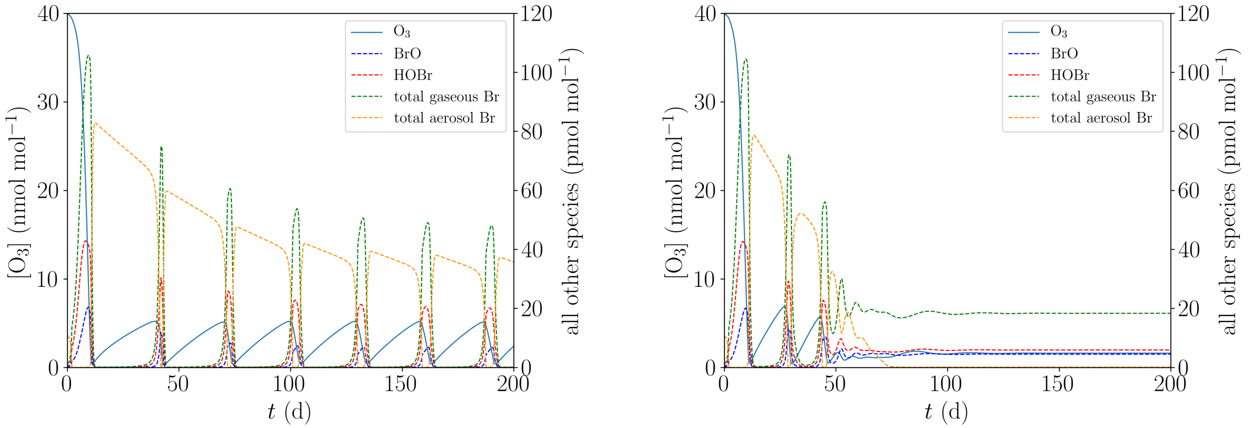

(a) $k_{\mathrm{t,inv}} = 10\,\mathrm{cm}^2\,\mathrm{s}^{-1}$

(b) $k_{\mathrm{t,inv}} = 20\,\mathrm{cm}^2\,\mathrm{s}^{-1}$

Figure 6. ~~Recurrence~~ Oscillation and termination of ODEs for different values of $k_{t,\mathrm{inv}}$

~~recurrences or can even result in an increase in the bromine concentration as shown in Fig. 7 where NO_2 is an ozone source leading to an increase of gaseous bromine after the first three recurrences.~~ efficiency reduce the drop in the total bromine mixing ratio in the gas and aerosol phase that occurs between successive oscillations. If the bromine release or ozone regeneration rate are sufficiently large, the bromine mixing ratio may increase for successive oscillations, as shown in Fig. 7. The additional ozone production due to an increased initial NO_y mixing ratio shortens the oscillation period and therefore limits the bromine losses occuring between successive bromine explosions.

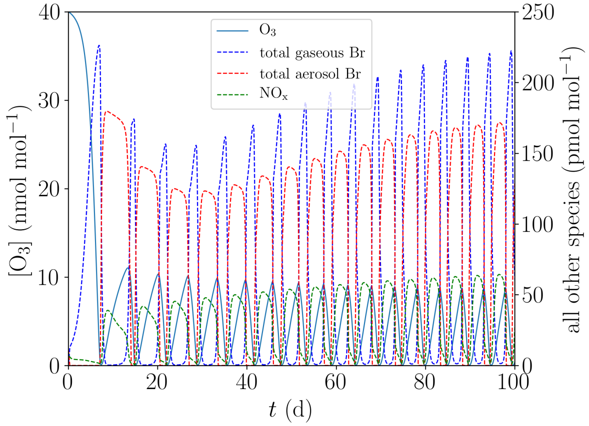

Figure 7. Evolution of O_3, NO_x, and total gaseous and aerosol bromine mixing ratios for the base case with $[NO_y] = 150\ \mathrm{pmol\,mol^{-1}}$

Termination may not occur at all during 200 days. Typically, the ~~recurrence~~ oscillation period becomes constant after the first few ~~recurrences~~ oscillations. The first ~~recurrences~~ oscillations are affected by the initial value of 40 $\mathrm{nmol\,mol^{-1}}$ for the ozone concentration. The fate of most of the bromine after an ODE is stored in aerosols as bromide. While the initial bromine explosion is mostly driven by heterogenous reactions on the ice/snow surface, the bromine explosions of the ~~recurrences~~ oscillations are driven by heterogenous reactions on the aerosols, which now hold a significant amount of bromide. After a few ~~recurrences~~ oscillations, the bromine deposited on the ice surface or diffused to the free troposphere between each ~~recurrence~~ oscillation becomes equal to the bromine released from the ice surface during each ~~recurrence~~ oscillation, resulting in a constant ~~recurrence~~ oscillation period thereafter.

In order to observe fast ~~recurrences~~ oscillations, an $\mathrm{O_3}$ recovery rate of about $\mathrm{nmol\,mol^{-1}}$ per day is required. However, as noted above, for an ODE to terminate properly, the $\mathrm{O_3}$ recovery rate during the termination of an ODE may not be too large. Figures 5 and 6 show a termination due to a sufficiently large $k_{\mathrm{t,inv}}$.

The effect of a strong inversion layer as well as the ozone formation via nitrogen ~~oxygen~~ oxides on ODEs will be studied in subsection 3.4. The next subsection concerns different ways of initialization of ODEs.

3.2 Initialization of an ODE with only aerosols

So far, the ODEs were initiated through the assumption of a fixed value of 0.3 $\mathrm{pmol\,mol^{-1}}$ $\mathrm{Br_x}$ inside the boundary layer (cf. Tab. 2). In the present subsection, another mechanism for the initiation is studied, where aerosols are used to initiate the ODEs. Five assumptions are changed with regard to the base case:

- The concentration of $\mathrm{Br^-}$ was set to $0.8\ \mathrm{mol\,l^{-1}}$, corresponding to a mixing ratio of 160 $\mathrm{pmol\,mol^{-1}}$ in the gas phase, which is different from the base setting of $0.05\ \mathrm{mol\,l^{-1}}$ (equivalent to 10 $\mathrm{pmol\,mol^{-1}}$) shown in Tab. 2.
- The turbulent diffusion coefficient in the inversion layer is set to zero.
- The initial concentration of gas phase bromine is set to zero.
- All heterogenous reactions on the ice/snow surface are turned off.
- The $[\mathrm{NO_y}]$ is increased from 50 to $100\ \mathrm{pmol\,mol^{-1}}$.

The large concentration of $\mathrm{Br^-}$ could be caused by a blowing snow event. In this simulation, the main source of the first reactive bromine is via the heterogenous reaction of ozone, see reaction (R19).

As a result of the different settings, the total bromine concentration is conserved during the simulation. Furthermore, the boundary layer is a closed system for this simulation. The results are shown in Fig. 8.

After one hour, already $0.1\ \mathrm{pmol\,mol^{-1}}$ of reactive bromine is reactivated, which is sufficient for the bromine explosion on aerosols to become the dominant reactivation mechanism. Also, $\mathrm{N_2O_5}$ can activate the first bromine by producing $\mathrm{BrNO_2}$. Reactive chlorine can also activate the first bromine, however more slowly. $0.3\ \mathrm{pmol\,mol^{-1}}$ of reactive chlorine takes several days to produce an initial seed of $0.1\ \mathrm{pmol\,mol^{-1}}$ reactive bromine. Only in the first time steps, bromine is reactivated by the

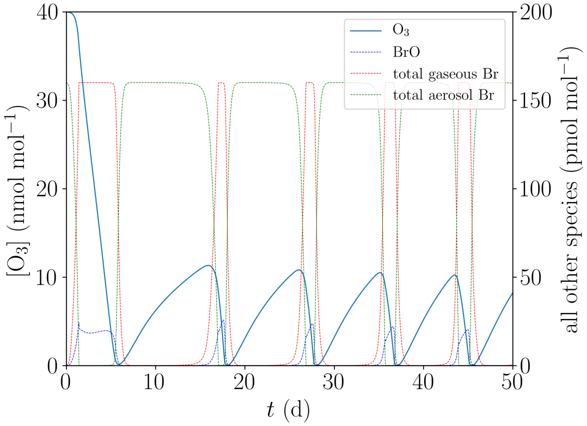

Figure 8. Simulation neglecting the snow pack and the exchange between the boundary and the inversion layers

very slow release of Br via HOCl, see reaction (R18).

After that, a regular bromine explosion occurs, albeit ~~starting at~~ restarting from very low concentrations of $10^{-4}\,\mathrm{pmol\,mol^{-1}}$ $[\mathrm{Br_x}]$. The initialization via reactivation of bromine on aerosols is much faster than reactivation via the ice surface, since ~~the aerosols are not diffusion limited~~ the multiphase reactions involving aerosols are not diffuson limited. All other ~~simulations~~ episodes start ~~with~~ from about 30 $\mathrm{pmol\,mol^{-1}}$ of ~~bromine~~ bromide in the aerosol phase, which is why they have longer induction stages of about 10 days compared to a few hours for this simulation.

It is of particular interest, that oscillations occur without any external sources and sinks, such as dry depositions, emissions or heterogenous reactions on the ice/snow surface. The density of each chemical element in the gas plus aerosol phase is conserved in this simulation, with hydrogen being the only exception due to the constant pH value of the aerosols. Due to the second law of thermodynamics, only reaction intermediates may oscillate. As an example, $\mathrm{CO_2}$ is a permanent sink for other organic species in this simulation. It is expected for the oscillations to terminate after a sufficient amount of reactive organics are converted to non-reactive organics.

3.3 Comparison to studies in the literature

The most relevant research in the area of oscillating ODEs was performed by Evans et al. (2003) which is used to validate the present model. Similar to the aerosol-only simulation of the previous subsection, aerosols are the only source and sink for bromine in the system studied by Evans et al. (2003).

A comparison between the model of Evans et al. (2003) and the present study is displayed in Fig. 9, where Fig. 9a is for a low NOx emission and an initial bromide mole fraction of $43\,\mathrm{pmol\,mol^{-1}}$ and Fig. 9b for elevated NOx emission by 35% and an initial bromide mole fraction of $60\,\mathrm{pmol\,mol^{-1}}$.

Differences in the model and in the conditions as follows.

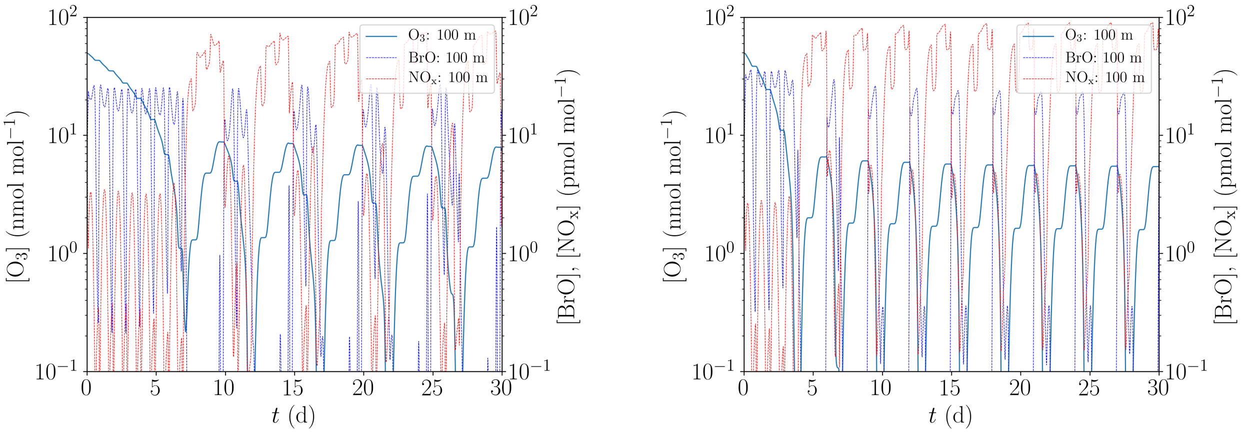

(a) Low NO_x emission and initial bromide mixing ratio of 43 $\mathrm{pmol\,mol^{-1}}$

(b) Increased NO_x emission by 35% and initial bromide mixing ratio of 60 $\mathrm{pmol\,mol^{-1}}$

Figure 9. Simulation of the ~~recurrences~~ oscillations of ODEs for the conditions of Evans et al. (2003)

- The ~~aerosol transfer~~ gas-aerosol mass transfer rates used by Evans et al. (2003) are approximately twenty times larger than these in the present work. Evans et al. (2003) employ the parameterization described by Michalowski et al. (2000). In that study, the diffusion-limit term k_{diff} (Eq. (9)), which appears in the gas-to-aerosol transfer constant k_{in} (Eq. (8)) of the present paper, is neglected and only k_{coll} (Eq. (11)) has been considered. However, the values used for k_{coll} and for k_{in} are also different. For the species HOBr, for instance, the base parameters in the present study are $k_{\mathrm{coll}} = 8.9 \times 10^{-4}\ \mathrm{s^{-1}}$ and $k_{\mathrm{in}} = 1.2 \times 10^{-4}\ \mathrm{s^{-1}}$. Using the values for the oscillating result of Evans et al. (2003) and estimating the aerosol radius via Eq. (10), which results in $r = 0.3\ \mathrm{\mu m}$, the corresponding values are $k_{\mathrm{coll}} = 2.0 \times 10^{-3}\ \mathrm{s^{-1}}$ and $k_{\mathrm{in}} = 5.0 \times 10^{-4}\ \mathrm{s^{-1}}$. These differences result not only from negligence of the diffusion limit but also from a larger accommodation coefficient ($\alpha = 0.8$ compared to $\alpha = 0.5$) as well as a larger aerosol surface area ($A = 4.4 \times 10^{-7}\ \mathrm{cm^2\,cm^{-3}}$ versus $A = 3 \times 10^{-7}\ \mathrm{cm^2\,cm^{-3}}$).
- NO_x and HCHO are emitted from the snowpack as described by Evans et al. (2003). The emission rate is proportional to the photolysis rate of NO_2 with an average emission rate of $1.2 \times 10^9\ \mathrm{molec.\,cm^{-2}\,s^{-1}}$ for NO_x and $3.6 \times 10^8\ \mathrm{molec.\,cm^{-2}\,s^{-1}}$ for HCHO.
- HNO_3 transfer to aerosols is considered and it acts as a sink for NO_y.
- All heterogenous reactions and depositions on the ice surface are neglected. However, following Evans et al. (2003), PAN and H_2O_2 undergo dry depositions with velocities of v_{d} = 0.004 $\mathrm{cm\,s^{-1}}$ and $v_{\mathrm{d}} = 0.09\ \mathrm{cm\,s^{-1}}$, respectively.
- The SZA is varied daily in the range of 65° to 97° following a cosine profile, which is consistent with a latitude of 73.4° on April 15, 2003.

- Initial concentrations and parameters are set to the values described by Evans et al. (2003). In particular, the initial mole fraction of bromide is set to $43\ \mathrm{pmol\,mol^{-1}}$. In contrast to the study of Evans et al. (2003), the mixing ratio of acetaldehyde CH_3CHO may evolve freely instead of being fixed to $18\ \mathrm{pmol\,mol^{-1}}$.
- Reactions involving the species $\mathrm{BrNO_2}$ are neglected since the species $\mathrm{BrNO_2}$ is not considered by Evans et al. (2003).

The results presented in Fig. 9 show that with an initial bromide mole fraction of $43\ \mathrm{pmol\,mol^{-1}}$, the ~~recurrence~~ oscillation period is approximately five days. The chemical reaction mechanism used in the present KINAL-T code predicts larger HBr and HOBr mixing ratios compared to the model employed by Evans et al. (2003), resulting in smaller BrO mixing ratios for the same total bromine mole fraction and thus slower ODEs: Ozone is completely depleted approximately one day after the ODE has started, which is more than twice as long as predicted by Evans et al. (2003). Also notably, ozone replenishes to approximately $8.5\ \mathrm{nmol\,mol^{-1}}$ before the ODE starts, whereas Evans et al. (2003) predict only approximately $4.5\ \mathrm{nmol\,mol^{-1}}$. This suggests that the bromine regeneration is slower or that less reactive bromine remains after an ODE in the present KINAL-T simulation. After an ODE, reactive bromine mixing ratios drop to approximately $10^{-4}\ \mathrm{pmol\,mol^{-1}}$ in the present simulation. The bromine regeneration rate is approximately one order of magnitude per day in the present simulation. This means that if the bromine regeneration rate is the same but the reactive bromine mixing ratio obtained by Evans et al. (2003) drops to $10^{-2}\ \mathrm{pmol\,mol^{-1}}$ after an ODE, which might explain the difference.

Negligence of the $\mathrm{BrNO_2}$ chemistry has been found to be of particular importance for finding ~~recurrences~~ oscillations of ODEs, since otherwise $\mathrm{BrNO_2}$ acts as a sink for both, bromine and NOx. If $\mathrm{BrNO_2}$ chemistry is considered, similar structures as seen in section 3.4.2 for large $\mathrm{NO_y}$ mixing ratios are found, where the large $\mathrm{NO_y}$ concentrations cause a termination of the ~~recurrences~~ oscillations.

Another issue of importance is the larger gas-aerosol mass transfer constants used by Evans et al. (2003) compared to the present study. The gas-to-aerosol transfer constants used by Evans et al. (2003) are of the order of $10^{-3}\mathrm{s^{-1}}$ compared to $10^{-4}\mathrm{s^{-1}}$ for the base case. In the present study, the latter value has been adjusted to that used by Evans et al. (2003) in order to match their results. These increased coefficients allow for a quick recycling of HOBr, HBr, and $\mathrm{BrONO_2}$. With smaller gas-aerosol mass transfer constants, the bromine regeneration after an ODE slows down and, more importantly, a larger initial bromide mixing ratio (more than $100\ \mathrm{pmol\,mol^{-1}}$) is necessary to achieve BrO mixing ratios of at least $20\ \mathrm{pmol\,mol^{-1}}$ during an ODE. At an initial bromide mixing ratio of $43\ \mathrm{pmol\,mol^{-1}}$, the ozone depletion occurs on a time scale of weeks with the slower gas-aerosol mass transfer constant.

As discussed above, Michalowski et al. (2000) and Evans et al. (2003) ignored the diffusion-limit. Staebler et al. (1994) measured a maximum value of $r = 0.1\ \mathrm{\mu m}$ in the aerosol size distribution at Alert, and therefore, Evans et al. (2003) assumed that the diffusion correction may be neglected for this small value of aerosol size. However, even at $r = 0.1\ \mathrm{\mu m}$, the HOBr transfer constants are calculated to decrease by a factor of two in the present study, which provides the motivation to consider its relevance in the present study. The aerosol transfer, however, is driven by the aerosol surface, which motivates the use of the aerosol surface distribution instead of the aerosol size distribution. This causes another shift towards larger aerosol sizes with an increased effect on the diffusion limit.

In order to reproduce the ~~recurrence~~ oscillation period of three days predicted by Evans et al. (2003), a second simulation with an increased initial bromide mixing ratio of $60\ \mathrm{pmol\,mol^{-1}}$ and increased NOx emissions by 35% was conducted, cf. Fig. 9b. The main effect of the increased initial bromide mixing ratio alone is a decrease of the duration of the ODEs from one day to somewhat less than half a day and as a consequence, the ~~recurrence~~ oscillation period reduces by about half a day. The increased initial bromide mixing ratio, however, barely affects the bromine regeneration speed, since it is limited by the low mixing ratio of reactive gas phase bromine (less than $10^{-4}\ \mathrm{pmol\,mol^{-1}}$) after the termination of the ODEs and not by the aerosol-phase bromide concentration. The increased $\mathrm{NO_x}$ emissions affect both, the ozone regeneration and the bromine regeneration. The latter is not only increased by the larger ozone regeneration speed, but also by the bromine explosion mechanism involving $\mathrm{BrONO_2}$. More BrO reacts to $\mathrm{BrONO_2}$, which quickly recycles bromide due to the large gas-aerosol mass transfer coefficients. Consequently, the ODEs start at an ozone mixing ratio of approximately $6\ \mathrm{nmol\,mol^{-1}}$ compared to the $8.5\ \mathrm{nmol\,mol^{-1}}$ for the previously used emission rate. Thus, the increased emissions reduce the ~~recurrence~~ oscillation period by about one and a half days, resulting in the shorter ~~recurrence~~ oscillation period of ODEs found by Evans et al. (2003). The differences between the numerical results by Evans et al. (2003) and the present study are most likely due to the different chemical reaction mechanisms. Even though Evans et al. (2003) used the reaction constants provided by the same group as the present study, the knowledge about chemical reaction constants has greatly improved in the last decade (Atkinson et al., 2007). Moreover, it should be noted that Evans et al. (2003) used a box model whereas in the present study, the one-dimensional KINAL-T code with a more advanced model for the heterogenous reactions and the aerosol treatment is used.

3.4 Study of model parameters influencing the ~~recurrence~~ oscillation period

This subsection concerns the variation of some environmental parameters that affect the ~~recurrence~~ oscillation of ODEs: The strength of the inversion layer, the turbulent diffusion in the free troposphere, the $\mathrm{NO_y}$ mixing ratio, the aerosol volume fraction as well as the solar zenith angle on the ~~recurrence~~ oscillation period of the ODEs, cf. Tab. 1. The variation of the $\mathrm{NO_y}$ mixing ratio is investigated for $T = 258$ K (base setting) and $T = 238$ K, as well as simulations where the chlorine mechanism is used (base setting) or neglected.

In the following, three properties of the ~~recurrences~~ oscillations of ODEs will be considered: The average ~~recurrence~~ oscillation period, i.e. the time difference between two ozone maxima, the number of ~~recurrence~~ oscillations, and the average maximum of the ozone mixing ratio; these characteristics are evaluated for a real time of 200 days.

3.4.1 Strength of the inversion layer

Diffusion from aloft is one of the two mechanisms that replenishes the ozone in the model. Since the thickness of the inversion layer is fixed, see Tab. 1, the turbulent diffusion constant $k_{\mathrm{t,inv}}$ is the most important parameter controlling the strength of this replenishment. The turbulent diffusion constant in the free troposphere, k_{f}, also plays an important role.

In order to eliminate the influence of the ozone regeneration by $\mathrm{NO_2}$, the concentration of $\mathrm{NO_y}$ is set to zero for evaluation purposes. In Fig. 10, the dependence of the ~~recurrence~~ oscillation characteristics on the variations of $k_{\mathrm{t,inv}}$ and k_{f} is shown, cf. Figs. 10a–10c, and the variation of the mixing ratios of $\mathrm{O_3}$ and Br at two different heights of 100 m and 225 m, Fig. 10d,

(a) Average ~~recurrence~~ oscillation period during 200 days

(b) Number of ~~recurrences~~ oscillations during 200 days

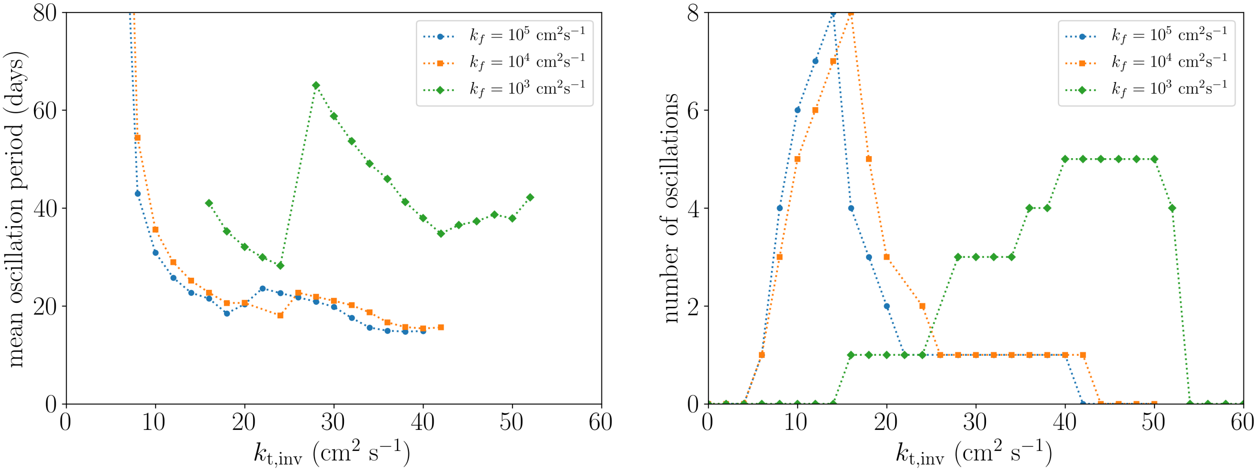

(c) Average maximum mixing ratio of ozone

(d) Profiles of the mixing ratios of O_3 and total gaseous Br

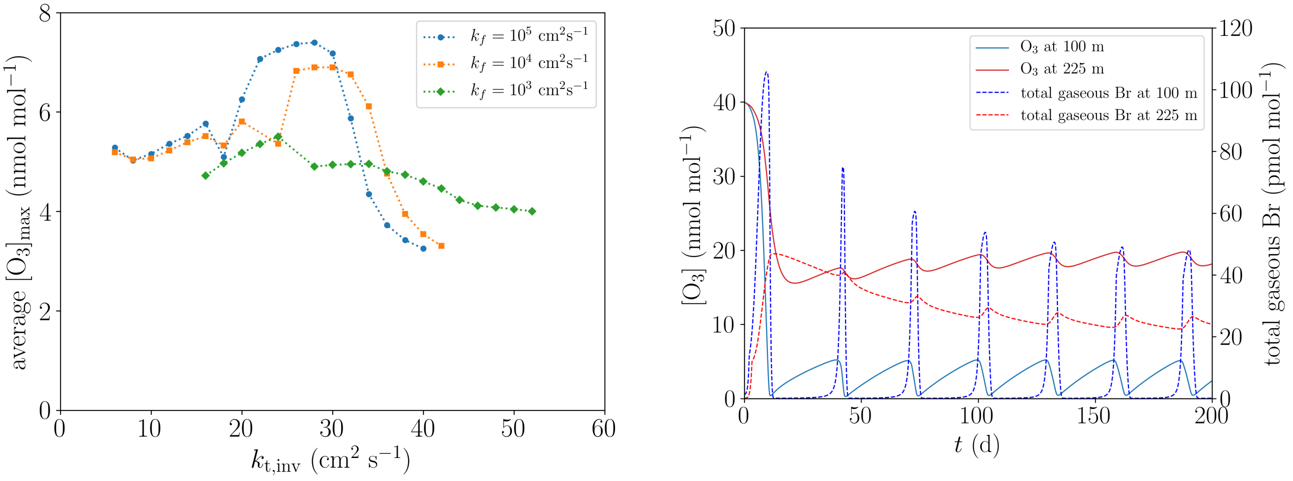

Figure 10. Dependence of the ~~recurrence~~ oscillation characteristics on the variations of $k_{\mathrm{t,inv}}$ and k_{f}, Figs. 10a–10c, and the variation of the mixing ratios of O_3 and Br at two different heights of 100 m and 225 m for the base settings, Fig. 10d

for the base settings.

The smallest ~~recurrence~~ oscillation period of approximately 20 days is found for the turbulent diffusion coefficient of $k_f = 10^5\ \mathrm{cm}^2\,\mathrm{s}^{-1}$ in the free troposphere and for $k_{\mathrm{t,inv}} \approx 40\ \mathrm{cm}^2\,\mathrm{s}^{-1}$. For very small turbulent diffusion coefficients of less than $k_{\mathrm{t,inv}} = 6\ \mathrm{cm}^2\,\mathrm{s}^{-1}$, no ~~recurrences~~ oscillations occur since the ozone regeneration rate is too slow in the considered time of 200 days.

The ~~recurrence~~ oscillation period does not increase linearly with $k_{\mathrm{t,inv}}$ since the ozone mixing ratio in the inversion layer changes with increased diffusion; three processes determine the ozone mixing ratio:

- In the inversion layer, ozone is lost by diffusion into the boundary layer.
- Ozone is ~~regenerated~~ replenished by its diffusion from the free troposphere into the inversion layer.
- Bromine is mixed into the inversion layer and lost to the free troposphere, resulting in a partial ODE inside the inversion layer.

Inside the inversion layer, reactive bromine may survive due to the sustained ozone supply from the free troposphere. It turns out that larger diffusion coefficients inside the inversion layer result in increased ozone mixing ratios, converging to approximately 20 $\mathrm{nmol\,mol^{-1}}$ for $k_{\mathrm{inv}} > 20\ \mathrm{cm^2\,s^{-1}}$, which is half of the value at the top boundary of the computational domain. This is the reason for the sharp, nonlinear increase in the number of ~~recurrences~~ oscillations during 200 days.

For $k_{\mathrm{inv}} < 14\ \mathrm{cm^2\,s^{-1}}$, the ~~recurrence~~ oscillation period decreases strongly, and for larger values of k_{inv}, termination is initiated. The mixing ratios for $\mathrm{O_3}$ and Br in the first regime, i.e. for $k_{\mathrm{inv}} = 10\ \mathrm{cm^2\,s^{-1}}$, are displayed in Fig. 10d. After the first ODE, the ozone regeneration due to diffusion is not very much affected by an ongoing ODE since the ozone mixing ratio is only slightly varying inside the inversion layer, severely limiting the ozone regeneration rate without termination.

Since the standard value of $k_{\mathrm{f}} = 10^5\ \mathrm{cm^2\,s^{-1}}$ used in the present simulation corresponds to an almost perfectly mixed free troposphere, even larger values do not affect the simulation results. By neglecting horizontal mixing and transport, it is essentially assumed that the air mass in the boundary layer is confined. However, the ~~upper~~ free troposphere will still have very different wind velocities, so it is reasonable that the air in the ~~upper~~ free troposphere is exchanged quickly with fresh air even though the boundary layer is confined. A large turbulent diffusion coefficient in the ~~upper~~ free troposphere ensures a quick exchange of the air with the upper simulation boundary.

The influence of a reduction of k_{f} to values of $10^4\ \mathrm{cm^2\,s^{-1}}$ and $10^3\ \mathrm{cm^2\,s^{-1}}$ is presented in Figs. 10a–10c. The value of $k_f = 10^4\ \mathrm{cm^2\,s^{-1}}$ still corresponds to nearly perfect mixing inside the free troposphere as can be seen by the negligible differences in the mean ~~recurrence~~ oscillation period between $k_f = 10^5\ \mathrm{cm^2\,s^{-1}}$ and $k_f = 10^4\ \mathrm{cm^2\,s^{-1}}$. All resulting profiles are very similar.

Reducing k_f to $10^3\ \mathrm{cm^2\,s^{-1}}$, however, has a large impact, since bromine transported to the free troposphere will stay there for several weeks (as may be estimated from the diffusion time scale) before being transported to the upper boundary. Ozone is also transported much ~~slower~~ more slowly to the lower layers of the free troposphere, causing the ozone levels to drop to approximately 15 $\mathrm{nmol\,mol^{-1}}$ at 500 m for $k_{\mathrm{t,inv}} = 25\ \mathrm{cm^2\,s^{-1}}$; ozone levels decrease further with increased values of $k_{\mathrm{t,inv}}$, ~~decreasing of course with larger $k_{\mathrm{t,inv}}$ and~~ converging to 12 $\mathrm{nmol\,mol^{-1}}$ for $k_{\mathrm{t,inv}}$ exceeding 50 $\mathrm{cm^2\,s^{-1}}$. The ozone mixing ratio in the inversion layer drops to less than 10 $\mathrm{nmol\,mol^{-1}}$, reducing the ozone ~~regeneration~~ recovery rate in the boundary layer and also limiting the maximum ~~ozone level that can be regenerated~~ levels to which ozone can be recovered.

~~Recurrence~~ Oscillations occur only at larger turbulent diffusion coefficients of $k_{\mathrm{t,inv}} > 14\ \mathrm{cm^2\,s^{-1}}$, and they terminate for $k_{\mathrm{t,inv}} > 50\ \mathrm{cm^2\,s^{-1}}$, see Fig. 10b. In contrast to the larger values k_{f}, the ozone mixing ratio in the inversion layer decreases with increasing $k_{\mathrm{t,inv}}$ in the present case. Also, the time between two ~~recurrences~~ oscillations tends to increase ~~with each further recurrence~~ progressively after each oscillation since a larger turbulent diffusion coefficient in the inversion layer causes ~~as strong~~ a greater loss of bromine to the free troposphere, which in turn decreases the speed of the bromine explosion in the boundary layer.

~~If~~ In cases where only two or three maxima occur, i.e. $k_{\mathrm{inv}} > 16\ \mathrm{cm}^2\,\mathrm{s}^{-1}$, due to the termination of the ~~recurrences~~ oscillations, the standard deviation of both the ~~recurrence~~ oscillation period and the ozone maxima increase sharply, since the first few ~~recurrences~~ oscillations are still affected by the first ODE, and the ~~recurrences~~ oscillations before the termination tend to have ozone maxima that are closer to the equilibrium mixing ratio of ozone.

3.4.2 The role of $\mathbf{NO_y}$, T and chlorine

In the present model, NOy is treated as a conserved quantity. In this subsection, the NOy mixing ratio is varied as the major parameter influencing NOx-catalyzed photochemical $\mathrm{O_3}$ formation, see reaction (R20) and its effect on the ODEs is investigated.

Figure 11 shows the variation of the ~~recurrence~~ oscillation period with $\mathrm{NO_y}$ mixing ratios of up to 300 $\mathrm{pmol\,mol^{-1}}$ for two different temperatures of 258 K (standard value) and the reduced value of 238 K, cf. Fig. 11a. ~~Recurrence~~ Oscillation periods of less than five days are obtained for 258 K. The number of ~~recurrences~~ oscillations increases linearly with the $\mathrm{NO_y}$ mixing ratio (Fig.11b), with a y-intercept given by the regeneration of ozone purely via diffusion through the inversion layer. At about $[\mathrm{NO_y}]$ = 200 $\mathrm{pmol\,mol^{-1}}$ for T = 258 K, ~~recurrences~~ oscillations tend to terminate. Once the mixing ratio of $\mathrm{NO_y}$ is very large, the bromine released during an ODE is not able to completely destroy all $\mathrm{NO_x}$. Thus, even during an ODE, ozone is produced by the $\mathrm{NO_2}$ photolysis, increasing ozone regeneration and making a termination more likely. The non-zero $\mathrm{NO_x}$ concentrations also result in more $\mathrm{BrNO_x}$ (which is the sum of $\mathrm{BrNO_2}$ and $\mathrm{BrONO_2}$) formation during the termination. $\mathrm{BrNO_x}$ then makes up approximately 60% of the total gas-phase bromine.

Moreover, the chlorine mechanism has been deactivated by setting all chlorine initial concentrations to zero and changing the heterogenous reaction of HOBr to only release $\mathrm{Br_2}$, see Figs. 11a and 11b. While the presence of chlorine may enhance the ODE by enhanced $\mathrm{O_3}$ destruction through the very fast reaction of BrO with ClO, the bromine explosion is actually slowed down by the presence of chlorine. This is due to the fact that when chlorine is included, part of the heterogenous reactions release BrCl instead of $\mathrm{Br_2}$, thus the amount of released bromine is reduced. Also, without chlorine, the slower ODE increases the duration of the bromine explosion, which also increases the bromine released, resulting overall in faster ~~recurrences~~ oscillations, since further ~~recurrences~~ oscillations contain more bromine in aerosols that can be reactivated. As a side effect, the ozone maximum value is slightly smaller without the chlorine chemistry.

For $T = 238$ K, the ~~recurrence~~ oscillation period is smaller compared to T = 258 K for small $[\mathrm{NO_y}]$, as can be seen in Fig. 11c. However, termination of ~~recurrences~~ oscillations starts already at around 70 $\mathrm{pmol\,mol^{-1}}$ of $\mathrm{NO_y}$ instead of at around 200 $\mathrm{pmol\,mol^{-1}}$ for $T = 258$ K. Figure 11d shows a termination for $T = 238$ K after 80 days. In this temperature region, $\mathrm{HNO_4}$ becomes very stable due to the decay of $\mathrm{HNO_4}$ being nearly two orders of magnitude slower, see (R 56) in Tab. A1, and replaces PAN as the most abundant nitrogen species. The shift towards $\mathrm{HNO_4}$ formation reduces the $\mathrm{NO_2}$ concentration,

(a) Average ~~recurrence~~ oscillation period during 200 days

(b) Number of ~~recurrences~~ oscillations during 200 days

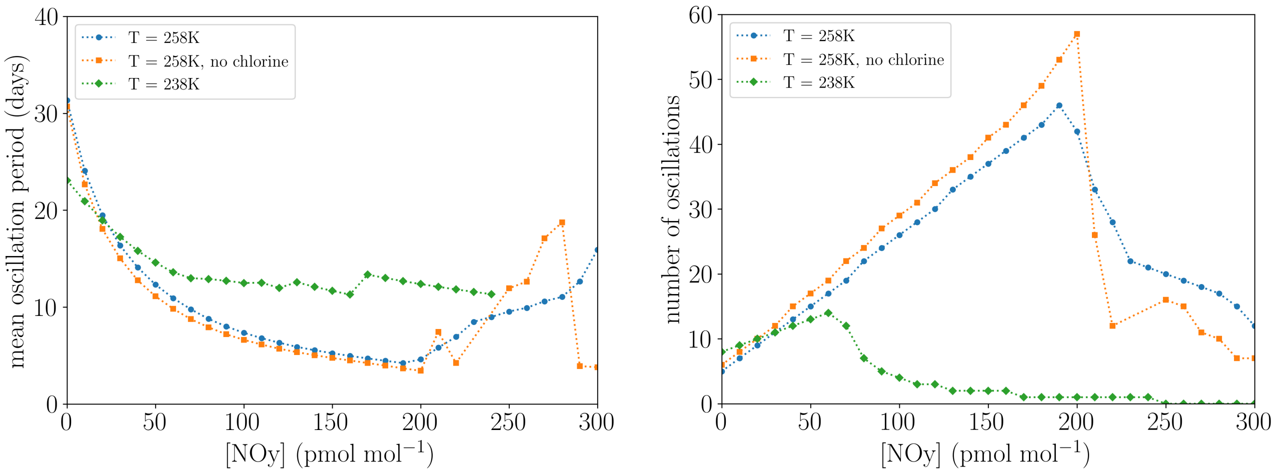

(c) Average maximum mixing ratio of ozone

(d) Profiles of the mixing ratios of O_3 and total gaseous Br

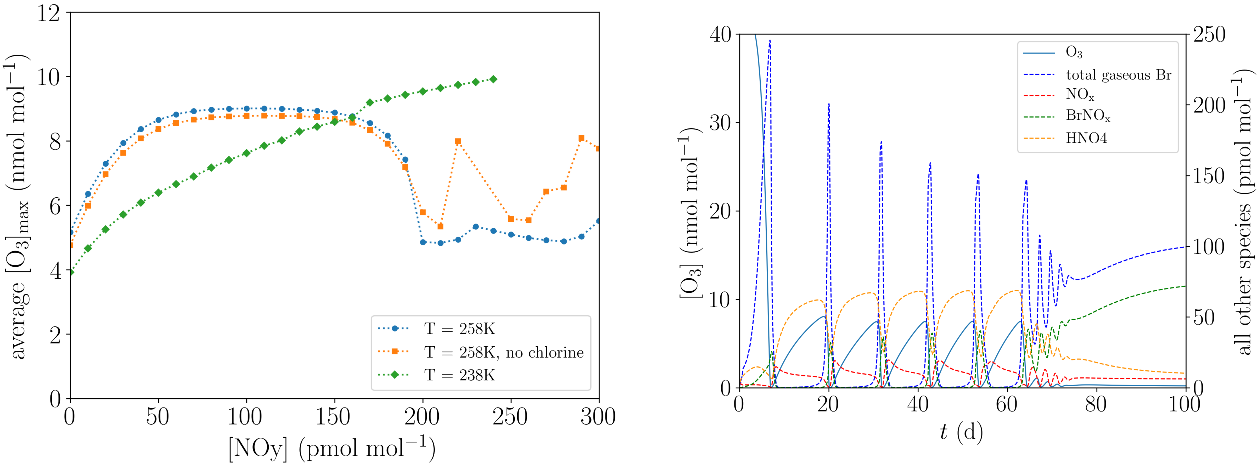

Figure 11. Dependence of the ~~recurrence~~ oscillation characteristics on the variations of $[NO_y]$, Figs. 11a–11c. Termination of an ODE: profiles of the mixing ratios of various species for the base settings and for 238 K and $[NO_y] = 100\ \mathrm{pmol\,mol^{-1}}$, Fig. 11d

retarding the ozone regeneration.

At the lower temperature, the ODE mechanism becomes more efficient, e.g. the reaction constant in the Br_2-producing BrO self-reaction increases by 33%, (R 5) in Tab. A1, while many of the HBr-producing reactions, e.g. (R 9) and (R 10) in Tab. A1, slow down by around around 20%. The total amount of bromine released for the first ODE increases whereas the amount of bromine released for the ~~recurrences~~ oscillations decreases due to the slower ozone regeneration.

The main reason for the earlier termination of the oscillations at $T = 238$ K is a strong shift towards the increased HNO_4 formation. During an ODE, the HNO_4 can be destroyed to directly produce NO_2 by reacting with OH or by decaying through

(R 56) and ~~(R 59)~~ (R 57) in Tab. A1. PAN, however, is more stable during an ODE at 258 K due to a larger formation of CH_3CO_3 via e.g. (R 34) in Tab. A1 caused by the larger OH formation during an ODE, consuming NO_2 ~~(R 67)~~ (R 65) instead of producing it through ~~(R 86)~~ (R 84) or through the photolysis of PAN. The shift from PAN as the most stable species towards HNO_4 for the lower temperature increases the ozone recovery during an ODE ~~, resulting in earlier terminations of the ODEs.~~ Since a larger ozone recovery during an ODE facilitates chemical equilibrium with the reactive bromine, this results in earlier terminations of the oscillations of ODEs.

3.4.3 The influence of the aerosol density

In order to study the influence of the aerosol characteristics, the standard value of the aerosol volume fraction of $10^{-11}\mathrm{m^3m^{-3}}$ is varied between $10^{-12}\mathrm{m^3m^{-3}}$ and $3\times10^{-10}\mathrm{m^3m^{-3}}$, see Fig. 12. For small aerosol concentrations, the recycling of HBr is too weak for a full ODE to occur since only small bromine concentrations are released before the termination of an ODE. Only a partial ODE and no ~~recurrences~~ oscillations take place.

For larger aerosol mixing ratios, the faster bromine recycling reduces the ~~recurrence~~ oscillation period, however the ozone does not regenerate faster. Thus, the ozone maximum decreases so that the ~~recurrences~~ oscillations release less bromine, resulting in a larger net bromine loss per ~~recurrence~~ oscillation. Also, the reactivation strength of aerosol bromine increases relative to the activation on the ice surface, resulting in a lower bromine release from the ice, also increasing the net bromine loss for each ~~recurrence~~ oscillation, which ultimately leads to the termination of the ~~recurrences~~ oscillations for aerosol volume fractions larger than about $5.5\times10^{-11}\mathrm{m^3m^{-3}}$.

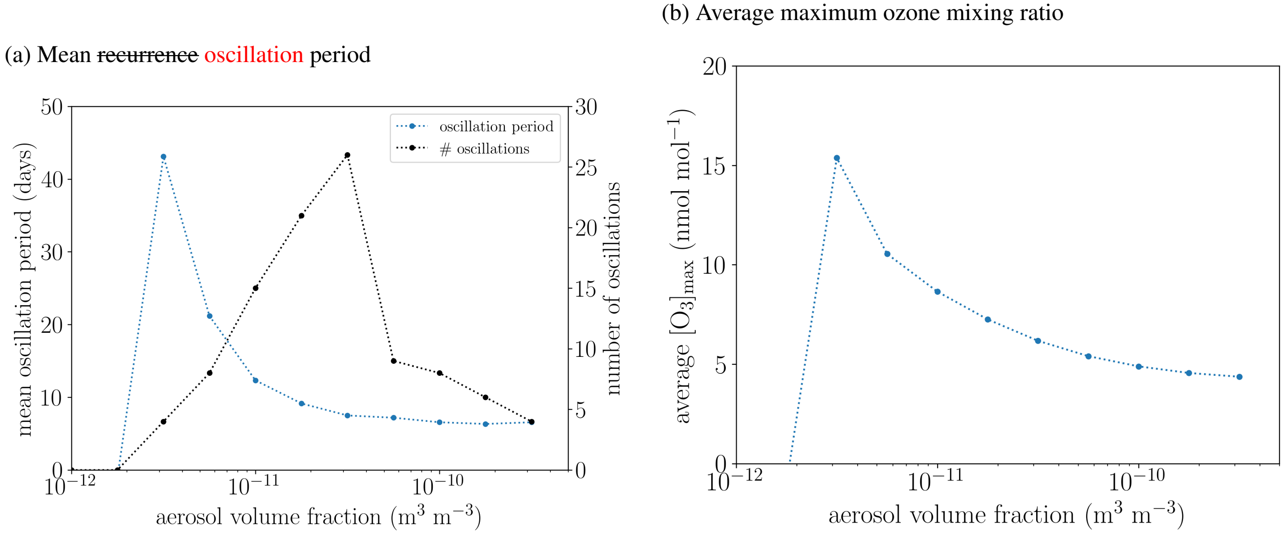

(a) Mean ~~recurrence~~ oscillation period

(b) Average maximum ozone mixing ratio

Figure 12. ~~Recurrence~~ Oscillation characteristics depending on the aerosol volume fraction after 200 days

3.4.4 Variation of the solar zenith angle

The mean ~~recurrence~~ oscillation period displayed in Fig. 13a hardly changes when the solar zenith angle SZA is varied from its standard value of 80° (see Tab. 1) within the range of 70° and 83°. The variations stay within one standard deviation. For SZA > 83°, the ODEs do no longer occur due to the slow photolysis frequencies. Surprisingly, the ~~recurrence~~ oscillation period does not monotonically decrease with increased SZA, instead, there is a minimum at SZA = 77°. For a lower SZA, some or even all ODEs are only partial as Fig. 13b demonstrates for the value of SZA = 70°. In particular, the minimum ozone mixing ratio for the six ~~recurrences~~ oscillations shown is approximately $10\ \mathrm{nmol\,mol^{-1}}$ and the ozone depletion restarts at an ozone mixing ratio of about $18\ \mathrm{nmol\,mol^{-1}}$. For a SZA of 70°, the $\mathrm{NO_2}$ mixing ratio decreases to about $5\ \mathrm{pmol\,mol^{-1}}$ during the ODEs instead of to nearly zero at 80°. Also, $\mathrm{BrNO_x}$ and PAN are photolyzed faster, increasing the $\mathrm{NO_x}$ formation. Only about $80\ \mathrm{pmol\,mol^{-1}}$ of bromine is released at SZA = 70° during the first ODE, which is about two-thirds of the value at 80°. Interestingly, gas-phase bromine does not drop to zero for the later ~~recurrences~~ oscillations, however, the BrO concentration drops to nearly zero. BrO mixing ratios do not exceed $10\ \mathrm{pmol\,mol^{-1}}$, which is much lower than the typical mixing ratio of 30-40 $\mathrm{pmol\,mol^{-1}}$ of numerical simulations with a SZA of 80°; this is most likely a result of the increased formation of $\mathrm{HO_2}$. Another characteristics are the faster photolysis reactions of BrO and HOBr for lower SZA. For SZA = 70°, 80% of the BrO photolyzes to Br and to $\mathrm{O_3}$, which results in a null cycle. The resulting smaller BrO mixing ratio also decreases the rate of self-recycling, which is part of the ozone-destroying cycle. 70% of the HOBr photolyzes to HO and Br, slowing down the bromine explosion substantially and consuming $\mathrm{HO_2}$ in the process. The faster $\mathrm{Br_2}$ photolysis, however, does not further enhance the ozone desctruction, since $\mathrm{Br_2}$ is already photolyzed extremely fast even at SZA = 80°.

For SZA = 70°, the fastest reaction of BrO is with NO, producing $\mathrm{NO_2}$ and Br in the process. $\mathrm{NO_2}$ is ~~photolyzrefered~~ pho-

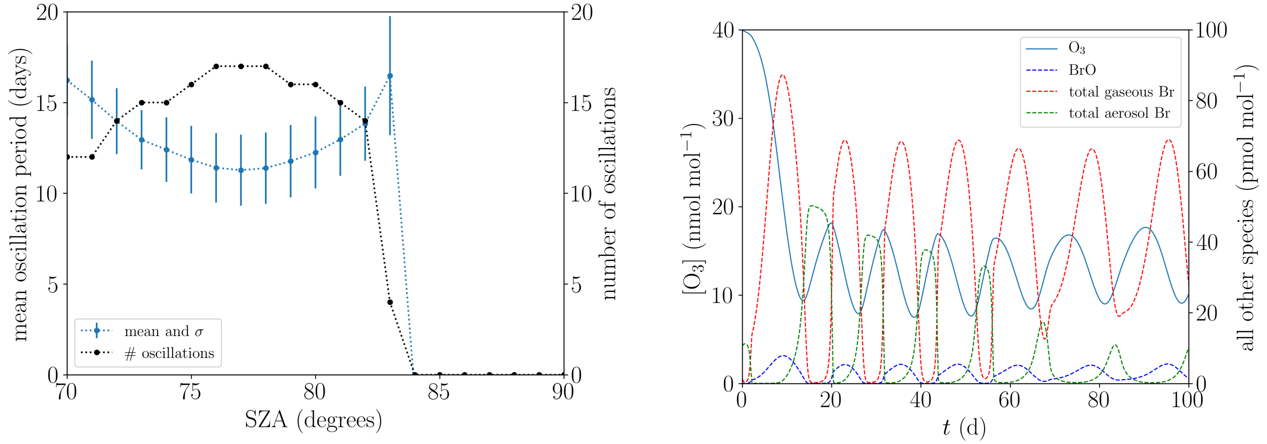
(a) ~~Recurrence~~ Oscillation period

(b) Partial ODE for SZA = 70°

Figure 13. (a) Mean ~~recurrence~~ oscillation period and number of ~~recurrences~~ oscillations versus the solar zenith angle during 200 days. (b) Evolution of the mixing ratios of $\mathrm{O_3}$ and the bromine species for SZA = 70°

tolyzed to ozone, resulting in a net null cycle. For SZA = 80°, the BrO self-reaction is stronger than its reaction with NO, favoring a full ODE.

4 Conclusions

In the present study, the one-dimensional model KINAL-T developed by Cao et al. (2016) was extended and optimized in order to study the potential of ODEs to recur. The extension concerns the chemical reaction mechanism as well as the treatment of aerosols and the improvement of the numerical solver. The model was employed to study both the ~~recurrence~~ oscillation and the termination of ODEs, and several parameters were varied to investigate their influence on the ~~recurrence~~ oscillation period, the maximum ozone mixing ratio, and the number of ~~recurrences~~ oscillations of the ODEs. After an ODE, ozone can be replenished by the diffusion of ozone from the free troposphere to the boundary layer and/or by the photolysis of NO_2; it is found that either of these two O_3 sources is sufficient to drive the ~~recurrences~~ oscillations. Another result of the present study is that the chemistry of ODEs coupled with the vertical diffusion alone can cause the ~~recurrence~~ oscillation of ODEs at the surface even without the existence of horizontal transport.

A strong inversion layer was found to be essential for the ~~recurrence~~ oscillation of ODEs since the steady mixing of the ozone back into the boundary layer may provide a sufficiently high ozone level to keep the reactive bromine in the boundary layer at a significant level, which then establishes chemical equilibrium with the remaining ozone.

Without the presence of reactive nitrogen oxides, the system is a heterogenous, diffusion-driven ~~recurrence~~ oscillation, the fastest periods of which were found to be approximately 20 days. Fast replenishment of the air in the free troposphere was found to lead to faster ~~recurrences~~ oscillations. It may be possible to find conditions leading to even shorter ~~recurrence~~ oscillation periods such as a slightly smaller SZA and moderately higher aerosol mixing ratios.

The replenishment of ozone via the photolysis of NO_2 is a chemical gas-phase process. Faster ~~recurrence~~ oscillation periods of approximately five days are found due to the destruction of NO_x during an ODE. However, at sufficiently high nitrogen oxide levels, the amount of bromine released during the bromine explosion is not large enough to keep the NO_2 mixing ratio low, so that the ~~recurrences~~ oscillations can terminate due to the ozone regeneration, keeping the reactive bromine at a significant level. With high NO_y mixing ratios, ~~recurrences~~ oscillations are possible even if the boundary layer does not interact at all with the free troposphere. Deactivation of the chlorine mechanism speeds up the bromine explosion, since the heterogenous reactions of HOBr on aerosols and snow/ice surfaces always produce Br_2 instead of Br_2 and $BrCl$. The absence of chlorine thus results in faster ~~recurrences~~ oscillations.

More sunlight, for a SZA up to 77°, and a higher aerosol volume fraction of up to 5.5×10^{-11} m^3/m^3 are beneficial for faster ~~recurrences~~ oscillations, at even higher values, the ~~recurrence~~ oscillation retards or terminates. Since bromine may be lost over time due to dry deposition and mixing into the upper troposphere, a strong release of bromine for each ~~recurrence~~ oscillation is important to enable the fast destruction of ozone so that no chemical equilibrium of bromine with the ozone may be established.

The present simulations were compared to results of an earlier study by Evans et al. (2003). Using the same initial bromide mixing ratio of $43\ \mathrm{pmol\,mol^{-1}}$ and the same NO_x emissions, a shorter ~~recurrence~~ oscillation period of five days was found in comparison with three days predicted by Evans et al. (2003). The difference in the ~~recurrence~~ oscillation periods is caused by a slower reactive bromine regeneration after an ODE or a stronger bromine depletion during the termination of the ODEs in the present model. By assuming an increased initial bromide mixing ratio of $60\ \mathrm{pmol\,mol^{-1}}$ and stronger $\mathrm{NO_x}$ emissions by 35%, the ~~recurrence~~ oscillation period of three days found by Evans et al. (2003) could be reproduced. The differences may be attributable to different chemical reaction mechanisms, a more advanced treatment of the aerosol in the present study as well as to the use of a box model by Evans et al. (2003) versus a 1D model in the present simulation.

Even though the present simulations are based on somewhat idealized assumptions, they demonstrate that there are additional reasons for the observed ~~recurrences~~ oscillations of ODEs that go beyond modified environmental conditions or advection of air masses with varying ozone and halogen content. Experimental validation of these simulations could be a challenge since these external causes of ~~recurrences~~ oscillations and intrinsic ~~recurrences~~ oscillations are likely to occur simultaneously. However, it is possible that the conditions simulated in the present paper can be found e.g. at high latitudes in the Arctic where day/night cycles do not play any role and ~~recurrences~~ oscillations may be observed. Thus, the present study provides valuable insight into parametric dependencies of the characteristics of the ~~recurrences~~ oscillations of ODEs and their termination.

An interesting extension of the present model could be the consideration of snow packs. A finite amount of sea salt that is consumed during the bromine explosion and redeposited after the bromine explosion may have an interesting effect on the ~~recurrences~~ oscillations. This may also allow for the modeling of $\mathrm{NO_x}$ emissions from the snow, relaxing the present assumption of a conserved $\mathrm{NO_y}$ mixing ratio.

The consideration of more realistic meteorological effects requires the use of more advanced 3D simulations which are currently being developed in extension of previous work of Cao and Gutheil (2013). The new simulations will include horizontal advection and vertical convection explicitly.

Appendix A: List of Reactions

A1 Gas phase reactions

Table A1: Gas phase reactions

# Reac.	Reaction	$k\ \left[\left(\mathrm{molec.\,cm}^{-3}\right)^{1-n}\mathrm{s}^{-1}\right]$	Reference
1	$O(^1D) + O_2 \rightarrow O_3$	$3.2 \times 10^{-11} \exp(670/T)$	Atkinson et al. (2004)
2	$O(^1D) + H_2O \rightarrow 2OH$	2.2×10^{-10}	Atkinson et al. (2004)
3	$O_3 + Br \rightarrow O_2 + BrO$	$1.7 \times 10^{-11} \exp(-800/T)$	Atkinson et al. (2007)
4	$2BrO \rightarrow 2Br + O_2$	2.7×10^{-12}	Atkinson et al. (2007)
5	$2BrO \rightarrow Br_2 + O_2$	$2.9 \times 10^{-14} \exp(840/T)$	Atkinson et al. (2007)
6	$BrO + HO_2 \rightarrow HOBr + O_2$	$4.5 \times 10^{-12} \exp(500/T)$	Atkinson et al. (2007)
7	$CO + OH \xrightarrow{O_2} CO_2 + HO_2$	$1.4 \times 10^{-13} \left[1 + [N_2] / \left(4 \times 10^{19}\right)\right]$	Atkinson et al. (2004)
8	$Br + HO_2 \rightarrow HBr + O_2$	$7.7 \times 10^{-12} \exp(-450/T)$	Atkinson et al. (2007)
9	$Br + CH_2O \xrightarrow{O_2} HBr + CO + HO_2$	$7.7 \times 10^{-12} \exp(-580/T)$	Atkinson et al. (2007)
10	$Br + C_2H_4O \xrightarrow{O_2} HBr + CH_3CO_3$	$1.8 \times 10^{-11} \exp(-460/T)$	Atkinson et al. (2007)
11	$Br_2 + OH \rightarrow HOBr + Br$	$2.0 \times 10^{-11} \exp(240/T)$	Atkinson et al. (2007)
12	$HBr + OH \rightarrow Br + H_2O$	$6.7 \times 10^{-12} \exp(155/T)$	Atkinson et al. (2007)
13	$Br + C_2H_2 \xrightarrow{3O_2} Br + 2CO + 2HO_2$	4.2×10^{-14}	Borken (1996)
14	$Br + C_2H_2 \xrightarrow{2O_2} HBr + 2CO + HO_2$	8.92×10^{-14}	Borken (1996)
15	$Br + C_2H_4 \xrightarrow{3.5O_2} Br + 2CO + H_2O + 2HO_2$	2.53×10^{-13}	Barnes et al. (1993)
16	$Br + C_2H_4 \xrightarrow{2.5O_2} HBr + 2CO + H_2O + HO_2$	5.34×10^{-13}	Barnes et al. (1993)
17	$CH_4 + OH \xrightarrow{O_2} CH_3O_2 + H_2O$	$1.85 \times 10^{-12} \exp(-1,690/T)$	Atkinson et al. (2006)
18	$BrO + CH_3O_2 \rightarrow Br + CH_2O + HO_2$	1.6×10^{-12}	Alfonso et al. (1997)
19	$BrO + CH_3O_2 \rightarrow HOBr + CH_2O + O_2$	4.1×10^{-12}	Alfonso et al. (1997)
20	$O_3 + OH \rightarrow O_2 + HO_2$	$1.7 \times 10^{-12} \exp(-940/T)$	Atkinson et al. (2004)
21	$HO_2 + OH \rightarrow O_2 + H_2O$	$4.8 \times 10^{-11} \exp(250/T)$	Atkinson et al. (2004)
22	$H_2O_2 + OH \rightarrow H_2O + HO_2$	$2.9 \times 10^{-12} \exp(-160/T)$	Atkinson et al. (2004)
23	$2OH \rightarrow H_2O + O(^3P)$	$6.2 \times 10^{-14} \times (T/298)^{2.6} \exp(-945/T)$	Atkinson et al. (2004)

# Reac.	Reaction	$k\ \left[\left(\mathrm{molec.\,cm}^{-3}\right)^{1-n}\mathrm{s}^{-1}\right]$	Reference
24	$O_3 + HO_2 \rightarrow 2O_2 + OH$	2.03×10^{-16} $\times (T/300)^{4.57} \exp(-693/T)$	Atkinson et al. (2004)
25	$2HO_2 \rightarrow O_2 + H_2O_2$	$2.2 \times 10^{-13} \exp(600/T)$	Atkinson et al. (2004)
26	$OH + C_2H_6 \rightarrow C_2H_5 + H_2O$	$6.9 \times 10^{-12} \exp(-1,000/T)$	Atkinson et al. (2006)
27	$O_2 + C_2H_5 \rightarrow C_2H_4 + HO_2$	3.8×10^{-15}	Atkinson et al. (2006)
28	$O_2 + C_2H_5 + M \rightarrow C_2H_5O_2 + M$	$k_0 = 5.9 \times 10^{-29} (T/300)^{-3.8} [N_2]$ $k_\infty = 7.8 \times 10^{-12}$ $F_c = 0.58 \exp(-T/1,250)$ $+0.42 \exp(-T/183)$	Atkinson et al. (2006)
29	$OH + C_2H_4 + M \overset{1.5O_2}{\rightarrow}$ $CH_3O_2 + CO + H_2O + M$	$k_0 = 8.6 \times 10^{-29} (T/300)^{-3.1} [N_2]$ $k_\infty = 9.0 \times 10^{-12} (T/300)^{-0.85}$ $F_c = 0.48$	Sander et al. (1997)
30	$O_3 + C_2H_4 \rightarrow CO + CH_2O + H_2O$	4.33×10^{-19}	Atkinson et al. (2006)
31	$OH + C_2H_2 + M \overset{1.5O_2}{\rightarrow}$ $CO + CH_2O + HO_2 + M$	$k_0 = 5.0 \times 10^{-30} (T/300)^{-1.5} [N_2]$ $k_\infty = 10^{-12}$ $F_c = 0.37$	Atkinson et al. (2006)
32	$OH + C_3H_8 \overset{2O_2}{\rightarrow}$ $CO + C_2H_5O_2 + 2H_2O$	$7.6 \times 10^{-12} \exp(-585/T)$	Atkinson et al. (2006)
33	$OH + CH_2O \overset{O_2}{\rightarrow} CO + HO_2 + H_2O$	$5.4 \times 10^{-12} \exp(135/T)$	Atkinson et al. (2006)
34	$OH + C_2H_4O \overset{O_2}{\rightarrow} CH_3CO_3 + H_2O$	$4.4 \times 10^{-12} \exp(365/T)$	Atkinson et al. (2006)
35	$HO_2 + CH_3O_2 \rightarrow CH_3O_2H + O_2$	$3.42 \times 10^{-13} \exp(780/T)$	Atkinson et al. (2006)
36	$OH + CH_3O_2H \rightarrow CH_3O_2 + H_2O$	$10^{-12} \exp(190/T)$	Atkinson et al. (2006)
37	$OH + CH_3O_2H \rightarrow$ $CH_2O + OH + H_2O$	$1.9 \times 10^{-12} \exp(190/T)$	Atkinson et al. (2006)
38	$Br + CH_3O_2H \rightarrow HBr + CH_3O_2$	$2.66 \times 10^{-12} \exp(-1,610/T)$	Mallard et al. (1993)
39	$2CH_3O_2 \rightarrow CH_3OH + CH_2O + O_2$	$6.29 \times 10^{-14} \exp(365/T)$	Atkinson et al. (2006)
40	$2CH_3O_2 \overset{O_2}{\rightarrow} 2CH_2O + HO_2 + H_2O$	$3.71 \times 10^{-14} \exp(365/T)$	Atkinson et al. (2006)
41	$OH + CH_3OH \overset{O_2}{\rightarrow}$ $CH_2O + HO_2 + H_2O$	$2.42 \times 10^{-12} \exp(-345/T)$	Atkinson et al. (2006)
42	$2C_2H_5O_2 \rightarrow 2C_2H_5O + O_2$	6.4×10^{-14}	Atkinson et al. (2006)
43	$O_2 + C_2H_5O \rightarrow C_2H_4O + HO_2$	7.44×10^{-15}	Atkinson et al. (2006)
44	$O_2 + C_2H_5O \rightarrow CH_2O + CH_3O_2$	7.51×10^{-17}	Sander et al. (1997)
45	$HO_2 + C_2H_5O_2 \rightarrow C_2H_5O_2H + O_2$	$3.8 \times 10^{-13} \exp(980/T)$	Sander et al. (1997)

# Reac.	Reaction	$k\left[\left(\text{molec. cm}^{-3}\right)^{1-n}\text{s}^{-1}\right]$	Reference
46	$OH + C_2H_5O_2H \rightarrow$ $C_2H_5O_2 + H_2O$	8.21×10^{-12}	Sander et al. (1997)
47	$Br + C_2H_5O_2H \rightarrow C_2H_5O_2 + HBr$	5.19×10^{-15}	Sander et al. (1997)
48	$2OH + M \rightarrow H_2O_2 + M$	$k_0 = 6.9 \times 10^{-31}$ $\times(T/300)^{-0.888}\,[N_2]$ $k_\infty = 2.6 \times 10^{-11}$ $F_c = 0.5$	Atkinson et al. (2004)
49	$NO + O_3 \rightarrow NO_2 + O_2$	$1.4 \times 10^{-12}\exp(-1,310/T)$	Atkinson et al. (2004)
50	$NO + HO_2 \rightarrow NO_2 + OH$	$3.6 \times 10^{-12}\exp(270/T)$	Atkinson et al. (2004)
51	$NO_2 + O_3 \rightarrow NO_3 + O_2$	$1.4 \times 10^{-13}\exp(-2,470/T)$	Atkinson et al. (2004)
52	$NO_2 + OH + M \rightarrow HNO_3 + M$	$k_0 = 3.3 \times 10^{-30}(T/300)^{-3}\,[N_2]$ $k_\infty = 4.1 \times 10^{-11}$ $F_c = 0.4$	Atkinson et al. (2004)
53	$NO + NO_3 \rightarrow 2NO_2$	$1.8 \times 10^{-11}\exp(110/T)$	Atkinson et al. (2004)
54	$HONO + OH \rightarrow NO_2 + H_2O$	$2.5 \times 10^{-12}\exp(260/T)$	Atkinson et al. (2004)
55	$NO_2 + HO_2 + M \rightarrow HNO_4 + M$	$k_0 = 1.8 \times 10^{-31}(T/300)^{-3.2}\,[N_2]$ $k_\infty = 4.7 \times 10^{-12}$ $F_c = 0.6$	Atkinson et al. (2004)
56	$HNO_4 + M \rightarrow NO_2 + HO_2 + M$	$k_0 = 4.1 \times 10^{-5}$ $\times\exp(-10,650/T)\,[N_2]$ $k_\infty = 4.8 \times 10^{15}\exp(-11,170/T)$ $F_c = 0.6$	Atkinson et al. (2004)
57	$HNO_4 + OH \rightarrow NO_2 + H_2O + O_2$	$3.2 \times 10^{-13}\exp(690/T)$	Atkinson et al. (2004)
58	$NO + OH + M \rightarrow HONO + M$	$k_0 = 7.4 \times 10^{-31}(T/300)^{-2.4}\,[N_2]$ $k_\infty = 3.3 \times 10^{-11}(T/300)^{-0.3}$ $F_c = 0.81$	Atkinson et al. (2004)
59	$NO_3 + OH \rightarrow NO_2 + HO_2$	2.0×10^{-11}	Atkinson et al. (2004)
60	$NO + CH_3O_2 \overset{O_2}{\rightarrow}$ $NO_2 + HO_2 + CH_2O$	$2.3 \times 10^{-12}\exp(360/T)$	Atkinson et al. (2006)
61	$NO_3 + CH_3OH \overset{O_2}{\rightarrow}$ $HNO_3 + HO_2 + CH_2O$	$9.4 \times 10^{-13}\exp(-2,650/T)$	Atkinson et al. (2006)
62	$NO_3 + CH_2O \overset{O_2}{\rightarrow}$ $HNO_3 + HO_2 + CO$	5.6×10^{-16}	Atkinson et al. (2006)

# Reac.	Reaction	$k\left[\left(\mathrm{molec.\,cm^{-3}}\right)^{1-n}\mathrm{s^{-1}}\right]$	Reference
63	$\mathrm{NO+C_2H_5O_2\overset{O_2}{\rightarrow}NO_2+HO_2+C_2H_4O}$	$2.6\times10^{-12}\exp(380/T)$	Atkinson et al. (2006)
64	$\mathrm{NO+CH_3CO_3\overset{O_2}{\rightarrow}NO_2+CO_2+CH_3O_2}$	$7.5\times10^{-12}\exp(290/T)$	Atkinson et al. (2006)
65	$\mathrm{NO_2+CH_3CO_3+M\rightarrow PAN+M}$	$k_0=2.7\times10^{-28}(T/300)^{-7.1}\,[\mathrm{N_2}]$ $k_\infty=1.2\times10^{-11}(T/300)^{-0.9}$ $F_c=0.3$	Atkinson et al. (2006)
66	$\mathrm{NO_2+Br+M\rightarrow BrNO_2+M}$	$k_0=4.2\times10^{-31}(T/300)^{-2.4}\,[\mathrm{N_2}]$ $k_\infty=2.7\times10^{-11}$ $F_c=0.55$	Atkinson et al. (2007)
67	$\mathrm{NO_3+Br\rightarrow NO_2+BrO}$	1.6×10^{-11}	Atkinson et al. (2007)
68	$\mathrm{NO_2+BrO+M\rightarrow BrONO_2+M}$	$k_0=4.7\times10^{-31}(T/300)^{-3.1}\,[\mathrm{N_2}]$ $k_\infty=1.8\times10^{-11}$ $F_c=0.4$	Atkinson et al. (2007)
69	$\mathrm{NO+BrO\rightarrow NO_2+Br}$	$8.7\times10^{-12}\exp(260/T)$	Atkinson et al. (2007)
70	$\mathrm{HNO_3+h\nu\overset{aero}{\rightarrow}NO_2+OH}$	3.3×10^{-4}	Cao et al. (2014)
71	$\mathrm{NO_2+O(^3P)\rightarrow NO+O_2}$	$5.5\times10^{-12}\exp(188/T)$	Atkinson et al. (2004)
72	$\mathrm{O_2+O(^3P)+M\rightarrow O_3+M}$	$6.0\times10^{-34}\,(T/300)^{-2.6}\,[\mathrm{N_2}]$ $+5.6\times10^{-34}\,(T/300)^{-2.6}\,[\mathrm{O_2}]$	Atkinson et al. (2004)
73	$\mathrm{N_2+O(^1D)\rightarrow N_2+O(^3P)}$	$1.8\times10^{-11}\exp(107/T)$	Atkinson et al. (2004)
74	$\mathrm{NO+O(^3P)+M\rightarrow NO_2+M}$	$k_0=10^{-31}(T/300)^{-1.6}\,[\mathrm{N_2}]$ $k_\infty=3.0\times10^{-11}(T/300)^{0.3}$ $F_c=0.85$	Atkinson et al. (2004)
75	$\mathrm{HO_2+O(^3P)\rightarrow OH+O_2}$	$2.7\times10^{-11}\exp(224/T)$	Atkinson et al. (2004)
76	$\mathrm{OH+O(^3P)\rightarrow HO_2+O_2}$	$2.4\times10^{-11}\exp(110/T)$	Atkinson et al. (2004)
77	$\mathrm{NO_2+O(^3P)+M\rightarrow NO_3+M}$	$k_0=1.3\times10^{-31}(T/300)^{-1.5}\,[\mathrm{N_2}]$ $k_\infty=2.3\times10^{-11}(T/300)^{0.24}$ $F_c=0.6$	Atkinson et al. (2004)
78	$\mathrm{NO_3+O(^3P)\rightarrow NO_2+O_2}$	1.7×10^{-11}	Atkinson et al. (2004)
79	$\mathrm{CH_2O+O(^3P)\rightarrow CO+HO_2+OH}$	$3.4\times10^{-11}\exp(-1,550/T)$	DeMore et al. (1997)
80	$\mathrm{NO+C_2H_5O_2\rightarrow NO_2+C_2H_5O}$	$2.6\times10^{-12}\exp(380/T)$	Atkinson et al. (2006)
81	$\mathrm{BrO+O(^3P)\rightarrow Br+O_2}$	$1.9\times10^{-11}\exp(230/T)$	Atkinson et al. (2007)

# Reac.	Reaction	$k\left[\left(\mathrm{molec.\,cm^{-3}}\right)^{1-n}\mathrm{s^{-1}}\right]$	Reference
82	$\mathrm{HOBr + O(^3P) \rightarrow BrO + O_2}$	$1.2\times10^{-10}\exp(-430/T)$	Nesbitt et al. (1995)
83	$\mathrm{PAN + OH \rightarrow CH_2O + NO_3}$	4.0×10^{-14}	Atkinson et al. (2006)
84	$\mathrm{PAN + M \rightarrow CH_3CO_3 + NO_2 + M}$	$k_0 = 4.9\times10^{-3} \times\exp(-12,100/T)\,[\mathrm{N_2}]$ $k_\infty = 5.4\times10^{16}\exp(-13,830/T)$ $F_c = 0.3$	Atkinson et al. (2006)
85	$\mathrm{2CH_3CO_3 \rightarrow 2CH_3O_2 + 2CO_2}$	$2.9\times10^{-12}\exp(500/T)$	Atkinson et al. (2006)
86	$\mathrm{NO_3 + C_2H_4O \xrightarrow{O_2} CH_3CO_3 + HNO_3}$	$1.4\times10^{-12}\exp(-1,860/T)$	Atkinson et al. (2006)
87	$\mathrm{CH_3CO_3 + CH_3O_2 \rightarrow CH_3O_2 + CH_2O + CO_2 + HO_2}$	$2.0\times10^{-12}\exp(500/T)$	Atkinson et al. (2006)
88	$\mathrm{NO_2 + NO_3 + M \rightarrow N_2O_5 + M}$	$k_0 = 3.6\times10^{-30}(T/300)^{-4.1}\,[\mathrm{N_2}]$ $k_\infty = 1.9\times10^{-11}(T/300)^{0.2}$ $F_c = 0.35$	Atkinson et al. (2004)
89	$\mathrm{N_2O_5 + M \rightarrow NO_2 + NO_3 + M}$	$k_0 = 1.3\times10^{-3}(T/300)^{-3.5} \times\exp(-11,000/T)\,[\mathrm{N_2}]$ $k_\infty = 9.7\times10^{14} \times(T/300)^{0.1}\exp(-11,080/T)$ $F_c = 0.35$	Atkinson et al. (2004)
90	$\mathrm{MPAN + M \rightarrow NO_2 + MCO_3 + M}$	$1.6\times10^{16}\exp(-13,500/T)$	Atkinson et al. (2006)
91	$\mathrm{NO_2 + MCO_3 + M \rightarrow MPAN + M}$	$1.1\times10^{-11}300/(T\,[\mathrm{N_2}])$	Atkinson et al. (2006)
92	$\mathrm{HOCl + O(^3P) \rightarrow ClO + OH}$	1.7×10^{-13}	Atkinson et al. (2007)
93	$\mathrm{ClO + O(^3P) \rightarrow Cl + O_2}$	$2.5\times10^{-11}\exp(110/T)$	Atkinson et al. (2007)
94	$\mathrm{OClO + O(^3P) \rightarrow ClO + O_2}$	$2.4\times10^{-12}\exp(-960/T)$	Atkinson et al. (2007)
95	$\mathrm{ClONO_2 + O(^3P) \rightarrow 0.5ClO + 0.5NO_3 + 0.5OClO + 0.5NO_2}$	$4.5\times10^{-12}\exp(-900/T)$	Atkinson et al. (2007)
96	$\mathrm{Cl + HO_2 \rightarrow HCl + O_2}$	3.4×10^{-11}	Atkinson et al. (2007)
97	$\mathrm{Cl + HO_2 \rightarrow ClO + OH}$	$6.3\times10^{-11}\exp(-570/T)$	Atkinson et al. (2007)
98	$\mathrm{Cl + H_2O_2 \rightarrow HCl + HO_2}$	$1.1\times10^{-11}\exp(-980/T)$	Atkinson et al. (2007)
99	$\mathrm{Cl + O_3 \rightarrow ClO + O_2}$	$2.8\times10^{-11}\exp(-250/T)$	Atkinson et al. (2007)
100	$\mathrm{Cl + HNO_3 \rightarrow HCl + NO_3}$	2.0×10^{-16}	Atkinson et al. (2007)
101	$\mathrm{Cl + NO_3 \rightarrow ClO + NO_2}$	2.4×10^{-11}	Atkinson et al. (2007)
102	$\mathrm{Cl + OClO \rightarrow 2ClO}$	$3.2\times10^{-11}\exp(170/T)$	DeMore et al. (1997)

# Reac.	Reaction	$k \left[\left(\mathrm{molec.\,cm^{-3}} \right)^{1-n} \mathrm{s}^{-1} \right]$	Reference
103	$\mathrm{Cl + ClONO_2 \rightarrow Cl_2 + NO_3}$	$6.2 \times 10^{-12} \exp(145/T)$	Atkinson et al. (2007)
104	$\mathrm{Cl_2 + OH \rightarrow Cl + HOCl}$	$3.6 \times 10^{-12} \exp(-1,200/T)$	Atkinson et al. (2007)
105	$\mathrm{HCl + OH \rightarrow Cl + H_2O}$	$1.7 \times 10^{-12} \exp(-230/T)$	Atkinson et al. (2007)
106	$\mathrm{HOCl + OH \rightarrow ClO + H_2O}$	5.0×10^{-13}	Atkinson et al. (2007)
107	$\mathrm{ClO + OH \rightarrow 0.94Cl + 0.94HO_2 + 0.06HCl + 0.06O_2}$	$7.3 \times 10^{-12} \exp(300/T)$	Atkinson et al. (2007)
108	$\mathrm{OClO + OH \rightarrow HOCl + O_2}$	$1.4 \times 10^{-12} \exp(600/T)$	Atkinson et al. (2007)
109	$\mathrm{ClONO_2 + OH \rightarrow HOCl + NO_3}$	$1.2 \times 10^{-12} \exp(-330/T)$	Atkinson et al. (2007)
110	$\mathrm{HCl + NO_3 \rightarrow Cl + HNO_3}$	5.0×10^{-17}	Atkinson et al. (2007)
111	$\mathrm{ClO + HO_2 \rightarrow HOCl + O_2}$	$2.2 \times 10^{-12} \exp(340/T)$	Atkinson et al. (2007)
112	$\mathrm{ClO + O_3 \rightarrow 0.06OClO + 0.96OClO + O_2}$	1.6×10^{-17}	Atkinson et al. (2007)
113	$\mathrm{ClO + NO \rightarrow Cl + NO_2}$	$6.2 \times 10^{-12} \exp(295/T)$	Atkinson et al. (2007)
114	$\mathrm{ClO + NO_2 + M \rightarrow ClONO_2 + M}$	$k_0 = 1.6 \times 10^{-31} (T/300)^{-3.4} [\mathrm{N_2}]$ $k_\infty = 7.0 \times 10^{-11}$ $F_c = 0.4$	Atkinson et al. (2007)
115	$\mathrm{ClO + NO_3 \rightarrow 0.74ClOO + 0.26OClO + NO_2}$	4.6×10^{-13}	Atkinson et al. (2007)
116	$\mathrm{2ClO \rightarrow Cl_2 + O_2}$	$10^{-12} \exp(-1,590/T)$	Atkinson et al. (2007)
117	$\mathrm{2ClO \rightarrow Cl + ClOO}$	$3.0 \times 10^{-11} \exp(-2,450/T)$	Atkinson et al. (2007)
118	$\mathrm{2ClO \rightarrow Cl + OClO}$	$3.5 \times 10^{-13} \exp(-1,370/T)$	Atkinson et al. (2007)
119	$\mathrm{2ClO + M \rightarrow Cl_2O_2 + M}$	$k_0 = 2.0 \times 10^{-32} (T/300)^{-4.0} [\mathrm{N_2}]$ $k_\infty = 10^{-11}$ $F_c = 0.45$	Atkinson et al. (2007)
120	$\mathrm{Cl_2O_2 + M \rightarrow 2ClO + M}$	$k_0 = 3.7 \times 10^{-7} \times \exp(-7,690/T) [\mathrm{N_2}]$ $k_\infty = 7.9 \times 10^{15} \exp(-8,820/T)$ $F_c = 0.45$	Atkinson et al. (2007)
121	$\mathrm{OClO + NO \rightarrow ClO + NO_2}$	$1.1 \times 10^{-13} \exp(350/T)$	Atkinson et al. (2007)
122	$\mathrm{OClO + Br \rightarrow ClO + BrO}$	$2.7 \times 10^{-11} \exp(-1,300/T)$	Atkinson et al. (2007)
123	$\mathrm{Cl_2O_2 + Br \rightarrow BrCl + ClOO}$	$5.9 \times 10^{-12} \exp(-170/T)$	Atkinson et al. (2007)
124	$\mathrm{BrO + ClO \rightarrow Br + OClO}$	$1.6 \times 10^{-12} \exp(430/T)$	Atkinson et al. (2007)
125	$\mathrm{BrO + ClO \rightarrow Br + ClOO}$	$2.9 \times 10^{-12} \exp(220/T)$	Atkinson et al. (2007)

# Reac.	Reaction	$k\left[\left(\mathrm{molec.\,cm}^{-3}\right)^{1-n}\mathrm{s}^{-1}\right]$	Reference
126	$\mathrm{BrO+ClO\rightarrow BrCl+O_2}$	$5.8\times10^{-13}\exp(170/T)$	Atkinson et al. (2007)
127	$\mathrm{BrCl+Cl\rightarrow Br+Cl_2}$	1.45×10^{-11}	Sander et al. (1997)
128	$\mathrm{Br_2+Cl\rightarrow Br+BrCl}$	$2.3\times10^{-10}\exp(135/T)$	Sander et al. (1997)
129	$\mathrm{Br+BrCl\rightarrow Br_2+Cl}$	3.3×10^{-15}	Sander et al. (1997)
130	$\mathrm{Br+Cl_2\rightarrow BrCl+Cl}$	1.1×10^{-15}	Sander et al. (1997)
131	$\mathrm{Cl+CH_4\xrightarrow{O_2}HCl+CH_3O_2}$	6.6×10^{-12}	Atkinson et al. (2006)
132	$\mathrm{Cl+C_2H_6\rightarrow HCl+C_2H_5}$	$8.3\times10^{-11}\exp(-100/T)$	Atkinson et al. (2006)
133	$\mathrm{Cl+C_3H_8\xrightarrow{2.5O_2}HCl+C_2H_5O_2+H_2O+CO_2}$	1.4×10^{-10}	Atkinson et al. (2006)
134	$\mathrm{Cl+CH_2O\xrightarrow{O_2}HCl+CO+HO_2}$	$8.1\times10^{-11}\exp(-34/T)$	Atkinson et al. (2006)
135	$\mathrm{Cl+C_2H_4O\xrightarrow{O_2}HCl+CH_3CO_3}$	8.0×10^{-11}	Atkinson et al. (2006)
136	$\mathrm{Cl+CH_3O_2H\rightarrow HCl+C_2H_4O+OH}$	5.9×10^{-11}	Atkinson et al. (2006)
137	$\mathrm{Cl+C_2H_5O_2H\rightarrow HCl+C_2H_5O_2}$	5.7×10^{-11}	Atkinson et al. (2006)
138	$\mathrm{Cl+C_2H_2\xrightarrow{3O_2}Cl+2CO+2HO_2}$	2.0×10^{-11}	Borken (1996)
139	$\mathrm{Cl+C_2H_2\xrightarrow{2O_2}HCl+2CO+HO_2}$	4.24×10^{-11}	Borken (1996)
140	$\mathrm{Cl+C_2H_4\xrightarrow{3.5O_2}Cl+2CO+H_2O+2HO_2}$	$k_0=1.26\times10^{-29}\times(T/300)^{-3.3}\,[\mathrm{N_2}]$ $k_\infty=6.0\times10^{-10}$ $F_c=0.4$	Atkinson et al. (2006)
141	$\mathrm{Cl+C_2H_4\xrightarrow{2.5O_2}HCl+2CO+H_2O+HO_2}$	$k_0=5.92\times10^{-30}\times(T/300)^{-3.3}\,[\mathrm{N_2}]$ $k_\infty=6.0\times10^{-10}$ $F_c=0.4$	Atkinson et al. (2006)
142	$\mathrm{Cl+O_2+M\rightarrow ClOO+M}$	$1.4\times10^{-33}\,(T/300)^{-3.9}\,[\mathrm{N_2}]+1.6\times10^{-33}\,(T/300)^{-2.9}\,[\mathrm{O_2}]$	Atkinson et al. (2007)
143	$\mathrm{ClOO+M\rightarrow Cl+O_2+M}$	$2.8\times10^{-10}\exp(-1,820/T)\,[\mathrm{N_2}]$	Atkinson et al. (2007)
144	$\mathrm{Cl+Cl_2O_2\rightarrow Cl_2+ClOO}$	$7.6\times10^{-11}\exp(65/T)$	Atkinson et al. (2007)
145	$\mathrm{Cl_2O_2+O_3\rightarrow ClO+ClOO+O_2}$	10^{-19}	Atkinson et al. (2007)
146	$\mathrm{Cl+ClOO\rightarrow 0.95Cl_2+0.95O_2+0.1ClO}$	2.42×10^{-10}	DeMore et al. (1997)
147	$\mathrm{ClO+CH_3O_2\rightarrow Cl+CH_2O+HO_2}$	$1.8\times10^{-12}\exp(-600/T)$	Atkinson et al. (2006)

Temperature T is given in Kelvin. Three-body reaction constants k_{3rd} appearing, for instance, in (R 28), are taken from (Atkinson et al., 2006)

$$k_{\mathrm{3rd}} = \frac{k_0}{1+k_0/k_\infty} F_c^{\frac{1}{1+\log_{10}(k_0/k_\infty)^2}}. \tag{A1}$$

Reaction (R 70) denotes the photolysis of $\mathrm{HNO_3}$ inside the aerosol phase. Since emissions of $\mathrm{NO_x}$ and transfers of $\mathrm{NO_y}$ to the aerosol phase are not considered in the present model, reaction (R 70) is necessary to recycle $\mathrm{HNO_3}$. Its rate is calculated by the transfer rate of $\mathrm{HNO_3}$ to the aerosol phase (Cao et al., 2014). Bottenheim et al. (1986) found that the majority of $\mathrm{NO_y}$ is in the form of PAN, as predicted by this model, whereas the $\mathrm{HNO_3}$ mixing ratio corresponds to a few percent of the $\mathrm{NO_y}$ mixing ratio. Without reaction (R 70) however, the model predicts that more than 80% of gas-phase $\mathrm{NO_y}$ is in the form of $\mathrm{HNO_3}$. It was proposed (Zhu et al., 2010; Ye et al., 2016) that a re-noxification of $\mathrm{HNO_3}$ may occur due to photolysis in the snow pack and aerosol phase, which occurs at a much faster rate than in the gas phase. Zhu et al. (2010) found a by three orders of magnitude enhanced absorption cross section of $\mathrm{HNO_3}$ on ice surfaces. Ye et al. (2016) found an enhancement of the photolysis rate of particulate $\mathrm{HNO_3}$ of 300 compared to the gas phase photolysis, corresponding to photolysis rates on the order of $10^{-4}\mathrm{s}^{-1}$, which is consistent with the rate of reaction (R 70).

A2 Photolysis reactions

The photolysis rates are calculated by a three-coefficient formula (Röth, 1992, 2002)

$$J(\mathrm{SZA}) = J_0 \exp\left(b\left[1-\sec(c\,\mathrm{SZA})\right]\right) \tag{A2}$$

with the solar zenith angle SZA. The coefficients are either taken from Lehrer et al. (2004) or from the Sappho module of the CAABA/MECCA model (Sander et al., 2011) as stated in Tab. A2.

A3 Gas-aerosol mass transfer constants

Table A3 shows the Henry's law constants H and mass accommodation coefficients α with their temperature dependence T_H and T_α as well their molecular mass M for all species undergoing a reaction of the form

$$\mathrm{X} \rightleftharpoons \mathrm{X_{aq}}.$$

All constants are taken from the CAABA/MECCA model (Sander et al., 2011). The calculation of the transfer constants is outlined in section 2.1.2. Perfect solubility is assumed for $\mathrm{BrONO_2}$ and $\mathrm{N_2O_5}$, which is denoted by a Henry's law constant of infinity. No transfer from the aerosol to the gas phase occurs for those species. These species directly undergo aqueous phase reactions where the reaction rate is proportional to the gas-to-aerosol transfer constant k_{in} in Eq. (8), see Tab. A4.

Table A2. Photolysis reactions

# Reac.	Reaction	$J_0\ [\mathrm{s}^{-1}]$	b	c	Reference
J1	$\mathrm{O_3 \rightarrow O(^1D) + O_2}$	6.85×10^{-5}	3.51	0.82	Lehrer et al. (2004)
J2	$\mathrm{O_3 \rightarrow O(^3P) + O_2}$	1.70×10^{-4}	1.71	0.85	Sander et al. (2011)
J3	$\mathrm{H_2O_2 \rightarrow 2OH}$	2.75×10^{-5}	1.60	0.848	Lehrer et al. (2004)
J4	$\mathrm{Br_2 \rightarrow 2Br}$	1.07×10^{-1}	0.73	0.9	Lehrer et al. (2004)
J5	$\mathrm{BrO \rightarrow Br + O(^3P)}$	1.27×10^{-1}	1.29	0.857	Lehrer et al. (2004)
J6	$\mathrm{HOBr \rightarrow Br + OH}$	2.62×10^{-3}	1.22	0.861	Lehrer et al. (2004)
J7	$\mathrm{BrONO_2 \rightarrow BrO + NO_2}$	3.11×10^{-3}	1.27	0.859	Lehrer et al. (2004)
J8	$\mathrm{BrNO_2 \rightarrow Br + NO_2}$	1.11×10^{-3}	1.48	0.851	Lehrer et al. (2004)
J9	$\mathrm{BrCl \rightarrow Br + Cl}$	3.41×10^{-2}	0.87	0.887	Lehrer et al. (2004)
J10	$\mathrm{Cl_2 \rightarrow 2Cl}$	7.37×10^{-3}	1.2	0.863	Lehrer et al. (2004)
J11	$\mathrm{ClO \rightarrow Cl + O(^3P)}$	1.08×10^{-4}	3.88	0.816	Lehrer et al. (2004)
J12	$\mathrm{HOCl \rightarrow Cl + OH}$	7.47×10^{-4}	1.40	0.855	Lehrer et al. (2004)
J13	$\mathrm{ClONO_2 \rightarrow Cl + NO_3}$	1.29×10^{-4}	1.29	0.861	Lehrer et al. (2004)
J14	$\mathrm{OClO \rightarrow ClO + O(^3P)}$	2.61×10^{-1}	1.06	0.872	Lehrer et al. (2004)
J15	$\mathrm{NO_2 \rightarrow NO + O(^3P)}$	2.62×10^{-2}	1.07	0.871	Lehrer et al. (2004)
J16	$\mathrm{NO_3 \rightarrow NO_2 + O(^3P)}$	6.2×10^{-1}	0.61	0.915	Lehrer et al. (2004)
J17	$\mathrm{NO_3 \rightarrow NO + O_2}$	7.03×10^{-2}	0.58	0.917	Lehrer et al. (2004)
J18	$\mathrm{HONO \rightarrow NO + OH}$	3.0×10^{-3}	0.76	0.925	Sander et al. (2011)
J19	$\mathrm{HNO_3 \rightarrow NO_2 + OH}$	1.39×10^{-6}	2.09	0.848	Lehrer et al. (2004)
J20	$\mathrm{N_2O_5 \rightarrow NO_2 + NO_3}$	8.13×10^{-5}	1.39	0.857	Sander et al. (2011)
J21	$\mathrm{PAN \rightarrow NO_2 + CH_3CO_3}$	3.682×10^{-5}	1.39	0.875	Lehrer et al. (2004)
J22	$\mathrm{HCHO \rightarrow 2HO_2 + CO}$	2.75×10^{-5}	1.15	0.91	Sander et al. (2011)
J23	$\mathrm{CH_3O_2H \rightarrow CH_2O + OH + HO_2}$	1.64×10^{-5}	1.49	0.861	Sander et al. (2011)
J24	$\mathrm{C_2H_4O \rightarrow CH_3O_2H + CO + HO_2}$	2.75×10^{-5}	1.15	0.91	Sander et al. (2011)
J25	$\mathrm{C_2H_5O_2H \rightarrow C_2H_5O + OH}$	1.64×10^{-5}	1.49	0.861	Sander et al. (2011)

A4 Aqueous phase reactions and equilibria

All aqueous reaction constants are taken from Sander et al. (2011). Acid/base equilibria are treated as very fast reactions where the ratio of the reaction constants is equal to the equilibrium constant. A few reactions are proportional to the gas-to-aerosol transfer constant k_{in} (Eq. (8)) of the depositing species.

A5 Heterogenous reactions and dry depositions

Table A5 shows all heterogenous reactions and dry depositions occurring on the snow surface. The calculation of the reaction constants, which are non-zero only in the lowest grid cell, is described in section 2.4. The mass accommodation coefficient

Table A3. Gas-aerosol mass transfer constants

Species	$H\left[\mathrm{M\,atm^{-1}}\right]$	$T_H\,[\mathrm{K}]$	$\alpha\,[1]$	$T_\alpha\,[\mathrm{K}]$	$M\left[\mathrm{g\,mol^{-1}}\right]$
HBr	1.3	10,240	0.032	3,940	80.91
HOBr	1,300.0	5,862	0.5	0	96.91
Br_2	0.77	3,837	0.038	6,546	159.8
N_2O_5	∞	0	0.1	0	108.0
HCl	0.1177	9,001	0.074	3,072	36.46
BrCl	0.94	5,600	0.038	6,546	115.4
Cl_2	0.092	2,081	0.038	6,546	79.0
HOCl	660.0	5,862	0.5	0	52.45
O_3	0.012	2,560	0.002	0	48.0
$BrONO_2$	∞	0	0.063	0	141.9

Table A4. Reactions occurring in the liquid phase, forward reaction rate coefficients are shown as well as backward reaction rate constants if applicable. $k_{\mathrm{in}}\,(\mathrm{X})$ denotes the gas-to-aerosol transfer rate for species X (Eq. (8)). $T_0 = 298.15$ K is the room temperature

# Reac.	Reaction	$k_{\mathrm{f}}\left[\mathrm{M^{1-n}s^{-1}}\right]$	$k_{\mathrm{b}}\left[\mathrm{M^{1-n}s^{-1}}\right]$
A1	$\mathrm{HOBr_{aq} + H^+ + Br^- \rightleftharpoons Br_{2,aq} + H_2O}$	1.6×10^{10}	$97.0\ \exp[-7{,}457\ \mathrm{K}\ (1/T - 1/T_0)]$
A2	$\mathrm{HOBr_{aq} + H^+ + Cl^- \rightleftharpoons BrCl_{aq} + H_2O}$	2.3×10^{10}	3.0×10^{6}
A3	$\mathrm{HOCl_{aq} + H^+ + Br^- \rightarrow BrCl_{aq} + H_2O}$	1.32×10^{6}	-
A4	$\mathrm{HOCl_{aq} + H^+ + Cl^- \rightleftharpoons Cl_{2,aq} + H_2O}$	$2.2\times10^{4}\ \exp[-3{,}508\ \mathrm{K}\ (1/T - 1/T_0)]$	$21.8\ \exp[-8{,}012\ \mathrm{K}\ (1/T - 1/T_0)]$
A5	$\mathrm{O_{3,aq} + Br^- \rightarrow BrO^-}$	$2.1\times10^{2}\ \exp[-4{,}450\ \mathrm{K}\ (1/T - 1/T_0)]$	-
A6	$\mathrm{O_{3,aq} + Cl^- \rightarrow ClO^-}$	3.0×10^{-3}	-
A7	$\mathrm{N_2O_{5,g} \rightarrow 2HNO_{3,g}}$	$k_{\mathrm{in}}\,(\mathrm{N_2O_5})$	-
A8	$\mathrm{N_2O_{5,g} + Br^- \rightarrow BrNO_{2,g} + HNO_{3,g}}$	$3.0\times10^{5}k_{\mathrm{in}}\,(\mathrm{N_2O_5})$	-
A9	$\mathrm{BrONO_{2,g} \rightarrow HOBr_{aq} + HNO_{3,g}}$	$k_{\mathrm{in}}\,(\mathrm{BrONO_2})$	-
A10	$\mathrm{BrONO_{2,g} + Br^- \rightarrow Br_{2,aq} + HNO_{3,g}}$	$3.0\times10^{5}k_{\mathrm{in}}\,(\mathrm{BrONO_2})$	-
E1	$\mathrm{HBr_{aq} \rightleftharpoons H^+ + Br^-}$	10^{15}	10^{6}
E2	$\mathrm{HCl_{aq} \rightleftharpoons H^+ + Cl^-}$	$1.53\times10^{-3}\ \exp(6{,}900/T)$	10
E3	$\mathrm{HOBr_{aq} \rightleftharpoons H^+ + BrO^-}$	$2.3\times10^{2}\ \exp[-3{,}091\ \mathrm{K}\ (1/T - 1/T_0)]$	10^{11}
E4	$\mathrm{HOCl_{aq} \rightleftharpoons H^+ + ClO^-}$	0.32	10^{7}
E5	$\mathrm{BrCl_{aq} + Cl^- \rightleftharpoons BrCl_2^-}$	5.0×10^{8}	$1.3\times10^{8}\ \exp[-1{,}191\ \mathrm{K}\ (1/T - 1/T_0)]$
E6	$\mathrm{BrCl_{aq} + Br^- \rightleftharpoons Br_2Cl^-}$	10^{9}	$5.6\times10^{4}\ \exp[-7{,}457\ \mathrm{K}\ (1/T - 1/T_0)]$
E7	$\mathrm{Br_{2,aq} + Cl^- \rightleftharpoons Br_2Cl^-}$	5.0×10^{7}	3.85×10^{7}
E8	$\mathrm{Cl_{2,aq} + Br^- \rightleftharpoons BrCl_2^-}$	7.7×10^{9}	$1{,}800\ \exp[-14{,}072\ \mathrm{K}\ (1/T - 1/T_0)]$

is $\gamma = 0.06$ (Sander and Crutzen, 1996) for most species. Since the strongest resistance is the species-independent turbulent resistance, the deposition velocities for the different species vary only slightly around 21 $\mathrm{cm\,s^{-1}}$. Deposition velocities in

Table A5. Heterogenous reactions and dry depositions occurring on the ice/snow surface

Reaction/Dry deposition	Accommodation coefficient γ
$\mathrm{HBr} \rightarrow$	0.06
$\mathrm{HOBr} \rightarrow 0.96\ \mathrm{Br_2} + 0.04\ \mathrm{BrCl}$	0.06
$\mathrm{HCl} \rightarrow$	0.06
$\mathrm{BrONO_2} \rightarrow \mathrm{HOBr} + \mathrm{HNO_3}$	0.06
$\mathrm{N_2O_5} \rightarrow \mathrm{BrNO_2} + \mathrm{HNO_3}$	0.09

the present model are relatively large since the lowest grid cell is at $10^{-4}\mathrm{m}$, reducing the turbulent resistance by a large factor compared to models using a linear grid. Also, the surface resistance is usually the largest resistance and widely calculated using parameterizations outlined by Wesely (1989), which, however, does not hold for ice/snow surfaces. Due to the large deposition velocity, the heterogenous reactions are rate limited by the downward diffusion of the depositing species, replenishing in the lowest grid cell.

Author contributions. MH developed the code that was used to perform the simulations and he created all figures presented in the paper. The code is based on previous work of LC, who helped to advance the present more extended code. HS contributed with respect to the model extension and validation of the results. UP and EG devised the methodology and supervised the project. The draft manuscript was edited by MH, and all authors contributed through numerous revisions of the draft paper.

Competing interests. The authors do not have any competing interests.

Acknowledgements. The authors thank R. Sander from the Max-Planck Institute for Chemistry, Mainz, Germany, for very fruitful discussions concerning the chemical reaction scheme and the aerosol treatment. Financial support of the German Research Foundation (DFG) through project GU-255/6-2 and through HGS MathComp is gratefully acknowledged. Le Cao is financially supported by the National Natural Science Foundation of China (Grant No. 41705103).

References

Abbatt, J. P. D., Thomas, J. L., Abrahamsson, K., Boxe, C., Granfors, A., Jones, A. E., King, M. D., Saiz-Lopez, A., Shepson, P. B., Sodeau, J., Toohey, D. W., Toubin, C., von Glasow, R., Wren, S. N., and Yang, X.: Halogen activation via interactions with environmental ice and snow in the polar lower troposphere and other regions, Atmospheric Chemistry and Physics, 12, 6237–6271, https://doi.org/10.5194/acp-12-6237-2012, http://www.atmos-chem-phys.net/12/6237/2012/, 2012.

Adams, J., Holmes, N., and Crowley, J.: Uptake and reaction of HOBr on frozen and dry NaCl/NaBr surfaces between 253 and 233 K, Atmospheric Chemistry and Physics, 2, 79–91, 2002.

Alfonso, A., Georges, L. B., Gérard, L. V., and Gilles, P.: The BrO + Ch3O2 reaction: Kinetics and role in the atmospheric ozone budget, Geophysical Research Letters, 24, 2745–2748, https://doi.org/10.1029/97GL02686, https://agupubs.onlinelibrary.wiley.com/doi/abs/10.1029/97GL02686, 1997.

Artiglia, L., Edebeli, J., Orlando, F., Chen, S., Lee, M.-T., Arroyo, P. C., Gilgen, A., Bartels-Rausch, T., Kleibert, A., Vazdar, M., et al.: A surface-stabilized ozonide triggers bromide oxidation at the aqueous solution-vapour interface, Nature Communications, 8, 700, 2017.

Atkinson, R., Baulch, D. L., Cox, R. A., Crowley, J. N., Hampson, R. F., Hynes, R. G., Jenkin, M. E., Rossi, M. J., and Troe, J.: Evaluated kinetic and photochemical data for atmospheric chemistry: Volume I - gas phase reactions of O_x, HO_x, NO_x and SO_x species, Atmospheric Chemistry and Physics, 4, 1461–1738, https://doi.org/10.5194/acp-4-1461-2004, https://www.atmos-chem-phys.net/4/1461/2004/, 2004.

Atkinson, R., Baulch, D. L., Cox, R. A., Crowley, J. N., Hampson, R. F., Hynes, R. G., Jenkin, M. E., Rossi, M. J., Troe, J., and Subcommittee, I.: Evaluated kinetic and photochemical data for atmospheric chemistry: Volume II ; gas phase reactions of organic species, Atmospheric Chemistry and Physics, 6, 3625–4055, https://doi.org/10.5194/acp-6-3625-2006, https://www.atmos-chem-phys.net/6/3625/2006/, 2006.

Atkinson, R., Baulch, D. L., Cox, R. A., Crowley, J. N., Hampson, R. F., Hynes, R. G., Jenkin, M. E., Rossi, M. J., and Troe, J.: Evaluated kinetic and photochemical data for atmospheric chemistry: Volume III - gas phase reactions of inorganic halogens, Atmospheric Chemistry and Physics, 7, 981–1191, https://doi.org/10.5194/acp-7-981-2007, https://www.atmos-chem-phys.net/7/981/2007/, 2007.

Barnes, I., Becker, K. H., and Overath, R. D.: Oxidation of Organic Sulfur Compounds, in: The Tropospheric Chemistry of Ozone in the Polar Regions, edited by Niki, H. and Becker, K. H., pp. 371–383, Springer Berlin Heidelberg, Berlin, Heidelberg, 1993.

Barrie, L., Bottenheim, J., Schnell, R., Crutzen, P., and Rasmussen, R.: Ozone destruction and photochemical reactions at polar sunrise in the lower Arctic atmosphere, Nature, 334, 138, 1988.

Beine, H., Domine, F., Ianniello, A., Nardino, M., Allegrini, I., Teinilä, K., and Hillamo, R.: Fluxes of nitrates between snow surfaces and the atmosphere in the European high Arctic, Atmospheric Chemistry and Physics, 3, 335–346, 2003.

Borken, J.: Ozonabbau durch Halogene in der arktischen Grenzschicht, Master's thesis, Heidelberg University, Germany, in German, 1996.

Bottenheim, J., Gallant, A., and Brice, K.: Measurements of NOy species and O3 at 82 N latitude, Geophysical Research Letters, 13, 113–116, 1986.

Bottenheim, J., Netcheva, S., Morin, S., and Nghiem, S.: Ozone in the boundary layer air over the Arctic Ocean: measurements during the TARA transpolar drift 2006–2008, Atmospheric Chemistry and Physics, 9, 4545–4557, 2009.

Bottenheim, J. W. and Chan, E.: A trajectory study into the origin of spring time Arctic boundary layer ozone depletion, Journal of Geophysical Research: Atmospheres, 111, https://doi.org/10.1029/2006JD007055, https://agupubs.onlinelibrary.wiley.com/doi/abs/10.1029/2006JD007055, 2006.

Briggs, T. S. and Rauscher, W. C.: An oscillating iodine clock, Journal of Chemical Education, 50, 496, https://doi.org/10.1021/ed050p496, https://doi.org/10.1021/ed050p496, 1973.

Cao, L. and Gutheil, E.: Numerical simulation of tropospheric ozone depletion in the polar spring, Air Quality, Atmosphere & Health, 6, 673–686, 2013.

Cao, L., Sihler, H., Platt, U., and Gutheil, E.: Numerical analysis of the chemical kinetic mechanisms of ozone depletion and halogen release in the polar troposphere, Atmos. Chem. Phys, 14, 377, 2014.

Cao, L., Platt, U., and Gutheil, E.: Role of the boundary layer in the occurrence and termination of the tropospheric ozone depletion events in polar spring, Atmospheric Environment, 132, 98–110, 2016.

Chu, L. and Anastasio, C.: Quantum yields of hydroxyl radical and nitrogen dioxide from the photolysis of nitrate on ice, The Journal of Physical Chemistry A, 107, 9594–9602, 2003.

Cotter, E., Jones, A., Wolff, E., and Bauguitte, S.-B.: What controls photochemical NO and NO2 production from Antarctic snow? Laboratory investigation assessing the wavelength and temperature dependence, Journal of Geophysical Research: Atmospheres, 108, 2003.

DeMore, W. B., Sander, S. P., Golden, D., Hampson, R., Kurylo, M. J., Howard, C. J., Ravishankara, A., Kolb, C., and Molina, M.: Chemical Kinetics and Photochemical Data for Use in Stratospheric Modeling. Evaluation No. 12, Tech. rep., Jet Propulsion Lab., California Inst. of Tech.; Pasadena, CA United Stat, 1997.

Dubowski, Y., Colussi, A., and Hoffmann, M.: Nitrogen dioxide release in the 302 nm band photolysis of spray-frozen aqueous nitrate solutions. Atmospheric implications, The Journal of Physical Chemistry A, 105, 4928–4932, 2001.

Evans, M. J., Jacob, D. J., Atlas, E., Cantrell, C. A., Eisele, F., Flocke, F., Fried, A., Mauldin, R. L., Ridley, B. A., Wert, B., Talbot, R., Blake, D., Heikes, B., Snow, J., Walega, J., Weinheimer, A. J., and Dibb, J.: Coupled evolution of BrOx-ClOx-HOx-NOx chemistry during bromine-catalyzed ozone depletion events in the arctic boundary layer, Journal of Geophysical Research: Atmospheres, 108, https://doi.org/10.1029/2002JD002732, https://agupubs.onlinelibrary.wiley.com/doi/abs/10.1029/2002JD002732, 2003.

Fan, S.-M. and Jacob, D. J.: Surface ozone depletion in Arctic spring sustained by bromine reactions on aerosols, Nature, 359, 522, 1992.

Fox, J. L., Wofsy, S. C., McElroy, M. B., and Prather, M. J.: A stratospheric chemical instability, Journal of Geophysical Research: Oceans, 87, 11 126–11 132, https://doi.org/10.1029/JC087iC13p11126, https://agupubs.onlinelibrary.wiley.com/doi/abs/10.1029/JC087iC13p11126, 1982.

Frieß, U., Hollwedel, J., König-Langlo, G., Wagner, T., and Platt, U.: Dynamics and chemistry of tropospheric bromine explosion events in the Antarctic coastal region, Journal of Geophysical Research: Atmospheres, 109, 2004.

Frieß, U., Sihler, H., Sander, R., Pöhler, D., Yilmaz, S., and Platt, U.: The vertical distribution of BrO and aerosols in the Arctic: Measurements by active and passive differential optical absorption spectroscopy, Journal of Geophysical Research: Atmospheres, 116, 2011.

Gottwald, B. A. and Wanner, G.: A reliable rosenbrock integrator for stiff differential equations, Computing, 26, 355–360, https://doi.org/10.1007/BF02237954, https://doi.org/10.1007/BF02237954, 1981.

Grannas, A. M., Jones, A. E., Dibb, J., Ammann, M., Anastasio, C., Beine, H. J., Bergin, M., Bottenheim, J., Boxe, C. S., Carver, G., Chen, G., Crawford, J. H., Dominé, F., Frey, M. M., Guzmán, M. I., Heard, D. E., Helmig, D., Hoffmann, M. R., Honrath, R. E., Huey, L. G., Hutterli, M., Jacobi, H. W., Klán, P., Lefer, B., McConnell, J., Plane, J., Sander, R., Savarino, J., Shepson, P. B., Simpson, W. R., Sodeau, J. R., von Glasow, R., Weller, R., Wolff, E. W., and Zhu, T.: An overview of snow photochemistry: evidence, mechanisms and impacts, Atmospheric Chemistry and Physics, 7, 4329–4373, https://doi.org/10.5194/acp-7-4329-2007, https://www.atmos-chem-phys.net/7/4329/2007/, 2007.

Grebel, J. E., Pignatello, J. J., and Mitch, W. A.: Effect of halide ions and carbonates on organic contaminant degradation by hydroxyl radical-based advanced oxidation processes in saline waters, Environmental science & technology, 44, 6822–6828, 2010.

Halfacre, J. W., Knepp, T. N., Shepson, P. B., Thompson, C. R., Pratt, K. A., Li, B., Peterson, P. K., Walsh, S. J., Simpson, W. R., Matrai, P. A., Bottenheim, J. W., Netcheva, S., Perovich, D. K., and Richter, A.: Temporal and spatial characteristics of ozone depletion events from measurements in the Arctic, Atmospheric Chemistry and Physics, 14, 4875–4894, https://doi.org/10.5194/acp-14-4875-2014, https://www.atmos-chem-phys.net/14/4875/2014/, 2014.

Hausmann, M. and Platt, U.: Spectroscopic measurement of bromine oxide and ozone in the high Arctic during Polar Sunrise Experiment 1992, Journal of Geophysical Research: Atmospheres, 99, 25 399–25 413, 1994.

Helmig, D., Boylan, P., Johnson, B., Oltmans, S., Fairall, C., Staebler, R., Weinheimer, A., Orlando, J., Knapp, D. J., Montzka, D. D., et al.: Ozone dynamics and snow-atmosphere exchanges during ozone depletion events at Barrow, Alaska, Journal of Geophysical Research: Atmospheres, 117, 2012.

Hess, P. G. and Madronich, S.: On tropospheric chemical oscillations, Journal of Geophysical Research: Atmospheres, 102, 15 949–15 965, https://doi.org/10.1029/97JD00526, https://agupubs.onlinelibrary.wiley.com/doi/abs/10.1029/97JD00526, 1997.

Honrath, R., Guo, S., Peterson, M. C., Dziobak, M., Dibb, J. E., and Arsenault, M.: Photochemical production of gas phase NO x from ice crystal NO3-, Journal of Geophysical Research: Atmospheres, 105, 24 183–24 190, 2000.

Hov, Ø., Schmidbauer, N., and Oehme, M.: Light hydrocarbons in the Norwegian Arctic, Atmospheric Environment (1967), 23, 2471–2482, 1989.

Huff, A. K. and Abbatt, J. P.: Gas-Phase Br2 Production in Heterogeneous Reactions of Cl2, HOCl, and BrCl with Halide- Ice Surfaces, The Journal of Physical Chemistry A, 104, 7284–7293, 2000.

Huff, A. K. and Abbatt, J. P.: Kinetics and product yields in the heterogeneous reactions of HOBr with ice surfaces containing NaBr and NaCl, The Journal of Physical Chemistry A, 106, 5279–5287, 2002.

Jacobi, H.-W., Morin, S., and Bottenheim, J. W.: Observation of widespread depletion of ozone in the springtime boundary layer of the central Arctic linked to mesoscale synoptic conditions, Journal of Geophysical Research: Atmospheres, 115, 2010.

Jones, A. E., Weller, R., Wolff, E. W., and Jacobi, H. W.: Speciation and rate of photochemical NO and NO2 production in Antarctic snow, Geophysical Research Letters, 27, 345–348, https://doi.org/10.1029/1999GL010885, https://agupubs.onlinelibrary.wiley.com/doi/abs/10.1029/1999GL010885, 2000.

Jones, A. E., Weller, R., Anderson, P. S., Jacobi, H. W., Wolff, E. W., Schrems, O., and Miller, H.: Measurements of NOx emissions from the Antarctic snowpack, Geophysical Research Letters, 28, 1499–1502, https://doi.org/10.1029/2000GL011956, https://agupubs.onlinelibrary.wiley.com/doi/abs/10.1029/2000GL011956, 2001.

Kalachev, L. V. and Field, R. J.: Reduction of a Model Describing Ozone Oscillations in the Troposphere: Example of an Algorithmic Approach to Model Reduction in Atmospheric Chemistry, Journal of Atmospheric Chemistry, 39, 65–93, https://doi.org/10.1023/A:1010649217616, https://doi.org/10.1023/A:1010649217616, 2001.

Keil, A. D. and Shepson, P. B.: Chlorine and bromine atom ratios in the springtime Arctic troposphere as determined from measurements of halogenated volatile organic compounds, Journal of Geophysical Research: Atmospheres, 111, 2006.

Koo, J.-H., Wang, Y., Kurosu, T., Chance, K., Rozanov, A., Richter, A., Oltmans, S., Thompson, A., Hair, J., Fenn, M., et al.: Characteristics of tropospheric ozone depletion events in the Arctic spring: analysis of the ARCTAS, ARCPAC, and ARCIONS measurements and satellite BrO observations, Atmospheric Chemistry and Physics, 12, 9909–9922, 2012.

Lehrer, E., Hönninger, G., and Platt, U.: A one dimensional model study of the mechanism of halogen liberation and vertical transport in the polar troposphere, Atmos. Chem. Phys., 4, 2427–2440, 2004.

Lotka, A. J.: Contribution to the Theory of Periodic Reactions, The Journal of Physical Chemistry, 14, 271–274, https://doi.org/10.1021/j150111a004, https://doi.org/10.1021/j150111a004, 1909.

Luther, G. W., Swartz, C. B., and Ullman, W. J.: Direct determination of iodide in seawater by cathodic stripping square wave voltammetry, Analytical Chemistry, 60, 1721–1724, 1988.

Mallard, W. G., Westley, F., Herron, J., Hampson, R. F., and Frizzell, D.: NIST chemical kinetics database, Version 5.0, National Institute of Standards and Technology, Gaithersburg, MD, 1993.

McConnell, J., Henderson, G., Barrie, L., Bottenheim, J., Niki, H., Langford, C., and Templeton, E.: Photochemical bromine production implicated in Arctic boundary-layer ozone depletion, Nature, 355, 150, 1992.

Michalowski, B. A., Francisco, J. S., Li, S.-M., Barrie, L. A., Bottenheim, J. W., and Shepson, P. B.: A computer model study of multiphase chemistry in the Arctic boundary layer during polar sunrise, Journal of Geophysical Research: Atmospheres, 105, 15 131–15 145, 2000.

Millero, F. J., Feistel, R., Wright, D. G., and McDougall, T. J.: The composition of Standard Seawater and the definition of the Reference-Composition Salinity Scale, Deep Sea Research Part I: Oceanographic Research Papers, 55, 50–72, 2008.

Moore, C. W., Obrist, D., Steffen, A., Staebler, R. M., Douglas, T. A., Richter, A., and Nghiem, S. V.: Convective forcing of mercury and ozone in the Arctic boundary layer induced by leads in sea ice, Nature, 506, 81, 2014.

Neff, W., Helmig, D., Grachev, A., and Davis, D.: A study of boundary layer behavior associated with high NO concentrations at the South Pole using a minisodar, tethered balloon, and sonic anemometer, Atmospheric Environment, 42, 2762–2779, 2008.

Nesbitt, F., Monks, P., Payne, W., Stief, L., and Toumi, R.: The reaction O (^{3}P)+ HOBr: Temperature dependence of the rate constant and importance of the reaction as an HOBr stratospheric loss process, Geophysical research letters, 22, 827–830, 1995.

Oltmans, S.: Surface ozone measurements in clean air, Journal of Geophysical Research: Oceans, 86, 1174–1180, https://doi.org/10.1029/JC086iC02p01174, https://agupubs.onlinelibrary.wiley.com/doi/abs/10.1029/JC086iC02p01174, 1981.

Oltmans, S. J., Johnson, B. J., and Harris, J. M.: Springtime boundary layer ozone depletion at Barrow, Alaska: Meteorological influence, year-to-year variation, and long-term change, Journal of Geophysical Research: Atmospheres, 117, 2012.

Oum, K., Lakin, M., and Finlayson-Pitts, B.: Bromine activation in the troposphere by the dark reaction of O3 with seawater ice, Geophysical Research Letters, 25, 3923–3926, 1998.

Palo, T., Vihma, T., Jaagus, J., and Jakobson, E.: Observations of temperature inversions over central Arctic sea ice in summer, Quarterly Journal of the Royal Meteorological Society, 143, 2741–2754, 2017.

Pielke, R. A. and Mahrer, Y.: Representation of the Heated Planetary Boundary Layer in Mesoscale Models with Coarse Vertical Resolution, Journal of the Atmospheric Sciences, 32, 2288–2308, https://doi.org/10.1175/1520-0469(1975)032<2288:ROTHPB>2.0.CO;2, https://doi.org/10.1175/1520-0469(1975)032<2288:ROTHPB>2.0.CO;2, 1975.

Platt, U. and Janssen, C.: Observation and role of the free radicals NO 3, ClO, BrO and IO in the troposphere, Faraday Discussions, 100, 175–198, 1995.

Platt, U. and Lehrer, E.: Arctic tropospheric ozone chemistry, ARCTOC, no. 64 in Air pollution research report, European Commission Directorate-General, Science, Research and Development, Luxembourg, 1997.

Pöhler, D., Vogel, L., Frieß, U., and Platt, U.: Observation of halogen species in the Amundsen Gulf, Arctic, by active long-path differential optical absorption spectroscopy, Proceedings of the National Academy of Sciences, 107, 6582–6587, 2010.

Poppe, D. and Lustfeld, H.: Nonlinearities in the gas phase chemistry of the troposphere: Oscillating concentrations in a simplified mechanism, Journal of Geophysical Research: Atmospheres, 101, 14 373–14 380, 1996.

Pratt, K. A., Custard, K. D., Shepson, P. B., Douglas, T. A., Pöhler, D., General, S., Zielcke, J., Simpson, W. R., Platt, U., Tanner, D. J., et al.: Photochemical production of molecular bromine in Arctic surface snowpacks, Nature Geoscience, 6, 351, 2013.

Pruppacher, H. R., Klett, J. D., and Wang, P. K.: Microphysics of clouds and precipitation, 1998.

Röth, E.-P.: A fast algorithm to calculate the photonflux in optically dense media for use in photochemical models, Berichte der Bunsengesellschaft für physikalische Chemie, 96, 417–420, 1992.

Röth, E.-P.: Description of the anisotropic radiation transfer model ART to determine photodissociation coefficients, Forschungszentrum, Zentralbibliothek, 2002.

Saiz-Lopez, A., Mahajan, A. S., Salmon, R. A., Bauguitte, S. J.-B., Jones, A. E., Roscoe, H. K., and Plane, J. M.: Boundary layer halogens in coastal Antarctica, Science, 317, 348–351, 2007.

Sander, R.: Modeling Atmospheric Chemistry: Interactions between Gas-Phase Species and Liquid Cloud/Aerosol Particles, Surveys in Geophysics, 20, 1–31, https://doi.org/10.1023/A:1006501706704, https://doi.org/10.1023/A:1006501706704, 1999.

Sander, R. and Crutzen, P. J.: Model study indicating halogen activation and ozone destruction in polluted air masses transported to the sea, Journal of Geophysical Research: Atmospheres, 101, 9121–9138, 1996.

Sander, R., Vogt, R., Harris, G. W., and Crutzen, P. J.: Modelling the chemistry of ozone, halogen compounds, and hydrocarbons in the arctic troposphere during spring, Tellus B: Chemical and Physical Meteorology, 45, 522–532, https://doi.org/10.3402/tellusb.v45i5.16001, https://doi.org/10.3402/tellusb.v45i5.16001, 1997.

Sander, R., Baumgaertner, A., Gromov, S., Harder, H., Jöckel, P., Kerkweg, A., Kubistin, D., Regelin, E., Riede, H., Sandu, A., Taraborrelli, D., Tost, H., and Xie, Z.-Q.: The atmospheric chemistry box model CAABA/MECCA-3.0, Geoscientific Model Development, 4, 373–380, https://doi.org/10.5194/gmd-4-373-2011, https://www.geosci-model-dev.net/4/373/2011/, 2011.

Seinfeld, J. H. and Pandis, S. N.: Atmospheric chemistry and physics: from air pollution to climate change, John Wiley & Sons, 2006.

Simpson, W., Glasow, R. v., Riedel, K., Anderson, P., Ariya, P., Bottenheim, J., Burrows, J., Carpenter, L., Frieß, U., Goodsite, M. E., et al.: Halogens and their role in polar boundary-layer ozone depletion, Atmospheric Chemistry and Physics, 7, 4375–4418, 2007.

Simpson, W. R., Alvarez-Aviles, L., Douglas, T. A., Sturm, M., and Domine, F.: Halogens in the coastal snow pack near Barrow, Alaska: Evidence for active bromine air-snow chemistry during springtime, Geophysical research letters, 32, 2005.

Simpson, W. R., Brown, S. S., Saiz-Lopez, A., Thornton, J. A., and von Glasow, R.: Tropospheric halogen chemistry: Sources, cycling, and impacts, Chemical reviews, 115, 4035–4062, 2015.

Staebler, R. M., den Hartog, G., Georgi, B., and Düsterdiek, T.: Aerosol size distributions in Arctic haze during the Polar Sunrise Experiment 1992, Journal of Geophysical Research: Atmospheres, 99, 25 429–25 437, https://doi.org/10.1029/94JD00520, https://agupubs.onlinelibrary.wiley.com/doi/abs/10.1029/94JD00520, 1994.

Stull, R. B.: An introduction to boundary layer meteorology, vol. 13, Springer Netherlands, https://doi.org/10.1007/978-94-009-3027-8, 1988.

Tang, J. and McConnell, J.: Surface ozone depletion in Arctic spring sustained by bromine reactions on aerosols, Geophysical Research Letters, 23, 2633–2636, 1996.

Tarasick, D. and Bottenheim, J.: Surface ozone depletion episodes in the Arctic and Antarctic from historical ozonesonde records, Atmospheric Chemistry and Physics, 2, 197–205, 2002.

Tinsley, M. R. and Field, R. J.: Steady State Instability and Oscillation in Simplified Models of Tropospheric Chemistry, The Journal of Physical Chemistry A, 105, 11 212–11 219, https://doi.org/10.1021/jp010571t, https://doi.org/10.1021/jp010571t, 2001.

Toyota, K., Kanaya, Y., Takahashi, M., and Akimoto, H.: A box model study on photochemical interactions between VOCs and reactive halogen species in the marine boundary layer, Atmospheric Chemistry and Physics, 4, 1961–1987, 2004.

Toyota, K., McConnell, J., Lupu, A., Neary, L., McLinden, C., Richter, A., Kwok, R., Semeniuk, K., Kaminski, J., Gong, S.-L., et al.: Analysis of reactive bromine production and ozone depletion in the Arctic boundary layer using 3-D simulations with GEM-AQ: inference from synoptic-scale patterns, 2011.

Tuckermann, M., Ackermann, R., Gölz, C., Lorenzen-Schmidt, H., Senne, T., Stutz, J., Trost, B., Unold, W., and Platt, U.: DOAS-observation of halogen radical-catalysed arctic boundary layer ozone destruction during the ARCTOC-campaigns 1995 and 1996 in Ny-Ålesund, Spitsbergen, Tellus Series B Chemical and Physical Meteorology B, 49, 533, https://doi.org/10.3402/tellusb.v49i5.16005, 1997.

Ueda, H., Fukui, T., Kajino, M., Horiguchi, M., Hashiguchi, H., and Fukao, S.: Eddy diffusivities for momentum and heat in the upper troposphere and lower stratosphere measured by MU radar and RASS, and a comparison of turbulence model predictions, Journal of the Atmospheric Sciences, 69, 323–337, 2012.

Wagner, T., Leue, C., Wenig, M., Pfeilsticker, K., and Platt, U.: Spatial and temporal distribution of enhanced boundary layer BrO concentrations measured by the GOME instrument aboard ERS-2, Journal of Geophysical Research: Atmospheres, 106, 24 225–24 235, 2001.

Wagner, T., Ibrahim, O., Sinreich, R., Frieß, U., von Glasow, R., and Platt, U.: Enhanced tropospheric BrO over Antarctic sea ice in mid winter observed by MAX-DOAS on board the research vessel Polarstern, Atmospheric Chemistry and Physics, 7, 3129–3142, https://doi.org/10.5194/acp-7-3129-2007, https://www.atmos-chem-phys.net/7/3129/2007/, 2007.

Wennberg, P.: Atmospheric chemistry: Bromine explosion, Nature, 397, 299, 1999.

Wesely, M.: Parameterization of surface resistances to gaseous dry deposition in regional-scale numerical models, Atmospheric Environment (1967), 23, 1293–1304, 1989.

White, W. H. and Dietz, D.: Does the photochemistry of the troposphere admit more than one steady state?, Nature, 309, 242–244, 1984.

Wilson, R.: Turbulent diffusivity in the free atmosphere inferred from MST radar measurements: a review, in: Annales Geophysicae, vol. 22 (11), pp. 3869–3887, 2004.

Wren, S. N., Donaldson, D., and Abbatt, J.: Photochemical chlorine and bromine activation from artificial saline snow, Atmospheric Chemistry and Physics, 13, 9789–9800, 2013.

Wu, M., Liu, X., Zhang, L., Wu, C., Lu, Z., Ma, P.-L., Wang, H., Tilmes, S., Mahowald, N., Matsui, H., et al.: Impacts of aerosol dry deposition on black carbon spatial distributions and radiative effects in the community atmosphere model CAM5, Journal of Advances in Modeling Earth Systems, 10, 1150–1171, 2018.

Ye, C., Zhou, X., Pu, D., Stutz, J., Festa, J., Spolaor, M., Tsai, C., Cantrell, C., Mauldin, R. L., Campos, T., et al.: Rapid cycling of reactive nitrogen in the marine boundary layer, Nature, 532, 489, 2016.

Zhu, C., Xiang, B., Chu, L. T., and Zhu, L.: 308 nm photolysis of nitric acid in the gas phase, on aluminum surfaces, and on ice films, The Journal of Physical Chemistry A, 114, 2561–2568, 2010.